SIMULATION OF OPEN QUANTUM DYNAMICS AND INVESTIGATION OF QUANTUM CORRELATIONS IN FINITE SYSTEMS

Massimo Borrelli, M.Sc. Physics

Submitted for the Degree of Doctor of Philosophy

Heriot-Watt University
EPS/IPaQS
Edinburgh, June 2014.

Abstract

This thesis reports a series of theoretical studies regarding the dynamics of few-body controllable quantum systems. Generally speaking, the main focus is on the behavior of correlations in open quantum systems and how these could be used both for applications to quantum technologies and investigations of more fundamental phenomena. The general physical setting for most of the results presented is trapped-ion systems. These have been proven to be an almost prefect practical platform for realizing a quantum computer. Furthermore, thanks to their exceptional degree of controllability, trapped ions have been lately employed to also simulate basic physics, ranging from condensed-matter to high-energy physics. Although the findings in this manuscript are theoretical, real experimental parameters have been taken into account in order to provide a more realistic modeling. To this aim, a mixed of analytical and numerical methods have been extensively utilized. Concluding, we do believe that the theory developed in this thesis could be experimentally tested to give a more insightful view on open quantum system dynamics, both from a foundational and applicative point of view.

Acknowledgments

Among the things that I learned from the time spent as a Ph.D. student, the most important one is that in this thesis there is much more than meets the eyes. This manuscript is the outcome of many people interacting and working together whom I really wish to thank now, at the very end of such an odyssey.

First of all, Sabrina. Working with you has been...amazing! You have been a constant source of enthusiasm and motivation for me, especially in those harsh times that very often come along with the Ph.D. package. Thank you for your open-mindedness and for the scientific and professional freedom you gave me. Last, but not least, thank you a lot for all the crazy fun projects that we carried on together! How many Ph.D. students manage to end up on a theatre stage during their post-graduate school years??

Secondly, our group members, both past and present and both in Turku and Edinburgh. Pinja, Laura, Janika, Ruggero, Carole, Suzanne, Stephen and Ollie. When one thinks of physicists, all sorts of nerdy and freaky stereotypes pop by, so thank you guys for being such stereotype breakers! I truly cannot imagine a better bunch of people to make my day so pleasant both at work and sometimes over a pint...

Furthermore, I am really thankful to all my collaborators, Mauro Paternostro, Carlos Sabin, Gerardo Adesso, Francesco Plastina, Gabriele De Chiara, Laura and Pinja. Without all of your contributions this manuscript would be much much shorter and far more boring, believe me!

I would also like to thank the Scottish Doctoral Training Center in Condensed Matter Physics for both the financial and personal support. This amazing postgraduate programme has allowed me to constantly grow as a young physicist.

Next, some people in Edinburgh that really made my time up there incredible and worth remembering. Dani, Silvia, Giuseppe, Francesca, Nathan, Chaytania and Aurora: thank you guys for the good atmosphere at Heriot-Watt and the good times spent mostly partying.

Un enorme grazie va alla mia famiglia, mami, papi, Sara e Sandra. Senza il vostro amore e il vostro appoggio non sono sicuro sarei arrivato tanto lontano, sia come

"scienziato"...sia in senso geografico! Grazie per aver creduto in me. [1]
Finally, Elsi. Thank you for your unconditional love and constant backup, no matter those annoying ≈ 1562.76 kilometers we very often had in between us and no matter the dozens of hours spent traveling to bridge them. It wasn't easy, but here we still are!

[1] A huge thank goes to my family, mom, dad, Sara and Sandra. Without your love and your backup I am not sure I would have gone this far, both as a "scientist" and...geographically speaking! Thank you for believing in me.

Contents

List of Publications

The contents of this manuscript are based upon the following publications:

- M. Borrelli, L. Mazzola, M. Paternostro and S. Maniscalco, *Simple trapped-ion architecture for high-fidelity Toffoli gates*, Physical Review A **84**, 012314 (2011)

- M. Borrelli, P. Haikka, G. De Chiara and S. Maniscalco, *Non-Markovian qubit dynamics induced by Coulomb crystals*, Physical Review A **88**, 010101(R) (2013)

- M. Borrelli, and S. Maniscalco *Effect of temperature on Non-Markovian dynamics in Coulomb crystals*, International Journal of Quantum Information **12**, 1461006 (2014)

- M. Borrelli, C. Sabín, G. Adesso, F. Plastina, and S. Maniscalco, *Dynamics of atom-atom correlations in the Fermi problem*, New Journal of Physics **14**, 103010 (2012)

Other papers published as a postgraduate student but not included in the thesis:

- M. Borrelli, N. Piovella, and M. G. A. Paris, *Stationary entanglement in N-atom subradiant degenerate cascade systems*, Physical Review A **83**, 013621 (2011)

- M. Borrelli, M. Rossi, C. Macchiavello, and S. Maniscalco, *Detecting entanglement via generalized structure factor*, submitted for publication in Physical Review A

Chapter 1

Introduction

This thesis collects the work that I carried out from 2011 to 2014 as a doctoral student at Heriot-Watt University. My research has been focused on the open dynamics of few-body systems, encompassing the study of quantum correlations as well as applications to quantum technologies and quantum simulators. Three main topics of the are discussed in three different chapters, where each of them refers to a particular publication and the contents of all the papers have been extended and reformatted in a fashion that is more suitable for a thesis. This includes, whenever necessary, a pedagogical introduction to the crucial concepts as well as a brief literature overview emphasizing the connection with previous works.

In the Chapter 2 we will introduce a novel quantum information scheme for implementing a three-qubit C-NOT gate, commonly known as Toffoli gate, in trapped ions. Over the last twenty years ion traps have been gathering increasing attention as a practical tool for realizing a quantum computer. Although the idea of a computing device operating on quantum mechanical laws had been around for a few decades already [1], it was only in 1995, when Ignacio Cirac and Peter Zoller demonstrated the feasibility of cold trapped ions for computational purposes [2], that this field of research was given a concrete motivational boost. In this seminal paper the authors showed how to implement a two-ion quantum gate using a sequence of properly tuned laser pulses. These pulses couple two specific electronic levels of each ion (which form the quantum bit or qubit) to its centre of mass kinetic degree of freedom. Shortly afterwards, two experimental groups succeeded to confirm the theoretical predictions by Cirac and Zoller in the laboratory [3,4]. From that point on, a myriad of theoretical proposals and experimental achievements have been reported. Many among these achievements proved trapped-ions to be an ideal platform for quantum computation. Relevant examples are the the possibility of efficient state initialization [5] and state read-out [6–8], extremely long coherence times [9] and the existence of decoherence-free subspaces [10], creation of multiple-ion entangled

states that are crucial for quantum computing [11–13]. Moreover, several quantum protocols have been demonstrated in trapped-ion systems, such as the Deutsch-Josza algorithm [14, 15], the realization of a universal set of quantum gates [16], quantum teleportation [17, 18], quantum error connection [19], and a three-ion C-NOT gate [20]. More recently, ion traps have been utilized to simulate relativistic physics [21], spin chains [22], and open quantum dynamics [23]. The strength of trapped ions lies in the almost perfect controllability that they offer, further supported by the flexibility of the laser-assisted manipulation, their robustness against environmental noise and an unprecedented 99.9% read-out efficiency achievable with fluorescence resonance techniques [24]. At present, the only major drawback affecting the realization of a trapped-ion-based quantum computer is the difficulty related to scaling up the number of ions while being still able to manipulate them efficiently. Most of the work done so far in trapped-ion-based quantum information, relies on single-ion laser-addressing and circuital decomposition of any protocol into single and two-ion operations [25]. This approach has been proven successful as long as the number of basic steps is not too big or, equivalently, the time required to implement a particular gate or protocol does not exceed the typical coherence times. Starting from this observation we show in Chapter 2 how a multi-qubit approach might be the path to take instead [26]. The case study is a three-qubit C-NOT gate, better known as the Toffoli gate [27]. As mentioned above, this was experimentally demonstrated in Innsbruck by using a standard circuital approach [20]. The total number of steps required, excluding state preparation and final read-out, amounted to 15 and the average probability of success obtained, known as gate fidelity, was about 71%. In the implementation we develop, which is a hybrid approach based on single-qubit operations, simultaneous multiple-ion laser addressing and the use of an enlarged computational space, we show that with the same experimental setup a drastic drop in the number of basic steps required can be achieved along with higher average fidelities [26].

Chapter 3 is devoted to characterizing critical behavior in trapped ions by using tools of open quantum system theory. Ion traps are an interesting platform not only for quantum computing but also for investigating fundamental physics [28]. In this respect, Coulomb crystals are among the most exciting physical systems that can be created in such devices [29]. These are self-organized structures where different geometries can be explored by tuning the trap parameters appropriately [30–32]. Interestingly, any change in the crystal geometry is accompanied by a structural phase transition [33, 34]. Loosely speaking, one can think of these phase transitions as resulting from an imbalance between the Coulomb repulsion, that tends to push the ions far apart, and the trapping potential aiming to confine them. Every time

the confinement reaches a certain critical value the crystal will abruptly enter a new phase with the atoms localized around some new equilibrium positions [35]. These equilibrium positions are the result of a restored balance between the two opposite forces. Structural phase transitions in Coulomb crystals have been subject of intense investigations, with particular attention to the linear to zig-zag phase transition [36, 37]. Here, the ions switch from a non-homogenous one-dimensional linear configuration to a planar zig-zag one. The main methods utilized to characterize this phase transition include numerical brute-force simulations [38], classical Landau theory [39], mapping to quantum critical systems [40, 41] and density matrix renormalization group [42].
In Chapter 3 we shall study the properties of a Coulomb crystal undergoing the linear-to-zig-zag phase transition from an open quantum system perspective [43].The theory of open quantum systems [44,45] has recently gained a lot of attention thanks to some pioneering works devoted to assessing non-Markovianity in a more rigorous and general fashion [46–49, 51, 129]. The underlying idea here is to cleverly design a protocol that simulates open system dynamics and to investigate how such a dynamics is affected by the critical behavior of the crystal. Alternatively, this engineered open system dynamics can be used to monitor and witness critical changes in the crystal structure. This latter interpretation goes along the idea of probing the properties of a many-body system by coupling it with a fully controllable single quantum system. This quantum-probe approach to investigating condensed matter physics has been explored lately in several different physical scenarios [52–56].

In Chapter 4 we shall investigate the connection between quantum and classical correlations and the relativistic concept of microcausality in an open system scenario. The motivation for this study originates from a well-known and long-standing open problem in quantum physics, the two-atom Fermi problem [57]. This is a gedanken experiment where two atoms, say A and B, that are far apart from each other are prepared in an excited and ground state, respectively. They both interact independently with a surrounding electromagnetic field in which no photons are initially present. Because of the interaction with the field the atom A will decay and emit a photon that can be absorbed by B. Is the dynamics of the atom B completely independent on the dynamics of A as long as the two atoms are causally disconnected? In quantum mechanical language: if we label r the atom-atom distance, can the excitation probability of B increase before $t = r/c$ where c is the speed light? Fermi tackled this problem first and found no violation of the causality principle. The excitation probability of B cannot increase before $t = r/c$ [57]. However, his original solution was flawed as based on some wrong approximations [58]. Since then, several authors have confronted this question regarding the very foundations of quantum

theory [59–62]. As a general remark, causality has been proven in several papers using different methods, models and approximations. However, no experimental verification has ever been carried out and the plethora of available findings is still purely theoretical. In this respect, particularly relevant is the analytical proof reported in [63] where causality is demonstrated exactly. Here the authors show that the excitation probability of B can be calculated starting from a projector operator that is the sum of three contributions arising from the field, the first atom A and the atom B itself. Although the field contribution starts increasing immediately at $t = 0$, the A contribution cannot increase until $t = r/c$. Hence, in order for the first atom to have any effect on the dynamics of the second, the two must become causally connected. In other words, the atom B has to wait for the A-emitted photon to arrive in order to see the atom A.
Motivated by such results we wonder about the behavior of atom-atom correlations. We do know that the excitation probability of B is completely independent of the atom A for $t > r/c$. Yet, the instantaneous field contribution can effectively correlate the two atoms starting from $t = 0$. In Chapter 4 we report a systematic analysis of the dynamics of quantum and classical atom-atom correlations in the two-atom Fermi problem [64]. More in detail, we study the time-evolution of entanglement [65], geometric quantum discord [66] and spin-spin correlation function [67]. Entanglement is probably one of the most striking and puzzling consequences of quantum mechanics. It arises in composite systems in the form of correlations that are classically unpredictable and impossible to generate. Quantum discord, a more recent concept, is as well a property of many-particle states. In the two-particle case it can be pictured as the minimum disturbance we induce on one of the two particles whenever we perform a measurement on the other [68, 69]. Generally speaking, we can anticipate that all of these correlations will be found to start increasing before the two atoms become causally connected [64]. However, different mechanisms are responsible for this effect depending on the correlation at hand. We underline that these findings do not violate the principle of causality: correlations do not represent any physical information unless they are concretely shared [63]. The action of sharing requires communication through transmission and this, as discussed above, is constrained by microcausality .

Chapter 5 will be devoted to drawing some conclusions.

Chapter 2

Trapped Ions

The first part of this Chapter is devoted to reviewing the basic principles of ion-trapping theory and introducing the essential ingredients for trapped-ion-based quantum computation [25]. This is meant to provide the reader with key concepts that are crucial to understand the content of paper [26], which is the topic of the second part of this Chapter.

2.1 Basics of ion trapping

2.1.1 Confining an ion: the linear Paul trap

Ions are charged particles and, as such, they can be confined in space by a suitable arrangement of electromagnetic fields. A three dimensional quadrupole field potential ϕ can be used for this purpose [28]

$$\phi(x,y,z;t) = \frac{U}{2}\left(\alpha_x x^2 + \alpha_y y^2 + \alpha_z z^2\right) + \frac{U'\cos\Omega t}{2}\left(\alpha'_x x^2 + \alpha'_y y^2 + \alpha'_z z^2\right), \quad (2.1)$$

where U, U' are the strengths of the potentials, the α, α's parameters are the oscillatory frequency and Ω is the modulation frequency. Thus, that such a potential is the sum of a static and a time-dependent part. Because of the Laplace theorem the only confinement we can achieve is dynamical and never globally static. Nevertheless, a fit choice of the drive frequencies as well as voltages can lead to an approximately harmonic confinement in three dimensions. A common choice of the αs and the α's is [70]

$$\begin{aligned} &\alpha_x + \alpha_y = -\alpha_z < 0, \\ &\alpha'_x = -\alpha'_y, \alpha'_z = 0, \end{aligned} \quad (2.2)$$

Given the potential (2.1) with the constraints (2.1) we are now able to write the equations of motion for an ion of mass m and charge e. Considering, for instance,

the x axes we obtain, straight from Newton's second law, the following equation

$$\frac{d^2x}{dt^2} = -\frac{e}{m}\left(U\alpha_x + U'\alpha'_x \cos\Omega t\right) x. \tag{2.3}$$

This can be recast in a more compact form where the relevant parameters are further highlighted. If we define $a_x = 4eU\alpha_x/m\Omega^2$, $q_x = 2eU'\alpha'_x/m\Omega^2$ and $\Omega t = 2\zeta$, the rescaled equation reads as

$$\frac{d^2x}{d\zeta^2} + \left(a_x - 2q_x \cos 2\zeta\right) x = 0. \tag{2.4}$$

This is a canonical Mathieu equation whose solutions are known [71, 72]. It is important to remark that the values of the a_x, q_x parameters are crucial in order to guarantee the stability of a particular solution and, in turn, the possibility of confining the ion's motion in the x direction. In other words, in the (a_x, q_x) plane both stability and instability regions exist [28]. By repeating the same steps for the y and z directions and bearing in mind the constraints dictated by (2.1), one obtains equations that are formally equivalent to (2.4) where $q_y = -q_x$ and $q_z = 0$. Obviously, each of them will present stable or unstable solutions depending on the values of the relevant Mathieu's parameters a_i, q_i. Hence, the ability of finding regions of global stability will result in the ability of confining the ion in three dimensions. The existence of bound trajectories is then what prevents the ion from escaping the electrode structure. This is what we mean by a *trapped ion*. It is instructive to spend a few words about the stable solutions of Eq.(2.4), whose analytical form follows from Floquet's theorem [71, 72]. These will read as

$$x(\zeta) = Ae^{i\beta_x\zeta}\sum_{n\in\mathbb{Z}} C_{2n}e^{2in\zeta} + Be^{-i\beta_x\zeta}\sum_{n\in\mathbb{Z}} C_{2n}e^{-2in\zeta}, \tag{2.5}$$

where both the β_x and the C_{2n} depend uniquely upon the values of a_x and q_x, whereas A and B are fixed by initial conditions. Recursion relations for the Fourier coefficients and β_x exist that link these quantities to the fundamental parameters a_x, q_x. As shown in [28], the boundaries of the stability zones for each of the three pairs (a_i, q_i) are set by the conditions $\beta_i = 0, 1$. At the lowest order of expansion for Eq.(2.5), which corresponds to looking for stable solutions fulfilling the condition $(|a_x|, q_x^2) \ll 1$ (small voltages), we can greatly simplify the analytical form of the ion's trajectory and identify the main frequencies associated to its motion

$$x(t) \propto 2\cos\left(\beta_x\frac{\Omega t}{2}\right)\left(1 - \frac{q_x}{2}\cos\Omega t\right), \tag{2.6}$$

where $\beta_x \approx \sqrt{a_x + q_x^2/2}$. The motion described by Eq.(2.6) is a superposition of two motions at very different frequencies: a slow secular motion at frequency $\omega = \beta_x \Omega/2 \ll \Omega$, and a much faster micromotion at frequency Ω. If the amplitude of the micromotion, which is proportional to q_x, can be neglected, then we can approximate the ion's motion as fully harmonic.
Several practical realizations of Eq.(2.1) are nowadays routinely achievable [24, 28]. Obviously, different arrangements of electrode structures lead to different confining potentials. In the following discussions, we will be concerned with the so-called linear Paul trap [73], which is schematically depicted in Fig. 2.1. The blue rods are subjected to an alternate potential oscillating at frequency Ω, whereas the others are held at the ground level. This guarantees localization in the $y-z$ plane (transverse), thanks to the quadrupole structure of the generated electric field. Along the $x-$axis (longitudinal) a positive potential is applied to the white segments, resulting in a potential well that confines the ions longitudinally also. Whenever the transverse potential is larger than the axial one this configuration allows for several ions to line up and be individually manipulated. Typical experimental values for the relevant trapping parameters are $U^{'} = 100 - 500$ V, $U = \pm 50$ V and $\Omega/2\pi = 100$ kHz $-$ 100 MHz [70]. Moreover, in typical quantum information experiments, the harmonic frequency$4\beta_x\Omega/2$ can be tuned to span from few kHz to few MHz.
The classical theory summarized above is the start point for a quantum treatment of the motional degrees of freedom of the trapped ion. The harmonic approximation is the most commonly accepted in almost all of the theoretical literature regarding the field of quantum information processing with cold trapped ions. In what follows we will stick to this approximation and use it throughly.

2.1.2 Quantization of the ion's motion

In the previous section we have reviewed the classical model of ion trapping and derived the equations of motion. We presented a solution to these equations and showed that, at the lowest order of expansion compatible with stability, the ion's trajectories are essentially harmonic. Obviously, a full quantum treatment requires solving a Schroedinger's equation where the ion's position and momentum are promoted to operators. This further step requires some clarification. By turning the potential (2.1) into an operator we obtain the following Hamiltonian governing the evolution of the ion's wave function

$$\hat{H}(t) = \frac{\hat{P}^2}{2m} + \frac{m}{8}\left[W_x(t)\hat{X}^2 + W_y(t)\hat{Y}^2 + W_z(t)\hat{Z}^2\right], \tag{2.7}$$

where $W_j(t) = \Omega^2 (a_j + 2q_j \cos\Omega t)$. The above Hamiltonian describes a three dimensional quantum harmonic oscillator with time-dependent oscillation frequencies

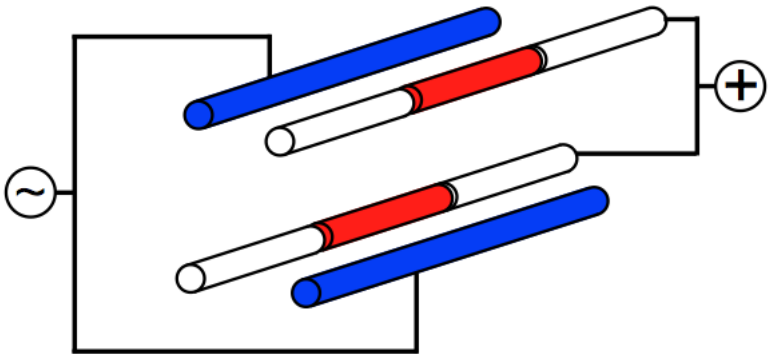

Figure 2.1: Scheme of a Paul trap.

$W_j(t)$. At this stage, one might wonder to what extent the classical approximation presented at the end of the previous section applies in the quantum case. The problem can be reformulated as follows: given the classical results, can we develop an exact quantum model where the harmonic approximation still holds? The answer is positive. It is of primary importance to underline that the the regions of classical and quantum stability coincide. This result was first obtained in [74], using an effective potential approach [28], and subsequently confirmed by Glauber in [75] exactly. The details of this calculations are exhaustively reported in Ref. [70], on which most of the discussion presented here is also based. We summarize the main points focusing on a one dimensional system only, since the Hamiltonian is the sum of three commuting harmonic Hamiltonians. Starting from Eq.(2.7) and writing the Heisenberg equations of motions for $\hat{X}$ and $\hat{P}$ we obtain

$$\frac{d^2\hat{X}}{dt^2} + W_x(t)\hat{X} = 0, \tag{2.8}$$

which is formally identical to Eq.(2.4). We choose $A = 1, B = 0$ in Eq.(2.5) and solve the classical equation (2.4)

$$x(t) = e^{\frac{i\beta_x\Omega t}{2}} \sum_{n\in\mathbb{Z}} C_{2n} e^{in\Omega t}. \tag{2.9}$$

At this point the following operator $\hat{C}(t)$ is introduced

$$\hat{C}(t) \equiv \sqrt{\frac{m}{2\hbar\nu}} \left[x(t)\dot{\hat{X}}(t) - \dot{x}(t)\hat{X}(t) \right], \tag{2.10}$$

where $\nu = \Omega \sum_{n\in\mathbb{Z}} C_{2n}(\beta_x/2+n)$, that satisfies the following equalities

$$\hat{C}(t) = \hat{C}(0) = \frac{1}{\sqrt{2m\hbar\nu}}\left[m\nu\hat{X}(0) + i\hat{P}(0)\right] \equiv \hat{a}, \tag{2.11}$$

where we have introduced the static bosonic ladder operator $\hat{a}$. Needless to say, its adjoint operator $\hat{a}^\dagger$ can be defined so to satisfy the standard bosonic commutation relation

$$\left[\hat{a}, \hat{a}^\dagger\right] = \hat{\mathbb{I}}. \tag{2.12}$$

It must be noted that the frequency ν is associated to the static bosonic mode described by $\hat{a}$. Hence, the time dependence of the ion's position and momentum operators $\hat{X}, \hat{P}$ in Heisenberg picture can be entirely encoded in the classical trajectory functions $x(t), x^*(t)$. The operatorial part is decomposed in terms of annihilation and creation operators

$$\begin{aligned}\hat{X}(t) &= \sqrt{\frac{\hbar}{2m\nu}}\left[x^*(t)\hat{a} + x(t)\hat{a}^\dagger\right], \\ \hat{P}(t) &= \sqrt{\frac{\hbar m}{2\nu}}\left[\dot{x}^*(t)\hat{a} + \dot{x}(t)\hat{a}^\dagger\right].\end{aligned} \tag{2.13}$$

It is instructive to compare this time-dependent quantum harmonic oscillator with its static counterpart. For a one dimensional quantum harmonic oscillator of mass m at frequency ω_0 the Hamiltonian reads as follows

$$\hat{H} = \frac{\hat{P}^2}{2m} + \frac{m\omega_0^2}{2}\hat{X}^2. \tag{2.14}$$

In terms of annihilation and creation operators $\hat{a}_0, \hat{a}_0^\dagger$ the time evolution of $\hat{X}$ and $\hat{P}$ in Heisenberg picture is

$$\begin{aligned}\hat{X}(t) &= \sqrt{\frac{\hbar}{2m\omega_0}}\left[e^{-i\omega_0 t}\hat{a} + e^{i\omega_0 t}\hat{a}^\dagger\right], \\ \hat{P}(t) &= i\sqrt{\frac{\hbar m}{2\omega_0}}\left[e^{i\omega_0 t}\hat{a}^\dagger - e^{-i\omega_0 t}\hat{a}\right].\end{aligned} \tag{2.15}$$

If we compare Eq.(2.13) with Eq.(2.15) it is clear that the former is a generalization of the latter. The the ion's classical trajectories $x(t)$ in the case of the quadrupole potential, modeled as a harmonic oscillator with time-varying frequency, replaces the oscillating exponential $e^{i\omega_0 t}$, which is the classical trajectory for a time-independent harmonic oscillator. At the end of the previous section we showed the influence of the micromotion on the ion's trajectory in the limit of small voltages: this resulted in rapid oscillations at frequency Ω superposed to a slower secular motion at frequency $\beta_x\Omega/2$. The same argument can be applied in the quantum case. However, unlike

classical physics, here we are interested in the time-evolution of the ion's wavefunction. As shown in Ref. [70] the time-evolution of the ground state wavefunction $|0\rangle$ as dictated by Hamiltonian (2.7) and again in the limit $(|a_x|, q_x^2) \ll 1$, reads as

$$\begin{aligned}\psi_0(x,t) = \left(\frac{m\nu}{\pi\hbar}\right)^{1/4} \sqrt{\frac{1+q_x/2}{1+(q_x/2)\cos\Omega t}} \\ \times \exp\left\{\left[i\frac{m\Omega\sin\Omega t}{2\hbar\,(2/q_x+\cos\Omega t)} - \frac{m\nu}{2\hbar}\right]x^2\right\},\end{aligned} \tag{2.16}$$

which, for $t = 0$ or $\Omega = 0$ reduces to the ground state of the static harmonic mode $\hat{a}$. As time goes by, the micromotion will cause the wavefinction $\psi_0(x,t)$ to breathe at frequency Ω. This breathing is the quantum analogue of the classical micro-oscillation exhibited by $x(t)$. Starting from this ground state one can construct the whole set of excited states by repeated actions of the $\hat{C}$ operator, in a fashion similar to the static case. It is important to underline that these states are quasi-stationary: they are the closest approximation of the eigenstates of the static harmonic Hamiltonian. In what follows we will ignore the breathing as it takes place on a much shorter time-scale than the one we are interested in. In all oncoming discussions, the ion will be considered as a static quantum harmonic oscillator at frequency ν whose possible quantum states $|\phi_M\rangle$ read as

$$|\phi_M\rangle = \sum_{n=0}^{+\infty} \phi_M^n |n\rangle, \tag{2.17}$$

where $\{|n\rangle\}_{n\in\mathbb{N}}$ are standard Fock states, such that, $\hat{a}|n\rangle = \sqrt{n}|n-1\rangle, \hat{a}^\dagger|n\rangle = \sqrt{n+1}|n+1\rangle$.

2.1.3 Multiple trapped ions

So far, we have sketched some basic trapping theory for a single ion. Needless to say, in order to both implement information protocols [25] and simulate complex systems [76], several ions are necessary. Nowadays, thanks to significant technical advancements, strings of ions can be easily and routinely trapped and manipulated. Most of the conclusions presented above are still applicable in the many-ion case. However, there is one fundamental difference with respect to the single-ion case, that is, the ions interact via Coulomb repulsion.

Let us assume that the static approximation is valid for the harmonic potential (2.7) generated inside a Paul trap and that the ions are so strongly bounded along the y, z direction that we can neglect this transverse motion. The motion along the trap axis x is instead harmonic. This condition can be easily achieved by setting $\nu_{y,z} \gg \nu_x$

where $\nu_j, j = x, y, z$ is the effective frequency along the j direction. Thus, with these assumptions, the Hamiltonian for a string of N ions of mass m and charge q is the sum of kinetic energy, harmonic potential and Coulomb repulsion

$$\hat{H} = \sum_{j=1}^{N} \frac{\hat{P}_j^2}{2m} + \frac{m\nu^2}{2}\hat{X}_j^2 + \sum_{i,j=1;i\neq j}^{N} \frac{q^2}{8\pi\varepsilon_0}\frac{1}{|\hat{X}_j - \hat{X}_i|}, \tag{2.18}$$

where ε_0 is the vacuum permittivity.

If we assume the whole chain to be at very low temperature we can expect to observe a stable configuration where each ion oscillates around its equilibrium position. Particularly relevant for tasks of quantum information and computation is the linear configuration. Here, all the ions are distributed along the trap axis in a linear one-dimensional array. Their equilibrium positions can be computed analytically (for $N = 2, 3$) or numerically (for $N > 3$) [35]. We must underline that, as a general feature, such positions are not equally spaced, except if we take a central segment when $N \gg 1$. This point will be further discussed in the next Chapter. As long as the amplitude of the oscillations is small compared to the equilibrium ion-ion separation we can expand each ion's position operator around its equilibrium position $X_j^{(0)}$

$$\hat{X}_j \approx X_j^{(0)} + \delta\hat{X}_j, \tag{2.19}$$

where $\delta\hat{X}_j$ is a small displacement operator. By carrying out the full expansion of Eq.(2.18) it is possible to derive an effective Hamiltonian describing a network of interacting harmonic oscillators. In Chapter 3, more details regarding the analysis of the chain stability will be presented. A chain of interacting harmonic oscillators can be mapped onto a system of non-interacting bosons by using the so-called normal-mode decomposition [77]. Loosely speaking, we can say that these normal modes represent all the possible ways the chain can oscillate and they are usually referred to as phonons. Analogously to the single-ion case, any operator $\delta\hat{X}_j$ can be expanded in terms of the annihilation and creation operators $\hat{a}_k, \hat{a}_k^\dagger$ of such normal modes

$$\delta\hat{X}_j = i\sqrt{\frac{\hbar}{2\nu m N}} \sum_k s_k^{(j)} \left(\hat{a}_k - \hat{a}_k^\dagger\right), \tag{2.20}$$

where the $s_k^{(j)}$ coefficients realize the normal mode transformation. It is important to remark that normal modes are delocalized in physical space but highly localized in momentum space. Exciting one normal mode, corresponds to a collective oscillation of the whole chain with a well defined wave-vector. The range of the allowed momenta k depends on the geometric pattern arising from the equilibrium positions. Concluding, we have reviewed some basics of ion-trapping theory. Starting from a

classical treatment we have derived the equation of motions for a single trapped ion and discussed the conditions under which its motion can be considered approximately harmonic. We later on quantized such theory and found that the quantum equations of motion are formally identical to the classical. The quantum version of the micromotion is a breathing effect of the ion's quantum wave-function at the same frequency of its classical countepart. We also briefly sketched how to generalize the treatment in the case of multiple ions. The next section will focus on introducing the key ingredients for implementing quantum information in trapped ions.

2.2 Trapped-ion systems for quantum information processing and quantum computation

2.2.1 Quantum information science in a nutshell

The first idea of a quantum computer dates back to 1980's [1] and still nowadays quantum information science is among the most fervent fields of research in the quantum community. The key idea is rather simple: is it possible to enhance the performances of a computing device by forcing it to operate according to the laws of quantum mechanics? After all, it is sensible to expect that if we keep moving towards smaller and smaller chips and electric components we will sooner or later cross the quantum border. Hence, the necessity of understanding both the possible advantages and disadvantages.

The theory of quantum information has been developing fast in the last 20 years and several approaches to the subject exist. Also, numerous experimental candidates have been proven to be better or worse depending on the task at hand. Examples of such candidates are nuclear magnetic resonance systems [78], quantum optical systems [79], superconducting circuit [80] and, obviously, trapped ion systems [25]. Quantum computers are believed to beat their classical counterparts when it comes to solving problems that are classically hard or impossible to tackle. Among these, the most prominent example is surely prime number factorization. Furthermore, the time required by some quantum algorithms is expected to be polynomial in the number of resources needed, in contrast to the exponential time typical of their classical counterparts [81]. This effect goes under the name of quantum speed-up. Quantum information has direct applications also to cryptography, communication and simulations of complex systems. This is a massive field of research, nearly impossible to summarize concisely. For an exhaustive introduction to quantum information theory, see [81]. In what follows we shall give a very basic introduction of quantum information theory.

In classical information theory the basic unit of information is a binary system whose

states are labelled 0 and 1. This is what we call a bit. Needless to say, a bit can be in either 0 or 1. In quantum information theory we replace such a classical object with its quantum counterpart, the qubit. The Hilbert space associated to a qubit is two-dimensional and we label the basis spanning it $|0\rangle, |1\rangle$. We call this basis the computational basis. Unlike in the classical case a qubit can be in an infinite number of basis-state linear combination. Generally speaking, a qubit in a pure state can be written as

$$|\psi\rangle = \cos\frac{\theta}{2}|1\rangle + e^{i\phi}\sin\frac{\theta}{2}|0\rangle, \tag{2.21}$$

where $\theta \in [0, \pi]$ and $\phi \in [0, 2\pi]$ are the polar and azimuthal angle respectively in the Bloch sphere representation [81]. For mixed states we have the following representation instead

$$\hat{\rho} = \frac{1}{2}\left(\hat{\mathbb{I}} + \vec{a}\cdot\vec{\sigma}\right), \tag{2.22}$$

where $\hat{\mathbb{I}}$ is the identity operator, $\vec{a} = (\sin\theta\cos\phi, \sin\theta\sin\phi, \cos\theta)$ is the so-called Bloch vector and $\vec{\sigma} = (\hat{\sigma}_x, \hat{\sigma}_y, \hat{\sigma}_z)$ is the vector of the spin 1/2 Pauli operators. We remark that $a_j = \mathrm{Tr}[\hat{\rho}\hat{\sigma}_j]$. We call a collection of N qubits a quantum register. In standard quantum information theory qubits are manipulated with single-qubit and multi-qubit unitary operations. Local operations act on the single-qubit Hilbert space and, as such, they can be represented by a 2×2 unitary matrix. An example of such a gate is the Hadamard gate

$$H = \frac{1}{\sqrt{2}}\begin{pmatrix} 1 & 1 \\ 1 & -1 \end{pmatrix}, \tag{2.23}$$

On the contrary, multi-qubit operations act on the tensor product space of single-qubit Hilbert space. Among these non-local multi-qubit gates can create non-classical correlations between different qubits, such as entanglement. These entangling gates are particularly relevant for better performances of quantum computers over classical. Any quantum logic protocol can be decomposed in a series of concatenated single and two-qubit operations in what is called the circuital approach to quantum computing. Particularly relevant among the multi-qubit gate is the C-NOT gate, which, in the 2-qubit case reads as

$$\mathrm{CNOT} = \begin{pmatrix} 1 & 0 & 0 & 0 \\ 0 & 1 & 0 & 0 \\ 0 & 0 & 0 & 1 \\ 0 & 0 & 1 & 0 \end{pmatrix}, \tag{2.24}$$

The 3-qubit version, namely the Toffoli gate, is very important in several quantum protocols, such as phase-estimation and error correction. The celebrated quantum

factorization algorithm itself relies on this gate.

As we just mentioned, any gate or protocol can be implemented as a series of subsequent universal and much simpler gates. We can think of these gates as the fundamental bricks for any computation we want to carry out. Obviously, whenever a quantum gate or protocol is implemented in some experimental setup, technical and fundamental limitations, which depend on the particular physical system used for the implementation, will affect the quality of the outcome. Typically such a standard implementation goes as illustrated in Fig.2.2. A certain quantum system is initialized to a well-defined input state $\hat{\rho}_{\mathrm{I}}$ that undergoes a set of quantum operations $\hat{\mathcal{G}}$ leading to an output state $\hat{\rho}_F$. We call $\hat{\mathcal{G}}$ a quantum map or, equivalently, a quantum channel. In a real experimental realization, assuming that no error is present in the initialization procedure to $\hat{\rho}_{\mathrm{I}}$, imperfections originating from the setup at hand will result in an approximate $\hat{\mathcal{G}}^{'}$ as well as an approximate $\hat{\rho}_{F}^{'}$. In order to quantify how good a particular experimental implementation is, a state-dependent characterization is required to estimate how close $\hat{\mathcal{G}}^{'}$ is to the ideal $\hat{\mathcal{G}}$. A powerful tool for this task is quantum process tomography [81], which we will briefly illustrate. For a system of N qubit, any completely positive map $\hat{\mathcal{G}}$ is specified by a set of 4^N orthogonal operators $\{\hat{\mathcal{K}}_m\}$

$$\hat{\mathcal{G}}\hat{\rho}_{\mathrm{I}}=\sum_{m,n}\chi_{mn}\hat{\mathcal{K}}_m\hat{\rho}_{\mathrm{I}}\hat{\mathcal{K}}_n^{\dagger}. \tag{2.25}$$

This is the so-called Kraus decomposition of the map $\hat{\mathcal{G}}$ and χ is the process matrix. Let us assume that we know both the real process matrix χ and the approximate process matrix $\chi^{'}$ associated to $\hat{\mathcal{G}}^{'}$. In order to quantify how well $\hat{\mathcal{G}}^{'}$ approximates $\hat{\mathcal{G}}$ we define the average gate fidelity

$$\mathcal{F}(\hat{\mathcal{G}}^{'})=\mathrm{Tr}(\chi\,\chi^{'}). \tag{2.26}$$

This quantity is connected to the average state fidelity [82, 83]

$$\overline{\mathcal{F}}_s(\hat{\mathcal{G}}^{'})=\frac{2^N\mathcal{F}(\hat{\mathcal{G}}^{'})+1}{2^N+1}. \tag{2.27}$$

which is obtained by first computing the fidelity between the ideal and the actual output state and the by averaging over all the possible initial pure states. Intuitively, this quantity measures the average probability of success in rearching a target state.

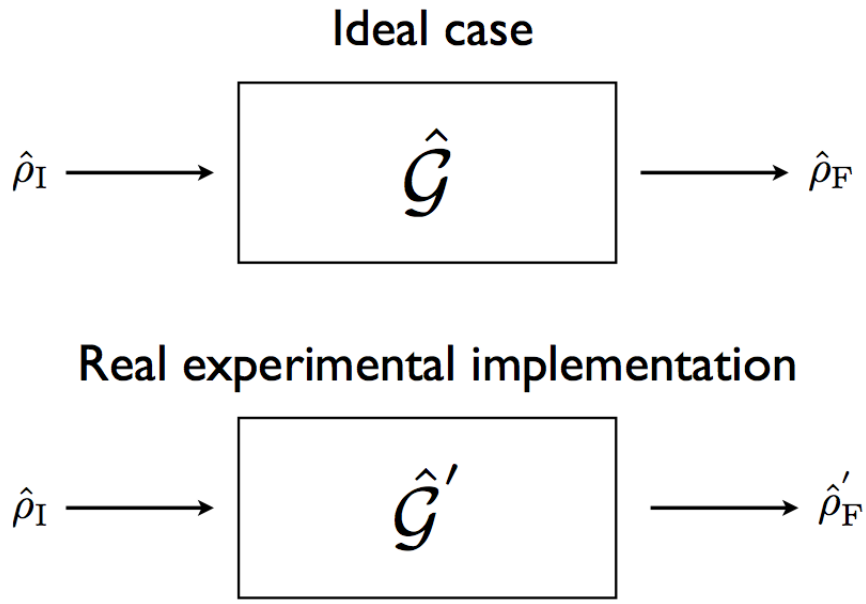

Figure 2.2: Typical scheme for the implementation of a quantum protocol.

2.3 Ion-trapped based quantum computers

In trapped-ion systems two choices for realizing a qubit exist. In the first scenario, the qubit is encoded in two sublevels of the hyperfine structure that are resolved using a static magnetic field and manipulated using two-photon Raman scattering [3] or direct microwave excitation [84]. The other approach relies on using the ion's ground state and an optically excited metastable state as qubit states. This requires the use of resonant laser pulse to perform all of the operations. For an extensive discussion, see Ref. [25]. Regardless of the practical implementation, these approaches can be described in a unique theoretical framework where one basic Hamiltonian can model them both [24].

As a general feature, the first qubit encoding has the advantage of exhibiting longer coherence times, up to few minutes. Nevertheless, also for the case of optical qubits the coherence times, usually amounting to seconds, are still longer than standard protocol-execution timescales, which typically correspond to microseconds [85]. A quantum register is composed by a linear string of ions and, at the present state of art, efficient manipulation up to 14 ions has been experimentally demonstrated [86]. Obviously, for any quantum protocol to be implemented the state of the quantum register has to be properly initialized. In trapped ions this is accomplished via optical pumping where preparation fidelities up to 0.99% are routinely achievable [87]. The preparation fidelity is defined as the overlap between the ideal target input state $\hat{\rho}_{\mathrm{I}}$ and the real initial state prepared in the lab $\hat{\rho}'_{\mathrm{I}}$ and reads as $\mathcal{F} = \mathrm{Tr}(\hat{\rho}_{\mathrm{I}}\hat{\rho}'_{\mathrm{I}})$,

similarly to the case of the average gate fidelity in Eq.(2.26).
The laser-assisted interactions utilized to manipulate the qubits allow for the implementation of the full spectrum of universal quantum gates, at least in principle. While single-qubit operations are realized by driving Rabi oscillations between the two internal states, two-qubit operations require an ancillary degree of freedom. This is encoded in the center of mass (COM) mode of the whole string. By coupling the internal levels of the single ion to the COM mode using properly tuned laser fields, an effective interaction between different qubits can be realized. Since, as mentioned above, coherence times for the ion's electronic structure are usually very long, the only obstacles to the implementation of any quantum protocol lie in heating and dephasing of the COM motional state. This effects will be discussed later in this chapter.
As mentioned at the beginning of this chapter, many theoretical and experimental hits in trapped-ion-based quantum computing have been reported in literature. The Cirac-Zoller gate (CZG) was the very first proposal for quantum information processing in a cold trapped-ion system [2]. In this seminal paper the laser-assisted and COM-mediated approach to the realization of a C-NOT gate for two qubits was for the first time investigated. A primary requirement for the protocol to work was the possibility of single-ion laser-addressing. The target gate was then decomposed in a chain of subsequent single-ion laser pulses. This CZG was experimentally implemented at NIST [3] and in Innsbruck [4]. In particular, in the Innsbruck experiment the complete gate for two $^{40}Ca^{+}$ qubits was efficiently performed leading to a 73% fidelity in the first run, later on raised to 91% after some technical improvements.
Another milestone in trapped-ion quantum computing is the Molmer-Sorensen gate (MSG) [88]. This is a two-qubit gate that relies on the possibility of creating virtual excitations of vibrational states. This feature leads to the important advantage that, unlike CZG, no cooling of the COM state is necessary and it also results in a major robustness of the whole gate to environment-induced heating. Furthermore, this MSG can be shown to be universal. This gate was experimentally implemented to achieve entanglement [11] and in quantum search algorithms [89].
Finally, we would like to mention the geometric phase gate (GPG) [90] which shares some technical similarities with MSG. The basic idea here is to give the ion's state an extra phase factor conditional to its internal state. This is carried out via a non-trivial force whose action depends on the non-linearity of the ion's electronic spectrum. We remark that no single-ion laser-addressing is required for this gate. In the remarkable experiment reported in Ref. [91] a fidelity of 97% in the implementation of the GPG was observed.
The next few sections are devoted to translating the basic concepts of quantum information to the trapped-ion language.

2.3.1 A trapped ion as a qubit

In the preceding sections we focused our attention on the motional degree of freedom of a single trapped ion. This turned out to be mappable onto a quantum harmonic oscillator that can be described in terms of standard bosonic annihilation and creation operators. In this section we are instead interested in the electronic structure of the ion which will be the other relevant degree of freedom for quantum information processing. The ion's spectrum consists of an infinite ladder of energy eigenstates, similar to the case of the hydrogen atom. However, for all the following discussions, we assume that only two of them will be relevant, which we name $|e\rangle$ and $|g\rangle$. This is the well-known two-level approximation, which has been utilized in many different physical contexts. In trapped ions, as discussed in the previous section, such two relevant states can be either selected in the Zeeman ion's sublevel structure or encoded using the ground state and an optically excited state [25]. In the following sections more details about the actual manipulation of electronic states will be presented.

Any two-level quantum system can be mapped onto a spin 1/2 system. Hence, the Pauli operatorial algebra can be used to model the dynamics of the ion's internal degree of freedom. The relevant operators read as follow

$$\begin{aligned} \hat{\sigma}^z &= |e\rangle\langle e| - |g\rangle\langle g|, \\ \hat{\sigma}^+ &= |e\rangle\langle g|, \\ \hat{\sigma}^- &= |g\rangle\langle e|, \end{aligned} \tag{2.28}$$

where $\hat{\sigma}^z$ measures the state-population difference and $\hat{\sigma}^{+(-)}$ creates(annihilates) an excitation in the two-level system. These operators obey the following commutation relations

$$\begin{aligned} \left[\hat{\sigma}^z, \hat{\sigma}^\pm\right] &= \pm 2\hat{\sigma}^+, \\ \left[\hat{\sigma}^+, \hat{\sigma}^-\right] &= \hat{\sigma}^z. \end{aligned} \tag{2.29}$$

The free Hamiltonian $\hat{H}$ of the two-level system is then

$$\hat{H} = \frac{\epsilon_0}{2}\hat{\sigma}^z, \tag{2.30}$$

where $\epsilon_0 = E_e - E_g$ is the transition energy between the two states, when we set the zero reference point half-way. We can now write the total Hamiltonian operator $\hat{H}_0$ governing the free evolution of the trapped ion

$$\hat{H}_0 = \frac{\epsilon_0}{2}\hat{\sigma}^z + \frac{\hat{P}^2}{2m} + \frac{m\nu^2}{2}\hat{X}^2 = \frac{\epsilon_0}{2}\hat{\sigma}_z + \hbar\nu\hat{a}^\dagger\hat{a}, \tag{2.31}$$

where we have rewritten the harmonic hamiltonian (2.14) in terms of the $\hat{a}$-mode number operator $\hat{a}^\dagger\hat{a} \equiv \hat{n}$. Since $\hat{H}_0$ is the direct sum of two local Hamiltonians, its eigenstates $\mathcal{S}$ are given by the tensor product of the local eigenstates

$$\mathcal{S} = \{|g,n\rangle, |e,n\rangle\}_{n\in\mathbb{N}}, \tag{2.32}$$

and the corresponding eigenvalues $\mathcal{E}$ read as

$$\mathcal{E} = \Big\{ -\frac{\epsilon_0}{2} + \hbar\nu n, \frac{\epsilon_0}{2} + \hbar\nu n \Big\}_{n\in\mathbb{N}}. \tag{2.33}$$

A schematic picture of the energy levels is displayed in Fig.2.3. A general pure state of the ion reads as

$$|\psi\rangle = \sum_{n=0}^{+\infty} c_{g,n}|g,n\rangle + c_{e,n}|e,n\rangle. \tag{2.34}$$

Summarizing, a trapped ion can be viewed as a single quantum object where we can combine two quantum subsystems of very different nature. On the one hand, we have the bosonic field associated to the quantized harmonic motion, with an infinite dimensional Hilbert space. On the other hand we have a fictitious two-level system whose Hilbert space is two-dimensional and that, thanks to the spin 1/2 mapping, can be represented as a fermionic system described by the Pauli operatorial algebra. The generalization to N ions follows straightforwardly. In the next section we will show how it is possible to couple these two ionic degrees of freedom by utilizing properly tuned lasers. We underline that this represents the start point for developing the theory of quantum information processing in trapped ions.

2.3.2 Coupling different degrees of freedom: the basic Hamiltonian

In this section we present a detailed analysis of the interaction Hamiltonian that allows to couple the internal levels of the ion to its vibrational degree of freedom. We anticipate that, in order to achieve such a coupling, a laser-assisted interaction is required. Generally speaking, the interaction between an atom *classically* located at a point $\vec{x}$ in space and a classical electromagnetic field $\vec{E}(\vec{x},t)$, in the dipole approximation, reads as

$$\hat{V} = -\hat{\vec{d}}\cdot\vec{E}(\vec{x},t) = -\frac{\hat{\vec{d}}\cdot\vec{E}}{2}\left[e^{i\left(\vec{k}_F\vec{x}-\omega_F t\right)} + e^{-i\left(\vec{k}_F\vec{x}-\omega_F t\right)}\right], \tag{2.35}$$

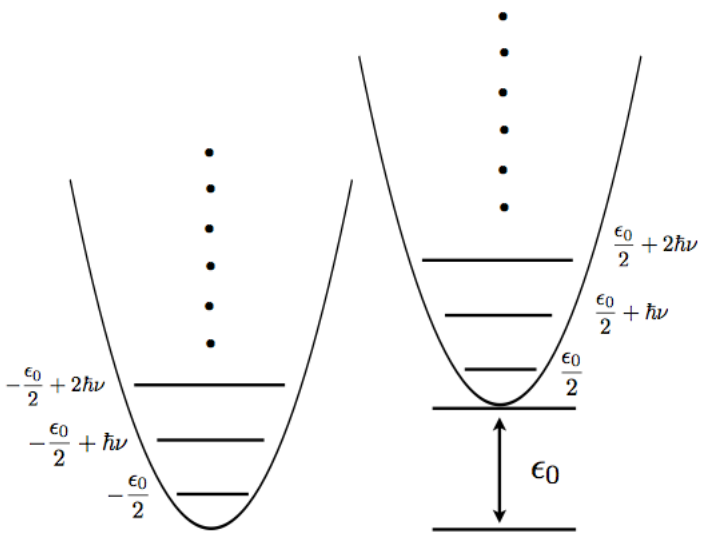

Figure 2.3: Energy levels of a single trapped ion, including internal and motional degrees of freedom.

where $\hat{\vec{d}}$ is the atomic dipole operator which, in the two level approximation reads as

$$\hat{\vec{d}} = \vec{d}_{eg} \left(\hat{\sigma}^+ + \hat{\sigma}^- \right), \tag{2.36}$$

where $\vec{d}_{eg} = \langle e|\hat{\vec{d}}|g\rangle = \langle g|\hat{\vec{d}}|e\rangle$ is taken real for the sake of simplicity. The Hamiltonian (2.35) can be recast in the following form

$$\hat{V} = \frac{\hbar\Omega_R}{2} \left(\hat{\sigma}^+ + \hat{\sigma}^- \right) \left[e^{i\left(\vec{k}_F\vec{x} - \omega_F t\right)} + e^{-i\left(\vec{k}_F\vec{x} - \omega_F t\right)} \right]. \tag{2.37}$$

It is important to underline that the above Hamiltonian is semiclassical: the internal structure of the atom is quantized whereas its position as well as the propagating field are treated as classical entities. Physically, this corresponds to assuming that the atom is effectively localized on a spatial scale much smaller then $\lambda_F = 2\pi/|\vec{k}_f|$. In other words, the propagating field sees the atom as a point-like-particle. The situation is, however, completely different for a trapped ion. Although the form of the interaction (2.37) remains the same, the ion's position needs to be treated as a quantum operator. Let us assume that the trapped ion is confined so strongly along the y and z directions that these two variables can be essentially treated as classical, whereas along the x direction the confinement leads to harmonic motion. This configuration can be easily achieved by a proper adjustment of the α_j and α'_j parameters in Eq.(2.1). Thus, we can use a one-dimensional model for the interaction (2.37) where the electromagnetic field, typically a laser, propagates along the x

direction. By using, in the usual limit of low voltages, the normal mode expansion (2.13) for the $\hat{X}$ operator, the $\hat{V}_I(t)$ operator in interaction picture reads as follows

$$\hat{V}_I(t) = \frac{\hbar\Omega_R}{2}\left(\hat{\sigma}^+ e^{i\frac{\epsilon_0 t}{\hbar}} + \text{h.c.}\right)\left\{\exp\left[i\eta\left(\hat{a}e^{-i\nu t} + \hat{a}^\dagger e^{i\nu t}\right) - i\omega_F t\right] + \text{h.c.}\right\}, \quad (2.38)$$

where the Lamb-Dicke parameter $\eta \equiv k_L\sqrt{\hbar/2m\nu}$ quantifies the ratio between the spatial dimension of the laser mode, as quantified by k_L, and the spatial delocalization of the motional ground state of the ion. Intuitively, this parameter measures the extent to which the electromagnetic field sees the ion as a delocalized quantum object rather than a point-like-particle. It is worth noticing that $\hat{V}_I(t)$ can be recast in the following more compact form

$$\hat{V}_I(t) = \frac{\hbar\Omega_R}{2}\left(\hat{\sigma}^+ e^{i\omega_0 t} + \text{h.c.}\right)\left[\hat{D}(i\eta e^{i\nu t})e^{-i\omega_F t} + \text{h.c.}\right], \quad (2.39)$$

where $\omega_0 = \epsilon_0/\hbar$ and $\hat{D}(i\eta e^{i\nu t})$ is a displacement operator with time-dependent displacement parameter. For the sake of completeness, we quickly recall the general definition of displacement operator $\hat{D}(\alpha), \alpha \in \mathbb{C}$ for a bosonic mode $\hat{a}$

$$\hat{D}(\alpha) = \exp\left(\alpha\hat{a}^\dagger - \alpha^*\hat{a}\right). \quad (2.40)$$

Interaction (2.39) displaces the state of the harmonic oscillator conditionally to the internal state of the ion and as such, it generates non-trivial correlations between the vibrational and the electronic degrees of freedom of the ion. The complexity of (2.39) can be easily understood in terms of the action of the displacement operator on the motional ground state $|n=0\rangle$

$$\hat{D}(\alpha)|n=0\rangle = |\alpha\rangle = e^{-|\alpha|^2/2}\sum_{n=0}^{+\infty}\frac{\alpha^n}{\sqrt{n!}}|n\rangle, \quad (2.41)$$

where $|\alpha\rangle$ is a so-called coherent state, first introduced by Glauber in [92]. Coherent states are the closest approximation to a classical state of a harmonic oscillator. We will return on them in Chapter 3. The important point here is that the action of a displacement operator generates an infinite number of excitations, even when it acts on the ground state of the harmonic oscillator. Therefore, unless some approximations are performed, calculating the dynamics governed by (2.39) may be an extremely hard task. The first approximation we perform is the rotating-wave approximation: if we expand the product in (2.38) we obtain four operators that oscillate at frequencies

$$\begin{aligned}\Delta &= \omega_0 - \omega_L,\\ \Sigma &= \omega_0 + \omega_L.\end{aligned} \quad (2.42)$$

The frequency Σ is obviously much larger than Δ, especially if the the ion and the laser are close to resonance. Since these fast oscillating terms average to zero on the time-scale set by Δ they will be further neglected. The next important approximation is the so-called Lamb-Dicke limit, that is

$$\eta \ll 1. \tag{2.43}$$

Recalling the physical meaning of the Lamb-Dicke parameter, the above equation tells us that the zero-point spread of the motional wavefunction is much smaller than the laser field wavelength. This limit is achievable, for instance, by increasing the confining frequency ν. Hence, the exponential operator in (2.38) can be expanded in powers of η and up to the first order the interaction operator is the sum of three terms

$$\begin{aligned}\hat{V}_I(t) \approx & \frac{\hbar\Omega_R}{2}\left(\hat{\sigma}^+ e^{i\Delta t} + \hat{\sigma}^- e^{-i\Delta t}\right) + \\ & \frac{i\eta\hbar\Omega_R}{2}\left[\hat{\sigma}^+\hat{a}e^{i(\Delta-\nu)t} - \hat{\sigma}^-\hat{a}^\dagger e^{-i(\Delta-\nu)t}\right] + \\ & \frac{i\eta\hbar\Omega_R}{2}\left[\hat{\sigma}^+\hat{a}^\dagger e^{i(\Delta+\nu)t} - \hat{\sigma}^-\hat{a}e^{-i(\Delta+\nu)t}\right].\end{aligned} \tag{2.44}$$

By adjusting the laser frequency it is possible to make any of these three contributions resonant, discarding the other two as they are time-independent. If we set $\Delta = 0$ the resonant term is

$$\hat{V}_C = \frac{\hbar\Omega_R}{2}\left(\hat{\sigma}^+ + \hat{\sigma}^-\right) = \frac{\hbar\Omega_R}{2}\hat{\sigma}_x, \tag{2.45}$$

which flips the population. By taking $\Delta = \nu$ the resonant term is instead

$$\hat{V}_R = \frac{i\eta\hbar\Omega_R}{2}\left(\hat{\sigma}^+\hat{a} - \hat{\sigma}^-\hat{a}^\dagger\right). \tag{2.46}$$

This interaction couples the harmonic oscillator to the internal levels and preserves the total number of excitations in the composite system. It is called first red sideband excitation and generates the same dynamics of the famous QED Jaynes-Cummings model. For instance, Rabi oscillations at a frequencies $\Omega_{n,n-1} = \sqrt{n}\eta\Omega_R$ can be observed. Finally, by setting $\Delta = -\nu$ we obtain

$$\hat{V}_B = \frac{i\eta\hbar\Omega_R}{2}\left(\hat{\sigma}^+\hat{a}^\dagger - \hat{\sigma}^-\hat{a}\right), \tag{2.47}$$

which is called the first blue sideband interaction. This Hamiltonian simultaneously creates or destroys excitation both in the internal structure and the motional degree of freedom of the ion. It should mentioned that we derived all the previous

results starting from the standard dipolar interaction Hamiltonian (2.35). However, the same type of interactions (2.45)-(2.47) can be engineered by using other coupling scheme such as quadrupole transitions or stimulated Raman transitions [24]. Furthermore, all these interactions provide an optimal platform not only for state engineering tasks, such as laser cooling or state read-out, but also for actual quantum computing. If we assume N laser-fields, each of them single-addressing a specific ion in the chain, the generalization of Hamiltonian (2.38) reads as

$$\hat{V}_I(t) = \frac{\hbar\Omega_R}{2}\hat{\sigma}_j^+ \exp\left[i\sum_{j=1}^{N}\eta_k^j\left(\hat{a}_k e^{-i\nu_k t} + \hat{a}_k^\dagger e^{i\nu_k t}\right) - (i\Delta t - \phi_j)\right] + \text{h.c.}, \tag{2.48}$$

where the generalized Lamb-Dicke parameters are $\eta_k^j \equiv k_L s_k^{(j)}$, ν_k is the frequency of the normal mode k and ϕ_j is the relative phase of the laser j.
As stressed above, any quantum algorithm can be decomposed using a circuit representation when a set of universal gates is well-identified and such gates are utilized as fundamental building blocks [81]. Single-qubit operations in trapped ions are implemented by employing the carrier Hamiltonian (2.45) where only the internal state of a single ion-qubit is changed. In the Bloch vector picture the most general form of a single-qubit unitary operation can be depicted as a rotation of the Bloch sphere. Equivalently, this can be also thought of as a rotation of the fictitious 1/2 spin. Two angles (θ, ϕ) uniquely identify such a rotation in the Bloch picture

$$\hat{R}(\theta,\phi) = \exp\left[i\frac{\theta}{2}\left(e^{i\phi}\hat{\sigma}_+ + e^{-i\phi}\hat{\sigma}_-\right)\right], \tag{2.49}$$

where ϕ represents the axis of rotation in the equatorial plane and θ is the rotation angle, which physically corresponds to the duration of the laser pulse. For two-qubit gates, which should physically couple two ions together, collective vibrational modes are used to mediate an ion-ion effective interaction. Once a specific mode is selected, usually the center of mass mode (COM), it acts as a sort of quantum bus that connects the ions and distributes information. Here, sideband interactions (2.46)-(2.47) are used. In the case of one ion the resulting operations read as

$$\begin{aligned}\hat{R}^{(-)}(\theta,\phi) &= \exp\left[i\frac{\theta}{2}\left(e^{i\phi}\hat{\sigma}_+\hat{a} + e^{-i\phi}\hat{\sigma}_-\hat{a}^\dagger\right)\right],\\ \hat{R}^{(+)}(\theta,\phi) &= \exp\left[i\frac{\theta}{2}\left(e^{i\phi}\hat{\sigma}_+\hat{a}^\dagger + e^{-i\phi}\hat{\sigma}_-\hat{a}\right)\right].\end{aligned} \tag{2.50}$$

Obviously, when the COM mode is excited and subsequent $\hat{R}^{(\pm)}$ pulses are applied to different ions, the net result is an effective many-ion logic gate. We conclude this section remarking that all the previous results were presented under the assumption

that no external influence on the ion's dynamics would be present at any time. Unfortunately, this is a rather unrealistic assumption, especially when it comes to experimental realizations. In a real laboratory one has to deal with several sources of imperfection that might jeopardize the dynamics dictated by (2.38). Some of these imperfections can, to some extent, be modeled in the general framework of decoherence theory, which is the topic of the next section.

2.4 Decoherence processes for a single trapped ion

Decoherence is the main obstacle to preserving the quantum properties of a quantum system [94]. Quantum mechanics in its standard formulation applies to isolated systems where no disturbance from the outside world is present. No matter how complicated a Hamiltonian can be, as long as we are dealing with closed systems, the dynamics will always be unitary, implying conservation of energy, quantum probabilities and coherences. However, in the real world, a quantum system S always couples with its surrounding environment E. In this case, we talk of an open quantum system. The effect of this coupling will lead to correlations between the system and the environment and loss of the system's quantum properties. More about this topic will be discussed in the next Chapter. In trapped-ion systems decoherence mostly affects the vibrational degrees of freedom and it originates from fluctuations of the trap parameters. These generate unwanted couplings between the ion's position and the thermal electric fields of the surrounding environment. Such fields can be depicted as electronic thermal noise in the resistance of the trap electrodes. Two lossy mechanisms arise, heating and dephasing of the COM. These two effects are described in terms of a master equation for the density matrix of the COM. In Chapter 3 we will spend a few more words about how to derive such an equation as well as the limit of validity for such a description. For the moment, we assume the equation to be applicable and analyze its solution. Heating can be modeled by using the amplitude damping model where a single harmonic oscillator $\hat{a}$ (COM) is coupled to a set of environment harmonic oscillators $\hat{b}_j$ at temperature T (the thermal electric fields) via an excitation-hopping interaction. The total Hamiltonian reads as follows [70]

$$\hat{H} = \hbar\nu\hat{a}^\dagger\hat{a} + \sum_{j=0}^{+\infty}\hbar\omega_j\hat{b}_j^\dagger\hat{b}_j + \sum_{j=0}^{+\infty}\hbar\left(g_j\hat{a}\hat{b}_j^\dagger + g_j^*\hat{a}^\dagger\hat{b}_j\right), \tag{2.51}$$

where ν is the frequency of the harmonic oscillator $\hat{a}$, ω_j the frequency of the environment harmonic oscillator $\hat{b}_j$ and g_j the coupling strength between the two. By

using a standard procedure, which will be clarified in Chapter 3, it is possible to derive an effective equation describing the time evolution of the reduced density operator of the COM boson $\hat{\rho}_a$ in interaction picture [44, 70]

$$\begin{aligned}\frac{d\hat{\rho}_a}{dt} = &-\frac{\gamma}{2}(N+1)\left(\hat{a}^\dagger\hat{a}\hat{\rho}_a + \hat{\rho}_a\hat{a}^\dagger\hat{a} - 2\hat{a}\hat{\rho}_a\hat{a}^\dagger\right) \\ &-\frac{\gamma N}{2}\left(\hat{a}\hat{a}^\dagger\hat{\rho}_a + \hat{\rho}_a\hat{a}\hat{a}^\dagger - 2\hat{a}^\dagger\hat{\rho}_a\hat{a}\right),\end{aligned} \tag{2.52}$$

where $N = \left(e^{\hbar\nu\beta} - 1\right)^{-1}$ is the average number of thermal excitations at frequency ν and the decay rate is $\gamma = R^2(\nu)g^2(\nu)$ with $R(\omega)$ being the density of states of the environment. The above equation describes how a bosonic thermal environment can de-excite (first term on the r.h.s.) or excite (second term on the r.h.s.) the harmonic oscillator $\hat{a}$. This can be explicitly seen by calculating the time-evolution of the average excitation number $\hat{N}_a = \hat{a}^\dagger\hat{a}$

$$\langle\hat{N}_a(t)\rangle = \langle\hat{N}_a(0)\rangle e^{-\gamma t} + N\left(1 - e^{-\gamma t}\right). \tag{2.53}$$

If the bath is initially at zero temperature ($N = 0$) the average energy of the system will decay and be lost in the environment. On the contrary, it the $T \neq 0$ the system will thermalize with its environment. A similar equation governs the COM dynamics in presence of dephasing. This destroys quantum coherences in the state of the system but leaves populations unaffected. In other words, this coupling turns an initial pure quantum state of the system into a classical statistical mixture and, as such, it can be considered as an archetypal model to explain quantum-to-classical transition. In this case the total Hamiltonian of system and environment reads as follows [70]

$$\hat{H} = \hbar\nu\hat{a}^\dagger\hat{a} + \sum_{j=0}^{+\infty}\hbar\omega_j\hat{b}_j^\dagger\hat{b}_j + \sum_{j=0}^{+\infty}\hbar\hat{a}^\dagger\hat{a}\left(g_j\hat{b}_j^\dagger + g_j^*\hat{b}_j\right). \tag{2.54}$$

Note that this time there is no energy exchange and the Hamiltonian commutes with the quantum number operators $\hat{a}^\dagger\hat{a}$ and $\hat{b}_j^\dagger\hat{b}_j$. Following the same approach as in the previous case it is possible to derive a new master equation for this model [44, 70]

$$\frac{d\hat{\rho}_a}{dt} = -\Gamma\left[\hat{a}^\dagger\hat{a}, \left[\hat{a}^\dagger\hat{a}, \hat{\rho}_a\right]\right], \tag{2.55}$$

where the dephasing rate Γ sets the time-scale at which the off-diagonal terms of $\hat{\rho}_a$ vanish. It is straightforward to show that

$$\begin{aligned}&\langle n|\frac{d\hat{\rho}}{dt}|n\rangle = \dot{\rho}_{nn} = 0, \\ &\langle n|\frac{d\hat{\rho}}{dt}|m\rangle = \dot{\rho}_{nm} = -\Gamma(n-m)^2\rho_{nm} \rightarrow \rho_{nm}(t) = \rho_{nm}(0)e^{-\Gamma(n-m)^2 t}.\end{aligned} \tag{2.56}$$

Hence, as anticipated above, in a dephasing process coherences decay exponentially whereas populations are untouched. As explained in the following the timescales associated to energy dissipation and dephasing are different. Nevertheless, for any quantum information protocol to be well-performed in trapped ions, they both have to be taken into account.

2.5 Implementing a Toffoli gate

In a recent experiment a C-NOT gate for a three-qubit system was experimentally implemented for the first time ever using a circuital decomposition [20]. By using single-ion laser-addressing a total of 15 steps was required to compose the whole gate along with state preparation and read-out. The mean gate fidelity achieved was around 71% and the execution time was about 1.5 ms. Here, we take a different approach and show how simultaneous laser-addressing of multiple ions can be used to implement a three-ion C-NOT gate with a good fidelity and a significant reduction of the number of operations required. We account for all the fundamental sources of imperfection introduced in section 2.4 as well as some of the technical ones. We demonstrate that as long as the relevant parameters are within the range as in [20], our gate is quite robust against most of the noise.

2.5.1 The setup

Let us consider three ions placed in a linear Paul trap located at their equilibrium positions [35]. We select three internal levels that we label $\{|l_j\rangle, |g_j\rangle, |e_j\rangle\}$. In order to couple these levels in pairs we utilize their COM mode $\hat{a}$ and exploit the flexibility of the following Hamiltonian

$$\hat{H}_I(t)=\frac{\Omega}{2}\hat{\sigma}_-^{(\alpha\beta)}\exp\left[i\eta\left(\hat{a}e^{-i\nu t}+\hat{a}^\dagger e^{i\nu t}\right)-i\left(\omega_{\alpha\beta}-\omega_L\right)t\right]+\text{h.c.}, \tag{2.57}$$

where, Ω is the Rabi frequency of the transition $|\alpha\rangle\leftrightarrow|\beta\rangle$, with $\alpha,\beta{=}e,g,l$, $\hat{\sigma}_-^{(\alpha\beta)}=|\alpha\rangle\langle\beta|$ is a jump operator, $\omega_{\alpha\beta}$ the corresponding transition frequency, ν the frequency of the mode $\hat{a}$ and η is the Lamb-Dicke parameter. The above interaction is a special case of Eq.(2.48) where we have pin-pointed only one among all vibrational modes. In an experimental setup a ionic species candidate could be $^{40}Ca^+$ with $|g\rangle=S_{1/2}(m=-1/2), |l\rangle=S_{1/2}(m=1/2)$ and $|e\rangle=D_{5/2}(m=-1/2)$. Interaction (2.57) allows for both $|e\rangle\leftrightarrow|g\rangle$ and $|e\rangle\leftrightarrow|l\rangle$ couplings, although through different schemes. The first transition can be guided via quadrupole coupling whereas the second can be driven by a far off-resonance Raman coupling (see Appendix A). In the first case the laser frequency ω_L is the frequency of the laser used, while in the

case of a Raman transition it would be the difference between the frequencies of the two laser-fields that off-resonantly couple $|l_j\rangle$ and $|g_j\rangle$ to a third suitable level, for instance the $P_{3/2}$ energy state. As discussed earlier in this chapter, the interaction Hamiltonian (2.57) can be expanded in powers of η and, up to the first order, three different resonant interactions can be engineered depending on the laser-ion tuning $\Delta_{\alpha\beta} = \omega_{\alpha\beta} - \omega_L$

$$\begin{aligned}
&\Delta_{\alpha\beta}{=}0 \rightarrow \hat{H}_C = \Omega\hat{\sigma}_x^{(\alpha\beta)}, \\
&\Delta_{\alpha\beta}{=}\nu \rightarrow \hat{H}_R = i\frac{\eta\Omega}{2}[\hat{a}\hat{\sigma_+}^{(\alpha\beta)} + \hat{a}^\dagger\hat{\sigma}_-^{(\alpha\beta)}], \\
&\Delta_{\alpha\beta}{=}-\nu \rightarrow \hat{H}_B = i\frac{\eta\Omega}{2}[\hat{a}^\dagger\hat{\sigma}_+^{(\alpha\beta)} + \hat{a}\hat{\sigma}_-^{(\alpha\beta)}].
\end{aligned} \tag{2.58}$$

In the following we will describe in details how to construct a Toffoli gate using the unitary evolution governed by the so-called Tavis-Cummings Hamiltonian [93]

$$\hat{H}_{\mathrm{TC}} = \sum_{j=1}^{3} g_j \left(\hat{a}|e_j\rangle\langle g_j| + \hat{a}^\dagger|e_j\rangle\langle g_j|\right), \tag{2.59}$$

where $g_j = \eta\Omega_j/2$ with Ω_j being the $|e_j\rangle \leftrightarrow |g_j\rangle$ Rabi frequency of the ion j, together with single-qubit operations to be performed before and after the dynamics induced by $\hat{H}_{\mathrm{TC}}$.

2.5.2 The protocol

For any quantum protocol to be implemented, we first need to identify appropriate qubit states. In this case the encoding goes as follows

$$\begin{aligned}
&|1_1\rangle = |e_1\rangle, \qquad |0_1\rangle = |g_1\rangle, \\
&|1_2\rangle = |l_2\rangle, \qquad |0_2\rangle = |g_2\rangle, \\
&|1_3\rangle = |l_3\rangle, \qquad |0_3\rangle = |g_3\rangle,
\end{aligned} \tag{2.60}$$

This allows us to immediately define the eight-state basis for the three-qubit system $\mathcal{B} = \{|000\rangle, |100\rangle, |010\rangle, |110\rangle, |001\rangle, |101\rangle, -i|011\rangle, -i|111\rangle\}$, where we have redefined the last two states to include an overall phase factor that will simplify further calculations. The COM mode will be utilized as an ancilla system. At this point, two important assumptions are necessary. First, we assume to work in the single-excitation subspace of the total Hilbert space, which includes the internal levels as well as the phononic mode. This implies that at any time during the protocol no more than one overall excitation will be present, at least in the ideal unitary case. Second, since we want to implement a three-qubit quantum gate, any correlation between the internal and motional degrees of freedom of the string both prior to and

after the protocol must be avoided. Hence, we enforce the phononic mode, initially prepared in the ground state $|0_a\rangle$, to return to this state once the gate is completed. Now, in order for interaction (2.59) to take place, we need to have at least one excitation overall. The protocol begins with the following single-ion operations

$$\begin{aligned}\hat{R}_A^+ &= \exp\left(i\hat{H}_B^{(eg)}\zeta\tau\right),\\ \hat{R}_B^- &= \exp\left(i\hat{H}_R^{(le)}\zeta\tau\right),\\ \hat{R}_C^- &= \exp\left(i\hat{H}_R^{(lg)}\zeta\tau\right),\end{aligned} \tag{2.61}$$

where $\zeta{=}\eta\Omega/2$ and the interaction time τ is chosen such that $\zeta\tau = \pi/2$. The concatenation of these three single-qubit operations performed in the following order

$$\hat{\mathcal{R}} = \hat{R}_C^-\hat{R}_B^-\hat{R}_A^+, \tag{2.62}$$

creates an excitation in the phononic ancilla $|0_a\rangle$ conditional to the state of the qubit 1, which, from now on, we will refer to as target qubit. Since we want to couple the target ion with the COM mode at each step, the frequencies of the laser fields must be tuned accordingly, that is $\omega_L^A{-}\omega_{ge}{=}{-}\nu, \omega_L^B{-}\omega_{le}{=}\nu, \omega_L^C{-}\omega_{gl}{=}\nu$. In the single-excitation subspace the action of $\hat{R}$ reads as

$$\begin{aligned}\hat{\mathcal{R}}|g_1, 0_a\rangle &= |g_1, 1_a\rangle,\\ \hat{\mathcal{R}}|e_1, 0_a\rangle &= |e_1, 0_a\rangle.\end{aligned} \tag{2.63}$$

After this dual-rail encoding we implement the Tavis-Cummings Hamiltonian $\hat{H}_{\mathrm{TC}}$. When solving the Schroedinger equation for each basis state we first observe that the set of all the states that are involved in the total dynamics can be split in four subspaces S_j that are invariant with respect the time-evolution operator $\exp\left(-i\hat{H}_{\mathrm{TC}}t\right)$

$$\begin{aligned}S_1 &= \{|g_1, g_2, g_3, 1\rangle, |e_1, g_2, g_3, 0\rangle, |g_1, e_2, g_3, 0\rangle, |g_1, g_2, e_3, 0\rangle\},\\ S_2 &= \{|g_1, g_2, l_3, 1\rangle, |e_1, g_2, l_3, 0\rangle, |g_1, e_2, l_3, 0\rangle\},\\ S_3 &= \{|g_1, l_2, g_3, 1\rangle, |e_1, l_2, g_3, 0\rangle, |g_1, l_2, e_3, 0\rangle\},\\ S_4 &= \{|g_1, l_2, l_3, 1\rangle, |e_1, l_2, l_3, 0\rangle\}.\end{aligned} \tag{2.64}$$

Hence, the dynamics can be separately solved in each of these four subspaces. Since we are interested in the time-evolution of those states that form the computational basis, that is the first two states in each S_j, we look at the population time evolution $P(t)$ of these eight states only. However, before proceeding, some remarks are needed. First, we briefly recall the matrix representation of the Toffoli gate T in the

computational basis $\mathcal{B}$

$$T = \begin{pmatrix} 1 & 0 & 0 & 0 & 0 & 0 & 0 & 0 \\ 0 & 1 & 0 & 0 & 0 & 0 & 0 & 0 \\ 0 & 0 & 1 & 0 & 0 & 0 & 0 & 0 \\ 0 & 0 & 0 & 1 & 0 & 0 & 0 & 0 \\ 0 & 0 & 0 & 0 & 1 & 0 & 0 & 0 \\ 0 & 0 & 0 & 0 & 0 & 1 & 0 & 0 \\ 0 & 0 & 0 & 0 & 0 & 0 & 0 & 1 \\ 0 & 0 & 0 & 0 & 0 & 0 & 1 & 0 \end{pmatrix}. \tag{2.65}$$

The action of T on the computational basis states leaves the first six states unaffected while swapping the last two. The idea is then to find a unique time t_T for the unitary operator

$$\hat{\mathcal{U}}_T = \mathrm{tr}_a \left[\left(\hat{\mathcal{R}}^\dagger \otimes \hat{\mathbb{I}}_{23} \right) \exp \left[-(i\hat{H}_{\mathrm{TC}} t_T \right] \left(\hat{\mathcal{R}} \otimes \hat{\mathbb{I}}_{23} \right) \right], \tag{2.66}$$

to be as close as possible to Eq.(2.65). The partial trace over the motional degree of freedom will reduce to a simple projection onto the ground state $|0_a\rangle$ in the unitary case. When solving the Schroedinger equation for each of the eight states in the basis we need to fix the initial conditions $|\phi_0\rangle$ accordingly

$$\begin{aligned}
|\phi_0\rangle = |g_1, g_2, g_3, 1\rangle \quad &\rightarrow \quad P_{g_1,g_2,g_3,1}(t) = \cos^2(\Theta_{123} t), \\
|\phi_0\rangle = |e_1, g_2, g_3, 0\rangle \quad &\rightarrow \quad P_{e_1,g_2,g_3,0}(t) = \left\{ 1 + \frac{g_{1c}^2}{\Theta_{123}^2} \left[\cos(\Theta_{123} t) - 1 \right] \right\}^2, \\
|\phi_0\rangle = |g_1, g_2, l_3, 1\rangle \quad &\rightarrow \quad P_{g_1,g_2,l_3,1}(t) = \cos^2(\Theta_{12} t), \\
|\phi_0\rangle = |e_1, g_2, l_3, 0\rangle \quad &\rightarrow \quad P_{e_1,g_2,l_3,0}(t) = \left\{ 1 + \frac{g_{1c}^2}{\Theta_{12}^2} \left[\cos(\Theta_{12} t) - 1 \right] \right\}^2, \\
|\phi_0\rangle = |g_1, l_2, g_3, 1\rangle \quad &\rightarrow \quad P_{g_1,l_2,g_3,1}(t) = \cos^2(\Theta_{13} t), \\
|\phi_0\rangle = |e_1, l_2, g_3, 0\rangle \quad &\rightarrow \quad P_{e_1,l_2,g_3,0}(t) = \left\{ 1 + \frac{g_{1c}^2}{\Theta_{13}^2} \left[\cos(\Theta_{13} t) - 1 \right] \right\}^2, \\
|\phi_0\rangle = -i|g_1, l_2, l_3, 1\rangle \quad &\rightarrow \quad P_{e_1,l_2,l_3,0}(t) = \sin^2(\Theta_1 t), \\
|\phi_0\rangle = -i|e_1, l_2, l_3, 0\rangle \quad &\rightarrow \quad P_{g_1,l_2,l_3,1}(t) = \sin^2(\Theta_1 t),
\end{aligned} \tag{2.67}$$

where the dressed frequencies are $\Theta_{123}{=}\hbar\eta(\sum_{j=1}^{3}\Omega_j^2)^{1/2}$, $\Theta_{1j}{=}\hbar\eta(\Omega_1^2{+}\Omega_j^2)^{1/2}$ $(j{=}2,3)$ and $\Theta_1{=}\hbar\eta\Omega_1$. Note that in the last two lines we want the states to swap. As anticipated earlier now we look for a single time t_T such that the $\hat{\mathcal{U}}_T(t)$ realizes the three-qubit-Toffoli T. This implies looking for a time t_T that maximizes all the previous probabilities $P_{\alpha_1,\alpha_2,\alpha_3,n_a}(t_T)$. Since we are dealing with trigonometric

functions we know exactly where their maximizing points on the time axis are

$$t_1 = \frac{\pi n_1}{\Theta_{123}}, \qquad t_2 = \frac{\pi n_2}{\Theta_{12}}, \qquad t_3 = \frac{\pi n_3}{\Theta_{13}}, \qquad t_4 = \frac{\pi(2n_4+1)}{2\Theta_1}, \tag{2.68}$$

with n_i's integer. By inspecting Eq.(2.67) and Eq.(2.68) it is obvious that an exact simultaneous maximization of all the probabilities can never be performed since the swapping operation causes the last two to be odd functions while the first six are even. However, an approximate simultaneous maximization is accessible by properly adjusting the Rabi frequencies Ω_j For instance, by setting

$$\Omega_1{:}\Omega_2{:}\Omega_3{=}1{:}\sqrt{143}{:}16, \tag{2.69}$$

at the optimal instant of time given by $t_T{=}\pi/\eta\Omega_1$, we obtain

$$\hat{\mathcal{U}}_T{=}\hat{T} - 10^{-3}|110\rangle\langle 110| - 2{\times}10^{-3}|001\rangle\langle 001|, \tag{2.70}$$

where $\hat{T}$ is the Toffoli operator. In matrix form this reads as

$$\mathcal{U}_{\mathcal{T}} = \begin{pmatrix} 1 & 0 & 0 & 0 & 0 & 0 & 0 & 0 \\ 0 & 1 & 0 & 0 & 0 & 0 & 0 & 0 \\ 0 & 0 & 1 & 0 & 0 & 0 & 0 & 0 \\ 0 & 0 & 0 & 1 & 0 & 0 & 0 & 0 \\ 0 & 0 & 0 & 0 & 0.999 & 0 & 0 & 0 \\ 0 & 0 & 0 & 0 & 0 & 0.998 & 0 & 0 \\ 0 & 0 & 0 & 0 & 0 & 0 & 0 & 1 \\ 0 & 0 & 0 & 0 & 0 & 0 & 1 & 0 \end{pmatrix}, \tag{2.71}$$

Needless to say, other choices can be found for the set of Rabi frequencies that achieve a gate close to $\hat{T}$. Clearly, the only important parameter in this model is the ratio of the Rabi frequencies rather than their actual value. The time needed in order to implement the whole gate is

$$t_G = \frac{\pi}{\eta}\left(\sum_{k=A,B,C}\frac{2}{\Omega_k} + \frac{1}{\Omega_1}\right), \tag{2.72}$$

where Ω_k is the Rabi frequency of the pulse $k{=}A,B,C$ in Eq.(2.61). It has to be remarked that the $\hat{\mathcal{R}}$ and $\hat{\mathcal{R}}^\dagger$ operations are fundamental in order to get rid of the photon label at the end of the whole gate, which is a very important step to perform in the whole scheme. In fact, the use of excited vibrational states opens the protocol to the effects of phononic heating and losses. The necessity of removing such excitations motivates the use of the encoding-decoding steps given by $\hat{\mathcal{R}}$. Also,

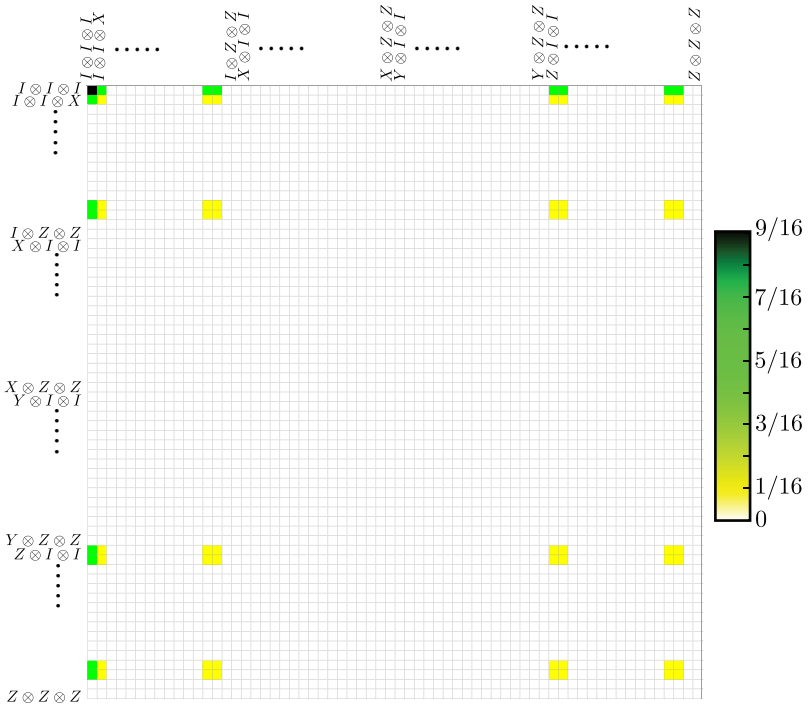

Figure 2.4: Reconstructed process matrix for $\hat{\mathcal{U}}_T$. The matrix is expressed in the three-qubit operator basis formed by $\{I{\equiv}\hat{\mathbb{I}}, X{\equiv}\hat{\sigma}_x, Y{\equiv}-i\hat{\sigma}_y, Z{\equiv}\hat{\sigma}_z\}$. We show the moduli of the matrix entries. The differences with respect to the elements of an ideal gate are $\mathcal{O}(10^{-4})$.

we emphasize that this protocol requires roughly 44% of the number of operations needed in [20]. The substantial difference between the two approaches lies in the usage of multiple-ion operations instead of the canonical single and 2-qubit circuital decomposition.

In Fig.2.4 we show the representation of the reconstructed process matrix in the tensorial operator-basis constructed with the single-qubit operators $\{\hat{\mathbb{I}}, \hat{\sigma}_x, -i\hat{\sigma}_y, \hat{\sigma}_z\}$. The entries of $\chi(t_G)$ differ from the ideal ones by $\mathcal{O}(10^{-4})$, showing the excellent quality of our gate, which has average infidelity $1-\overline{\mathcal{F}}_s(t_G)$ as small as 10^{-5}.

2.5.3 Sources of imperfections

All the discussions presented so far refer to the ideal case in which the evolution is unitary and not affected by any external influence. In order to draw more realistic conclusions about the goodness of the protocol our model has to be extended to include noise. The experimental setup we have in mind is the one utilized in [20] and we shall consider the most severe sources of imperfections of this particular ion-trap architecture. We concentrate on quality-limiting effects of non-technical nature for which a well-defined analytical description in terms of dissipation and decoherence of the COM mode exists. As pointed out earlier in this chapter, both these effects are connected to heating caused by noisy electric potentials at the surface of the

trap electrodes, resulting in an effective bath at non-zero temperature. Now, the presented protocol consists of three steps: a dual-rail encoding that involves the target ion and the COM mode, the multiple-ion interaction as ascribed by Hamiltonian (2.59) and the final dual rail decoding aimed to remove unwanted correlations between the internal levels and the COM mode. In [20, 70] it was shown that by taking fast and intense optical pulses, the duration of sideband-resolved light-ion interactions that are required to implement $\hat{\mathcal{R}}$ can be made much shorter than the radiative lifetime of the ionic excited states, the heating rate of the COM mode and the trap period. Thus, we neglect any decoherence effect occurring during the realization of single-ion gates and assume the dynamics at this stage to be still purely unitary. This was experimentally achieved in [20], where it was also shown that single-ion-addressing errors in $\hat{\mathcal{R}}$ are rather small and do not fundamentally limit the accuracy of one-qubit operations. Obviously, the same conclusions apply to $\hat{\mathcal{R}}^{\dagger}$. Hence, we focus our attention on the intermediate step that effectively realizes the Toffoli gate. As anticipated earlier, both decoherence and heating of the COM can be investigated in an open quantum system framework where a master equation for the dynamics of the COM mode can be set

$$\begin{aligned}\frac{d\hat{\rho}}{dt}=&-i\left[\hat{H}_{\mathrm{TC}},\hat{\rho}\right]-\frac{\kappa\left(\bar{n}+1\right)}{2}\left(\hat{a}^{\dagger}\hat{a}\hat{\rho}+\hat{\rho}\hat{a}^{\dagger}\hat{a}-2\hat{a}\hat{\rho}\hat{a}^{\dagger}\right)\\&-\frac{\kappa\bar{n}}{2}\left(\hat{a}\hat{a}^{\dagger}\hat{\rho}+\hat{\rho}\hat{a}\hat{a}^{\dagger}-2\hat{a}^{\dagger}\hat{\rho}\hat{a}\right)-\gamma\left[\hat{a}^{\dagger}\hat{a},\left[\hat{a}^{\dagger}\hat{a},\hat{\rho}\right]\right],\end{aligned}\tag{2.73}$$

where $\hat{\rho}$ is the density matrix of the ionic string and the vibrational mode, κ is the heating rate, $\bar{n}$ is the mean number of phononic quanta of the bath at a given temperature and γ is the dephasing rate. Analogously to the unitary case, the dynamical map $\mathcal{E}_H$ arising from Eq. (2.73) is to be preceded and followed by the $\hat{\mathcal{R}}$ gate. That is, any initial state $\hat{\rho}(0)$ of the three-ion system density matrix evolves until time t_G according to

$$\hat{\rho}(t_G)=\hat{\mathcal{R}}^{\dagger}\left[\mathcal{E}_H\left(\hat{\mathcal{R}}\hat{\rho}(0)\hat{\mathcal{R}}^{\dagger}\right)\right]\hat{\mathcal{R}}.\tag{2.74}$$

The resulting open-system dynamics implies, in principle, leakage from the computational space that could spoil the desired gate. In particular, the thermal background could lead to populating Hilbert subspaces with more than one excitation. The lossy dynamics dictated by Eq.(2.73) is to be solved numerically. Furthermore, by applying QPT it is possible to obtain a more realistic estimation of the gate quality in presence of noise. The rates are set to the values $1/\kappa = 140$ms and $1/\gamma = 85$ms which are fully consistent with the COM mode and in line with the most recent experiments [20]. First we investigate thermal effects in the worst case scenario by setting $\bar{n} = 5$ [20]. Once the process matrix $\tilde{\chi}(t_G)$ is computed, its resemblance

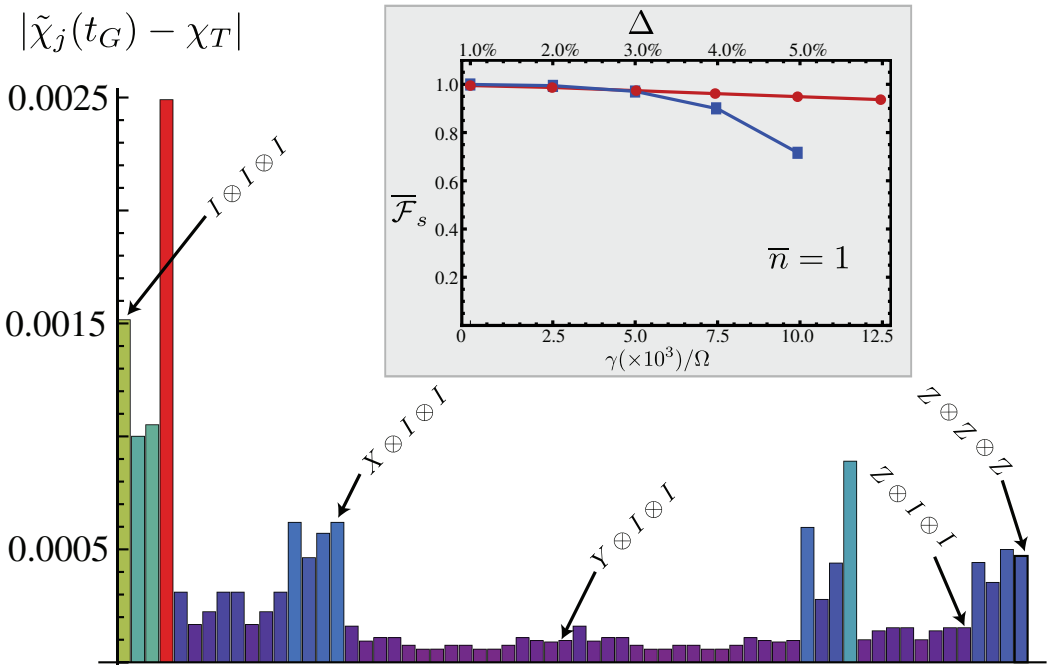

Figure 2.5: Main panel.- We take the largest entry per row in the discrepancy matrix $|\tilde{\chi}(t_G)-\chi_T|$ for $\bar{n}$=5, γ/Ω=10^{-3}. We have highlighted the bars corresponding to some of the operator-basis elements. Inset.- Lower horizontal axis and circle-shaped points: Average state fidelity for the $\hat{\mathcal{U}}_T$ gate against the dephasing γ/Ω. At γ=0 it is $\overline{\mathcal{F}}_s$=0.999988, while for the larger dephasing rate that we have considered we have $\overline{\mathcal{F}}_s$>0.93. Upper horizontal axis and square-shaped points: Average gate fidelity for $\hat{\mathcal{U}}_T$ against the variance Δ of the uniform distribution determining the amplitudes of laser fluctuations in our model. The solid lines are only guides to the eye.

to χ_T is analyzed by calculating the discrepancy $|\tilde{\chi}(t_G)-\chi_T|$. The main panel of Fig. 2.5 shows the maximum value per row of such a discrepancy matrix. The largest deviation we observe out of the 64 values gathered in this way is $\simeq 2.5\times10^{-3}$. Moreover, the average gate fidelity turns out to be $\overline{F}_s$=0.994855, which is 99.5% the value achieved for the best case scenario $\bar{n}$=1. It is worth noticing that the protocol appears to be well robust against the influence of a thermal background. Thus, we can conclude that the dynamics realized by $\mathcal{E}_H$ can be approximated as follows

$$\rho(t_G) \approx \rho_q(t_G) \otimes |0\rangle\langle 0|, \tag{2.75}$$

where $\rho_q(t_G)$ is the density matrix of the three-ion system. This result is consistent with the Markovian approximation.

The next step is the evaluation of the dephasing effect. In this case we set $\bar{n} = 1$ and solve Eq. (2.73) for increasing values of γ and plot the corresponding average state fidelity of the effective gate, which is shown in the inset of Fig. 2.5, red circles. Remarkably, the protocol is almost insensitive to an increase of γ by at least one order of magnitude from the value estimated in Ref. [20].

By inspecting Eq.(2.69) it should be clear that a key point in the implementation of the protocol is the maintenance of precise ratios among the Rabi frequencies. Intensity fluctuations may jeopardize the required stability and so they have to be investigated throughly. We solve Eq.(2.73) treating the Ω_j's as stochastic variables that randomly oscillate around their ideal values. In practice, we define

$$\Omega_j^{'}=\Omega_j+\delta\Omega_j, \tag{2.76}$$

where $\delta\Omega_j/\Omega_j$ is a uniformly distributed zero-mean variable with variance $\Delta\in[1,5]\%$. Using a sample of 500 randomly drawn values of $\delta\Omega_j$ and evaluating the corresponding dynamical evolution, we calculate the sample-averaged $\overline{\mathcal{F}}_s$. In the worst case scenario given by Δ=5%, which grossly underestimate the current experimental capabilities, an average fidelity of $\simeq$71% is achievable. This behavior is displayed again in the inset of Fig. 2.5, blue squares.

The final point we address regards the initialization of the COM mode to its ground state. If this is not perfectly achieved we might expect the performance of the protocol to worsen and we would like to estimate to extent to which this happens. This effect translates to preparing the ancillary phonon mode in a low-temperature thermal state with a mean number of initial thermal excitations up to $\bar{n}_{\rm TH}=10^{-1}$.

$$\hat{\rho}_a=\sum_{n=0}^{+\infty}\frac{e^{-\beta\nu n}}{Z_a}. \tag{2.77}$$

We have proven this effect to influence the efficiency of the protocol fairly little, with a gate fidelity that in the unitary case is never smaller than 0.901. In the open-system case we find a fidelity equal to 0.8962 for $\bar{n}=5$ and γ=85msec, while $\overline{\mathcal{F}}_s$=0.6396 for the case of fluctuating Rabi frequencies with Δ=5%.

2.6 Conclusions

In this chapter, after introducing the basic theory of quantum computing in trapped ions, we have discussed an alternative scheme for implementing the TOFFOLI gate in such systems. The protocol presented relies on both single and multi-qubit operations and, at least in principle, it requires only 44% of the operations needed in the experiment reported in [20]. Furthermore, a quite good robustness against the most common sources of imperfections and noise has been demonstrated.

Chapter 3

Non-Markovian dynamics and criticality in Coulomb Crystals

3.1 A quantum probe

The traditional approach to investigating the physics of a many-body system relies on measuring its response to a weak and controllable *classical* perturbation. For instance, if we are interested in determining the features of a crystal, such as its periodicity or density-density correlation function, all we need to do is to shine some light on the sample and study the resulting diffraction pattern [95, 96]. More complicated techniques can be engineered depending on the type of information that we want to extract from the system under scrutiny, all pretty much based on the same idea.

Now, let us imagine a different kind of scenario. Let us assume that we are given a many-body system whose Hamiltonian is known from first principles but rather complicated to study. This time though, along with the many-body system comes a single, fully controllable quantum system and a suitable interaction between the two can be efficiently engineered. Furthermore, the dynamics of the single quantum system, as resulting from the interaction with the many-body system, can be monitored. We call this scheme *quantum probe*. We ask ourselves the following questions: what kind of information regarding the complex many-body system can we gain by looking at the dynamics of the quantum probe only? Is there any improvement with respect to a more standard probing scheme? Needless to say, a general answer to any of these questions is not available yet, since a general theory of quantum probes is missing. However, this approach is surely interesting from a foundational point of view.

The dynamics of a single quantum system interacting with a large many-body system can be theoretically modeled within the framework of open quantum system

theory [44,45]. In this approach the many-body system serves as an environment E and its features determine what kind of dynamics the single quantum system S will undergo. In the spirit of open quantum system theory, this is the only dynamics we are interested in as we trace out the environmental degrees of freedom. Such a reduced dynamics can be either Markovian or non-Markovian. Even though a proper definition will be given in what follows, for now we can anticipate that a Markovian dynamics lacks in memory. Markovian processes can always be modeled by a suitable master equation [97,98]. Textbook examples of such a process are spontaneous emission of an atom placed in vacuum and thermalization of an optical cavity field [99,100]. A universal definition of non-Markovian dynamics is far more elusive. Several possible solutions have been presented [46–49,51,129] that capture different aspects of what non-Markovianity could be. Now let us imagine that not only is the environment a complex many-body system, but it also shows some critical behavior whenever one of its Hamiltonian parameters is tuned to a certain critical value. If we have a single quantum system embedded in and interacting with it can we, by any chance, observe a drastic change in the system's dynamics when we drive the environment across criticality? Furthermore, if this turns out to be the case, could this provide a new way to interpret critical behavior?

This novel approach has been utilized in a series of recent papers [52–56]. The general finding in all of these investigations is that if we look at a critical many-body system as an environment for some kind of single quantum system, then a link between the Markovian/non-Markovian character of the latter and its critical behavior does exist.

In the following we will apply this idea to Coulomb crystals [29]. Coulomb crystals are many-body systems that are routinely achievable in many trapped-ion labs and exhibit structural critical behavior. In the following we will show and explain in detail how this critical behavior can be witnessed by using an open quantum system approach.

3.2 Open quantum systems: a brief introduction

The field of open systems is among the vastest in quantum theory. It is the aim of this section to provide the reader with some general concepts, highlighting some later developments.

A general open quantum system can be depicted as follows. Let us assume a single and well-identified quantum object, namely the systems S, interacting with a much larger quantum system, namely the environment E. Here, by much larger we mean that the relevant degrees of freedom of the environment are way too many to be controlled or even monitored. We assume the free evolution of both S and E to be

governed by local Hamiltonians that we label $\hat{H}_S$ and $\hat{H}_E$. If no system-environment interaction was present S and E would evolve separately and never influence each other.

However, as soon as we switch on the interaction- $\hat{V}$- this is no longer true. The total time-evolution is then dictated by the following unitary operator

$$\hat{U}(t) = \exp\left[-\frac{it}{\hbar}\left(\hat{H}_S + \hat{H}_E + \hat{V}\right)\right], \tag{3.1}$$

and the time-evolution of a general initial state of system and environment $\hat{\rho}_{SE}(0)$ reads as follows

$$\hat{\rho}_{SE}(t) = \hat{U}(t)\hat{\rho}_{SE}(0)\hat{U}(t)^\dagger. \tag{3.2}$$

Now, since we have assumed that we can only keep track of the system's dynamics we need to discard the environment's degrees of freedom. This operation is carried out by tracing out the environment's degrees of freedom from the above equation. The reduced dynamics of the system only reads as

$$\hat{\rho}_S(t) = \mathrm{Tr}_E\left[\hat{U}(t)\hat{\rho}_{SE}(0)\hat{U}(t)^\dagger\right]. \tag{3.3}$$

Physically speaking, this corresponds to ignoring the presence of the environment and focusing on the system's dynamics only. Furthermore, this is the only operation that allows to recover the correct statistics when we perform measurements on the sole system. The effect of the environment on the system survives, to some extent, in the new density matrix elements that we obtain after performing the partial trace. A crucial assumption that one usually makes is that system and environment are initially totally uncorrelated $\hat{\rho}_{SE}(0) = \hat{\rho}_S(0) \otimes \hat{\rho}_E(0)$. With this simplification, it is always possible to define a completely positive and trace-preserving (CPT) map $\Phi(t, 0)$ describing the time evolution of the system [44]

$$\hat{\rho}_S(t) = \Phi(t, 0)\hat{\rho}_S(0) \equiv \mathrm{Tr}_E\left[\hat{U}(t)\hat{\rho}_{SE}(0)\hat{U}(t)^\dagger\right]. \tag{3.4}$$

The reduced dynamics of the system can also be written in the following differential form

$$\frac{d}{dt}\hat{\rho}_S = -\frac{i}{\hbar}\mathrm{Tr}_E\Big\{\left[\hat{H}_S + \hat{H}_S + \hat{V}, \hat{\rho}_{SE}\right]\Big\}. \tag{3.5}$$

All the above equations are exact but, unfortunately, untreatable in most of the cases unless a series of approximations are employed. A few approximations make Eq.(3.5) solvable. The first, named the Born approximation, assumes weak coupling between system and environment so that a perturbative expansion of the commutator in (3.5) is possible and the state of the environment does not significantly change during the evolution. The second, the Markov approximation, is essentially an

assumption about the different time-scales involved in the total dynamics, that is, the decay time of environment correlations is much shorter than any relevant time scale of the system. Two silghtly more technical approximations are still required. The interaction between S and E must be of the type $\hat{V} = \sum_j \hat{A}_j^{(S)} \otimes \hat{B}_j^{(E)}$ where $\hat{A}_j^{(S)}, \hat{B}_j^{(E)}$ are a set of system and enviroment operators respectively. Furthermore, the well-known secular approximation is employed for the enviroment operators [44]. When these approximations are carried out in Eq.(3.5) we obtain the following general Markovian master equation in Lindblad form [97, 98]

$$\frac{d}{dt}\hat{\rho}_S = -\frac{i}{\hbar}\left[\hat{H}_S, \hat{\rho}_S\right] + \sum_n \gamma_n \left(\hat{A}_n \hat{\rho}_S \hat{A}_n^\dagger - \frac{1}{2}\{\hat{A}_n^\dagger \hat{A}_n, \hat{\rho}_S\}\right), \tag{3.6}$$

where γ_n are positive constant decay rates and $\hat{A}_n, \hat{A}_n^\dagger$ are called jump operators. These are system's operators that carry the information regarding what kind of processes the environment induces on the system. The above equation can be derived in more than one fashion. As long as the dynamics of an open quantum system can be modeled using Eq.(3.6) with positive rates γ_n, we call the open quantum system Markovian. In Markovian dynamics the future state of the system solely depends upon the present one and memory effects are absent. This typically results in a complete loss of all the quantum properties initially stored in the system. This point will be further clarified in the next section.

3.3 A possible characterization of non-Markovian dynamics: information backflow

It should be clear at this point that a solid definition of Markovian systems exists, based on the ability to describe the dynamics of an open quantum system in terms of a Markovian master equation or, equivalently, of a CPT dynamical map that is a semigroup [44].

Defining what is non-Markovian is, however, a bit more subtle business. This topic has recently gained a considerable attention in the quantum physics community and a significant number of possible points of view have been presented [46–49, 51, 129]. Of course different definitions pertain to different aspects or properties of open systems with memory.

In what follows we will focus our attention on one specific definition of non-Markovian dynamics, based on the idea of information flow [47]. The reason for this choice lies in the interpretation of non-Markovianity that this definition offers. This point will be further clarified at the end of this section and when we get to the physical model studied in this chapter.

We start by introducing the key mathematical quantity for the definition of information flow. Let us imagine we are given two general quantum states $\hat{\rho}_1$ and $\hat{\rho}_2$ and we want to quantify how distinguishable from each other they are. To this aim, we introduce the trace distance

$$D(\hat{\rho}_1, \hat{\rho}_2) \equiv \frac{1}{2}\|\hat{\rho}_1 - \hat{\rho}_2\|_1, \tag{3.7}$$

where $\|\hat{O}\|_1 = \mathrm{Tr}\sqrt{\hat{O}\hat{O}^\dagger}$. This quantity measures the distinguishability between two arbitrary quantum states.

Now, let us consider a physical process that we know to always be representable in terms of a semigroup of $t-$parametrized CPT maps $\Phi(t,0)$. It can easily be proven that, such a map is always contractive with respect to D. This translates to the following inequality [47]

$$D(\Phi(t,0)\hat{\rho}_1(0), \Phi(t,0)\hat{\rho}_2(0)) \leq D(\hat{\rho}_1(0), \hat{\rho}_2(0)) \qquad \forall\hat{\rho}_1, \hat{\rho}_2 \forall t \geq 0. \tag{3.8}$$

Hence, all quantum dynamical semigroups are contractive. The trace distance between any pair of initial states never increases in time. Since the solution of a Markovian master equation (3.6) is always a dynamical semigroup of CPT maps, we conclude that two states undergoing Markovian dynamics become less and less distinguishable: the information about the quantum system of interest will be inevitably lost. The idea is then to define non-Markovian dynamics as deviations from Eq.(3.8). If for some time we are able to gain back some knowledge about the system, that is, the distinguishability of two initial states temporarily increases, we say that this information is flowing back into the system. Hence, the positivity of the following quantity

$$\sigma(t, \hat{\rho}_{1,2}(0)) = \frac{d}{dt}D(\hat{\rho}_1(t), \hat{\rho}_2(t)), \tag{3.9}$$

for some pair of states and some time intervals is an indicator of non-Markovianity. To further quantify the degree of non-Markovianity authors in [47] define the following measure

$$\mathcal{N}(\Phi(t,0)) = \max_{\rho_{1,2}(0)} \int_{\sigma>0} dt\sigma(t, \rho_{1,2}(0)). \tag{3.10}$$

The maximization is to be performed over all the possible pairs of initial states in the state space of the open system and the integration to be extended over time intervals where the trace distance increases. This formula is absolutely general and neither it requires any approximation nor it assumes the knowledge of the master equation. We again stress that it is a property of the dynamical map $\Phi(t,0)$ only.

3.4 Coulomb Crystals: some general facts

A Coulomb crystal is a self-organized spatial arrangement of ions achievable in a linear or ring ionic trap. For a detailed review regarding trapping, cooling and formation of Coulomb crystals, see Ref. [29]. These systems show clear critical features and have been the subject of the intense studies. They can be considered as a toy-model for solid state physics since various spatial equilibrium configurations can be easily explored in a controllable way. The geometry of a particular pattern is a direct consequence of the balance between the repulsive Coulomb force acting between the ions and the three-dimensional confining potential induced in the trap. By appropriately tuning the trap parameters it is possible to explore different geometries and, switching from a particular configuration to another, results in a structural phase transition where critical behavior arises.

Investigations concerning the decoherence of a single two-level system embedded in a Coulomb crystal near criticality have been previously reported in [101]. In this theoretical paper, the authors make use of Ramsey interferometry to monitor collective properties of the crystal, such as correlation functions, in the neighborhood of a critical point. Two electronic levels of one of the ions in the crystal are coupled to the collective vibrations of the whole chain via suitable lasers. The interaction is dependent upon the state of the two-level system and initial superposition states lead to interfering dynamical paths. The authors study the behavior of the interference fringe visibility when the chain is driven across a critical point and exhibits a linear-to-zig-zag structural phase transition. This quantity is connected to the ground state probability of the two-level system and the general finding is that the closer the crystal is to criticality, the more the damped the fringe visibility is. In the following, we take a step further and, by using the same interferometric scheme, we provide a time-independent way to characterize such decoherence. Needless to say, our approach relies on looking at this scenario from an open quantum system perspective and studying the non-Markovian character of the resulting dynamics and its connection to the criticality of the chain.

In what follows we will review some general facts about Coulomb crystals. This is intended to provide the reader with a minimum set of notions that are crucial to understand further results. The classical Hamiltonian governing the dynamics of a N-ion Coulomb crystal reads as

$$H = \sum_{j=1}^{N} \frac{p_j^2}{2m} + \frac{1}{2} m \left[\nu^2 x_j^2 + \nu_t^2 \left(y_j^2 + z_j^2 \right) \right] + \frac{1}{2} \sum_{j \neq i=1}^{N} \frac{Q^2}{|\vec{r}_j - \vec{r}_i|}, \tag{3.11}$$

where $\vec{p}_j$ is the momentum of the $j-$th ion, $\vec{r}_j = (x_j, y_j, z_j)$ its position, ν and ν_t the axial and transverse trap frequencies, respectively. In writing Eq.(3.11) we

have assumed the static harmonic approximation for the quadrupole potential (2.1) discussed in Chapter 2. The relevant and controllable parameters here are the trap frequencies, as compared to the strength of the Coulomb interaction, and the number of ions N. The above Hamiltonian can be straightforwardly turned into an operator by standard quantization procedure.

From now on we will focus on the first transition we can observe, namely, the linear-to-zig-zag. As the name suggests, here the crystal switches from a one-dimensional linear equilibrium configuration, with equally spaced ions, to a planar one where the new equilibrium positions of the ions form a zig-zag segment. This transition takes place for a critical value $\nu_t^{(c)}$ of the transverse trapping frequency ν_t, see Fig.3.1. It has been the subject of theoretical investigations [36, 38, 39] and experimentally observed [33, 34]. In particular, in [39] the authors demonstrated this transition to be of the second order, in agreement with earlier numerical investigations [38] and in a later paper it was argued to be a quantum phase transition [40, 41]. In what follows some features of both the linear and the zig-zag phase are discussed.

Assuming a stable linear configuration with strong transverse confinement $\nu_t > \nu$ and small oscillations around the equilibrium positions $\vec{r}_j^{(0)} = (ja, 0, 0)\,, j = 1, \ldots, N$ with a the equilibrium inter-particle distance, the Hamiltonian (3.11) can be expanded up the second order in the displacement variables $\vec{r}_j = \vec{r}_j^{(0)} - \delta\vec{r}_j$. The resulting effective Hamiltonian describes a set of interacting harmonic oscillators with effective couplings Γ_{ij}

$$\Gamma_{ij} = \frac{2Q^2}{|x_i^{(0)} - x_j^{(0)}|^3}. \tag{3.12}$$

We observe a uniformly spaced chain as long as $\nu_t > \nu_t^{(c)}$ [36, 39],

$$\nu_t^{(c)} = \omega_0 \sqrt{\frac{7\zeta(3)}{2}}, \tag{3.13}$$

where $\omega_0 = \sqrt{Q^2/ma^3}$ is a natural frequency that only depends on the ion's species and number and ζ is the standard Riemann function. This linear regime is the simplest structural pattern arising from ion's localization, where all the vibrational degrees of freedom are uncoupled from each other. As extensively discussed in Chapter 2, this is also the regime implemented for quantum information and computation tasks. The excitation spectrum of the chain can be easily calculated leading

to [39, 103]

$$\omega_{\parallel}(k) = \omega_0 \sqrt{8 \sum_{j=1}^{N/2} \frac{1}{j^3} \sin^2\left(\frac{jka}{2}\right)},$$
$$\omega_{\perp}(k) = \sqrt{\nu_t^2 - 4\omega_0^2 \sum_{j=1}^{N/2} \frac{1}{j^3} \sin^2\left(\frac{jka}{2}\right)}, \tag{3.14}$$

where the sbscripts $\parallel, \perp$ refer to longitudinal (along the $x-$axis) and perpendicular ($y - z$ plane), respectively, and the normal mode's wave vectors are $k = 2\pi n/Na$ with $n = 0, \pm 1, \pm 2, \ldots, N/2$, for N even. When the transition to the zig-zag phase takes place the transverse component of the spectrum vanishes at $k = \pi/a$. This vibrational mode is called the soft-mode of the chain and corresponds to the shortest wavelength and with the lowest energy in the $\omega_{\perp}$ dispersion relation.
In Ref. [39] it was shown that the soft mode drives the chain across the mechanical instability that is responsible for the transition. More precisely, this mode is associated to a deformation of the chain that leads to a planar zig-zag structure with periodicity $2a$. The order parameter is the transverse equilibrium distance b from the longitudinal axis and it is a function of a and ν_t respectively. When the chain enters the zig-zag regime the new equilibrium positions are $\vec{r}_j^{(0)} = [ja, (-1)^j b/2, 0], j = 1, \ldots, N$. In this case the x and y vibrational degrees of freedom of the chain are all coupled and the first Brillouin zone is now $[0, \pi/2a]$, with $k = 2\pi n/Na$ and $k = 0, 1, \ldots, N/4$, that is reduced by a factor of 2. The excitation spectra, which displays multiple branches depending also on the parity of each mode, are far more structured than the linear case. For a detailed derivation and description of the system see Ref. [39].
We conclude this section by mentioning that all of the vibrational modes, both in the linear and in the zig-zag regime, can be easily quantized through standard quantization procedure. Moreover, by means of Taylor expansion up to the second order in terms of the ion's displacement from the equilibrium positions, the full Hamiltonian (3.11) can be mapped onto an effective harmonic oscillator. Thus the eigenmodes, within the validity of this approximation, follow a bosonic statistics. This, in turn, implies that each ion's displacement operator can be linearly expanded in terms of annihilation and creation operators of the eigenmodes, by following the same procedure discussed in Chapter 2 that led to Eq.(2.20).

3.5 Ramsey interferometry in the zero-temperature limit

In this section we show in detail the protocol we use to probe a $N-$ion Coulomb crystal near criticality. First, in order to use an open quantum system approach we

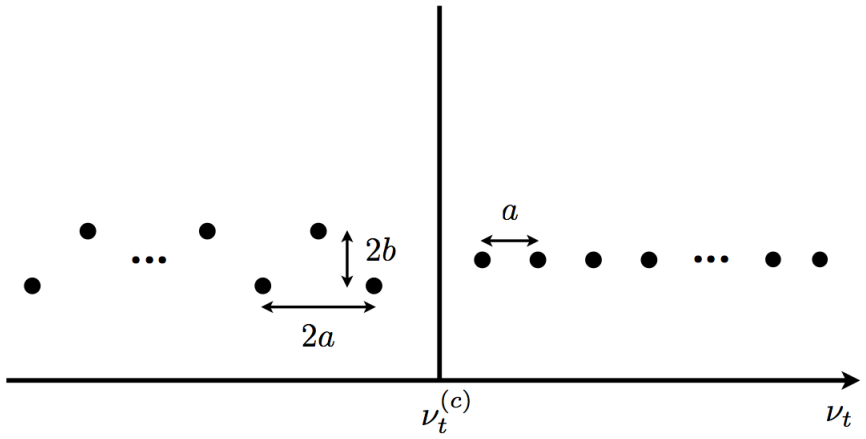

Figure 3.1: Linear and zig-zag equilibrium configurations in a Coulomb crystal.

need to identify the system S and its environment E. We pinpoint the first ion in the chain and we select two internal states that we label $\{|e\rangle, |g\rangle\}$. This will be our open system S. The rest of the ionic chain is taken to be the surrounding environment E. The relevant degrees of freedom of E are the vibrational ones and so we can use the normal-mode decomposition and picture E as a bosonic environment with a non-trivial discretized excitation spectrum, both in the linear and the zig-zag regime.

Each ion's displacement operator $\delta\hat{\vec{r}}$ in the chain can be expanded in terms of annihilation and creation operators of the normal modes. For instance, for the target ion in the linear phase this reads as [101]

$$\begin{aligned}
\delta\hat{x}_1 &= \sum_k \sqrt{\frac{\hbar}{Nm\omega_x(k)}}\Big\{ \cos ka \left[\hat{b}_x(k,+) + \text{h.c.}\right] + \sin ka \left[\hat{b}_x(k,-) + \text{h.c.}\right] \Big\}, \\
\delta\hat{y}_1 = \hat{y}_1 &= \sum_k \sqrt{\frac{\hbar}{Nm\omega_y(k)}}\Big\{ \cos ka \left[\hat{b}_y(k,+) + \text{h.c.}\right] + \sin ka \left[\hat{b}_y(k,-) + \text{h.c.}\right] \Big\}, \\
\delta\hat{z}_1 = \hat{z}_1 &= \sum_k \sqrt{\frac{\hbar}{Nm\omega_z(k)}}\Big\{ \cos ka \left[\hat{b}_z(k,+) + \text{h.c.}\right] + \sin ka \left[\hat{b}_z(k,-) + \text{h.c.}\right] \Big\},
\end{aligned} \tag{3.15}$$

where $\pm$ indicates the mode parity under $k \to -k$ reflection and the $\omega_{x/y/z}(k)$ are given by Eq.(3.14). The $\hat{b}, \hat{b}^\dagger$ operators satisfy the usual commutation relations for bosons. The coupling between the two-level system and the rest of the chain is engineered via the following resonant laser pulse in the transverse direction y

$$\hat{H}_{\text{INT}} = \hbar\Omega \left[\hat{\sigma}^+ e^{-i(\omega_L t - k_L \hat{y}_1)} + \text{h.c.}\right], \tag{3.16}$$

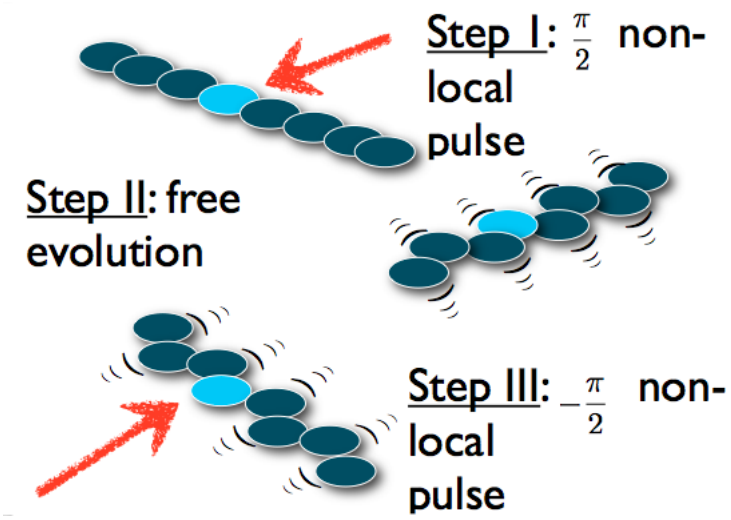

Figure 3.2: Ramsey interferometry of a single spin (light blue) in a Coulomb crystal (dark blue).

where $\hat{\sigma}^+ = |e\rangle\langle g|, \hat{\sigma}^- = |g\rangle\langle e|$, Ω is the Rabi frequency of the laser, ω_L, k_L are the laser frequency and wave-vector respectively. The target ion receives a state-dependent mechanical 'kick' in the y direction due to recoil caused by laser-photon absorption. It immediately starts oscillating and excites all the transverse vibrational normal modes of the chain. The operator $e^{-ik_L\hat{y}_1}$ is nothing but a common displacement operator for the y normal modes of the chain:

$$e^{-ik_L\hat{y}_1} = \bigotimes_{k,\sigma} \hat{D}(\alpha_{k,\sigma}) = \bigotimes_{k,\sigma} \exp\left[\alpha_{k,\sigma}\hat{b}_y^\dagger(k,\sigma) - \alpha_{k,\sigma}^*\hat{b}_y(k,\sigma)\right], \tag{3.17}$$

where σ labels the mode parity and the coherent amplitudes are [101]

$$\alpha_{k,+} = i\sqrt{\frac{\hbar}{Nm\omega_z(k)}}\cos ka, \qquad \alpha_{k,-} = i\sqrt{\frac{\hbar}{Nm\omega_z(k)}}\sin ka. \tag{3.18}$$

Analogous, but slightly more complicated expressions, are found for the zig-zag phase.

We are now in the position of describing the complete Ramsey interferometric protocol used to probe the Coulomb crystal. We label with T_L the laser pulse duration and with ω_M the largest frequency of the composite system $S + E$ and assume $\omega_M T_L \ll 1$. This corresponds to having a strong and practically instantaneous laser pulse. We set $\Omega T_L = \pi/4$ in Eq.(3.16), therefore applying a $\pi/2$ pulse, after which we let S and E evolve freely for a time t. The time-dependent dynamics is then governed by the following Hamiltonian

$$\hat{H}_0 = \frac{\hbar\hat{\sigma}_z}{2} + \sum_{k,\sigma} \hbar\omega_y(k)\hat{b}_y^\dagger(k,\sigma)\hat{b}_y(k,\sigma). \tag{3.19}$$

Finally, we apply a $-\pi/2$ pulse. The total evolution operator reads as follows

$$\hat{U}(t) = \hat{U}_{INT}(-\pi/2)\hat{U}_0(t)\hat{U}_{INT}(\pi/2). \tag{3.20}$$

It is important to remark that t is the time elapsed between the two pluses. Using the Bloch-sphere representation (θ, ϕ) for S, we choose a generic pure initial state of the form

$$|\psi_i\rangle = \left[\cos\left(\frac{\theta}{2}\right)|e\rangle + e^{i\phi}\sin\left(\frac{\theta}{2}\right)|g\rangle\right] \bigotimes |\underline{0}\rangle, \tag{3.21}$$

where $|\underline{0}\rangle$ is the total phononic vacuum state, which is defined as $|\underline{0}\rangle = \bigotimes_{k,\sigma} |0_{k,\sigma}\rangle$. After applying (3.20) to $|\psi_i\rangle$ we obtain the following final system-environment state

$$\hat{U}(t)|\psi_i\rangle = |\psi_f\rangle = \frac{1}{2}\left[|g, \chi_g(t)\rangle + |e, \chi_e(t)\rangle\right], \tag{3.22}$$

where

$$\begin{aligned} |\chi_g\rangle &= c_g|0\rangle + ic_e|-\underline{\alpha}\rangle + c_g\hat{D}(-\underline{\alpha})|\underline{\alpha}(t)\rangle - ic_e|-\underline{\alpha}(t)\rangle, \\ |\chi_e\rangle &= c_e|0\rangle + ic_g|\underline{\alpha}\rangle + c_e\hat{D}(\underline{\alpha})|-\underline{\alpha}(t)\rangle - ic_g|\underline{\alpha}(t)\rangle, \end{aligned} \tag{3.23}$$

and we have introduced the short-hand notation $c_e = \cos(\theta/2), c_g = e^{i\phi}\sin(\theta/2)$, $|\underline{\alpha}\rangle \equiv \bigotimes_{k,\sigma} |\alpha_{k,\sigma}\rangle$, $\alpha_{k,\sigma}(t) = \alpha_{k,\sigma}e^{-i\omega_y(k)t}$ and $\hat{D}(\underline{\alpha}) \equiv \bigotimes_{k,\sigma} \hat{D}(\alpha_{k,\sigma})$. At this stage we make use of the open quantum system approach. We are interested in the reduced dynamics of the two-level system. Hence, we trace out the environment degrees of freedom to get the state of the probe qubit

$$\hat{\rho}_S(r) = [1 - \rho_{gg}(t)]\,|e\rangle\langle e| + \rho_{gg}(t)|g\rangle\langle g| + \rho_{eg}(t)|e\rangle\langle g| + \text{h.c.}. \tag{3.24}$$

The density matrix elements of the two-level system after partial trace read

$$\rho_{gg}(t) = \frac{1}{4}\Big\{2 - \xi\sin\theta\sin\phi[1 - e^{-2A(t)}] + 2\cos\theta\cos[B(t)]e^{-A(t)}\Big\}, \tag{3.25}$$

$$\begin{aligned} \rho_{eg}(t) = \frac{1}{4}\Bigg\{ & \frac{\sin\theta}{2}\Big[e^{-i\phi}\left(1 + 2e^{-A(t)}\cos[B(t)] + e^{-4A(t)}\right) - \\ & 2e^{i\phi}\xi^4\left(e^{A(t)}\cos[B(t)] - 1\right)\Big] + i\xi\left[e^{-2A(t)} - 1\right]\times \\ & \left[\sin^2\left(\frac{\theta}{2}\right)e^{2iB(t)} - \cos^2\left(\frac{\theta}{2}\right)e^{-2iB(t)}\right]\Bigg\}, \end{aligned} \tag{3.26}$$

where the A, B and ξ functions are

$$\begin{aligned} A(t) &= 2\sum_{k,\sigma} |\alpha_{k,\sigma}|^2 \sin^2\left[\frac{\omega_y(k)t}{2}\right], \\ B(t) &= \sum_{k,\sigma} |\alpha_{k,\sigma}|^2 \sin\omega_y(k)t, \\ \xi &= e^{-\sum_{k,\sigma}|\alpha_{k,\sigma}|^2/2}. \end{aligned} \tag{3.27}$$

At this point we need to make a remark. As discussed in section 3.2 a standard open system interacts with its environment via a fixed interaction that does not usually change in time. Since here the overall evolution is made up of three different building blocks, two laser pulses and a free evolution, one may argue that this case study is a bit atypical. However, the operation of tracing out the environment's degrees of freedom in the Ramsey scheme is perfectly legitimate and a dynamical map for the two-level system is well defined as long as we start from a factorized state. In this respect, it is interesting to notice that the overall process admits two complementary viewpoints: If we set the initial time $t_0 = 0$, then the system time-evolution is dictated by a complex quantum map, analogous to a black box, to which we cannot assign a unique global Hamiltonian describing its action. Nevertheless, the reduced evolution is described by a CPT map. If, instead, we set $t_0 = +T_L$ we are looking at the free evolution of an initially correlated system-environment state. Obviously, in the second case, a CPT map is not guaranteed to exist. However, either way, we are effectively engineering and simulating an open system dynamics where both dissipation and decoherence processes can take place. In the following we will quantify the degree of non-Markovinaity associated to this dynamical process.

3.6 Non-Markovian Coulomb crystal

In this section we will study the Markovian/non-Markovian character of Ramsey interferometry of a single 1/2 spin embedded in a Coulomb crystal that undergoes a linear-to-zig-zag phase transition. First, we define the reduced tuning parameter $\Delta = \nu_t/\nu_c - 1$. When $\Delta = 0$ the chain is at criticality. Once again, we recall the dynamical map for the reduced density matrix

$$\hat{\rho}_S(t) = \Lambda_t \hat{\rho}_S(0) = \mathrm{tr}_E\left[\hat{U}(t)\hat{\rho}_{S+E}\hat{U}^\dagger(t)\right], \tag{3.28}$$

where $\hat{U}(t)$ is given in (3.20). Since we are dealing with a single two-level system only initial pairs formed by orthogonal pure states are to be considered when it comes to the state space maximization in Eq.(3.10) [102]. However, given the complexity of (3.28), see Eq.(3.25)-(3.26), it is impossible to perform such a maximization exactly

even for a few ions in the chain. Numerical evidences, based on the rate of change of $D(t)$ for several initial pairs of orthogonal pure states spanning the whole Bloch sphere, seem to suggest that the maximizing pair is formed by the eigenstates of σ_x, which we label $|+\rangle, |-\rangle$. The corresponding trace distance reads as

$$D_{\text{opt}}(t) = \left|\rho_{eg}^{(+)}(t) - \rho_{eg}^{(-)}(t)\right|, \tag{3.29}$$

Interestingly, the dynamics of the $|+\rangle, |-\rangle$ pair is purely dephasing, *i.e.*, neither $|+\rangle$ nor $|-\rangle$ exchanges energy with the bosonic chain. The time-evolution of D is strongly sensitive to changes in the tuning parameter Δ. In Ref. [101] an exact expression of the visibility of the Ramsey protocol was derived for the case of the two-level system initially in the ground state

$$\mathcal{V}(t) = \exp\left[-A(t)\right], \tag{3.30}$$

By further simplifying Eq.(3.29) it can be shown analytically that the optimal trace distance is a function of the visibility $\mathcal{V}(t)$

$$D_{\text{opt}}(t) = \frac{1}{4}\left|1 + 2\cos\left[B(t)\right]\left(\mathcal{V}(t) - \frac{\xi^4}{\mathcal{V}(t)}\right) + \mathcal{V}^4(t) + 2\xi^4\right|, \tag{3.31}$$

This result is of great importance for two reasons. First, it establishes an exact analytical link between the fringe visibility $\mathcal{V}(t)$, which is experimentally measurable, and the non-Markovian character of the process as measured by $\mathcal{N}$. Second, and more important, in order to obtain $D_{\text{opt}}(t)$ in a real experiment we only need to initialize the spin in the ground state. No pair initialization is required, nor the creation of superposition states.

It is worth mentioning that the term $\mathcal{V}(t) - \xi^4/\mathcal{V}(t)$ in (3.31) accounts for the overlap between time-dependent coherent states of opposite sign and the initially laser-generated coherent states. This feature is a consequence of the optimal pair of states and shows notable similarity to the critical model of Ref. [52].

Let us remark that the above formula is completely general and specific of the dynamical steps (3.20) only. The nature of the chain, that is either linear or zig-zag, is fully encoded in ξ, $A(t)$ and $B(t)$ only. In the following subsections we will analyze in detail the behavior of both $D_{\text{opt}}(t)$ and $\mathcal{N}$ in two complementary time regimes.

3.6.1 Short time scale

In this section we analyze the short time behavior of the backflow of information. First, let us clarify how we define this regime. Since we are dealing with a finite system recurrences in any kind of interferometric signal are expected. The exci-

tation created by the initial laser pulse propagates across the crystal and results in oscillations of the chain that will be asynchronous up to a certain time t_R. At this instant a quasi-synchronous collective behavior will occur, leading to a strong revival in the fringe visibility. This revival time can also be seen as the time that it takes for the initial excitation to travel through the crystal and back to the target ion. It can be estimated with the following formula

$$t_R = \frac{Na}{v_{\max}}, \tag{3.32}$$

where $v_{\max} = \partial\omega_y/\partial k|_{\max}$ is the maximum group velocity allowed in the first Brillouin zone. Thus, we set an upper bound $t_M < t_R$ to the elapsed time and this will also be the upper integration limit in Eq.(3.10). In the experimental set up in [33], this t_M would roughly correspond to 250μs.

We first investigate the time-evolution of the optimal trace distance on the linear side of the phase transition for two different values of the tuning parameter, see Fig.3.3 with $\tau = \omega_0 t$. The black curve shows the behavior at $\Delta = 10^{-1}$, hence not very close to the critical point. After a significant initial drop we observe some lightly damped oscillations up to a revival time $\tau_R \approx 150$. When the chain is instead pushed very close to criticality, red curve at $\Delta = 10^{-5}$, we observe a completely different behavior for D_{opt}. The trace distance is abruptly damped up to a shorter revival time $\tau_R \approx 120$. Some tiny oscillations are still present and the revival peak is more pronounced that in the black curve. Based on this plot we expect the non-Markovianity measure $\mathcal{N}$ to show a local minimum at $\Delta = 0$, at least as long as the elapsed time is smaller than τ_R. In this way, all the memory effects we observe are due only to the exchange of information between the two-level system and the rest of the chain and no finite-size effects are involved.

The behavior of $\mathcal{N}$ as a function of Δ is shown in Fig.3.4 for $N = 100, 1000$. The point $\Delta = 0$ represents the critical point and in the harmonic approximation employed here we can go as close to it as 10^{-6} on both sides. A clear and rather sudden change in the behavior of $\mathcal{N}$ very near the critical point is observed. This minimum coincides with the occurring of the structural phase transition and is in perfect agreement with the time-evolution of the optimal trace distance for smaller and smaller values of Δ.

Even though the non-Markovianity measure is not symmetric around the critical point, $\mathcal{N}_{\Delta\to 0^-}$ and $\mathcal{N}_{\Delta\to 0^+}$ converge to the same value, which appears to be a non-zero absolute minimum, at least in the Δ range here considered. As the environment approaches the critical point the dynamics of the probe becomes less non-Markovian. We would like to stress that the behavior shown in Fig.3.4 is characteristic of a second order phase transition. Even if $\mathcal{N}$ is a continuous function when $\Delta \to 0^{\pm}$, its

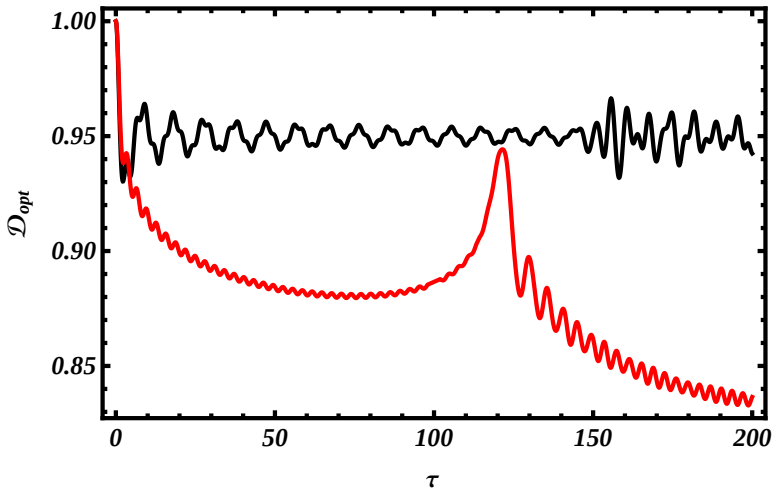

Figure 3.3: Short-time-scale dynamics: Time-evolution of the trace distance for the maximizing pair $\{|+\rangle, |-\rangle\}$ for $N = 100$, far from the critical point (black line, $\Delta = 10^{-1}$) and very close to it (red line, $\Delta = 10^{-5}$).

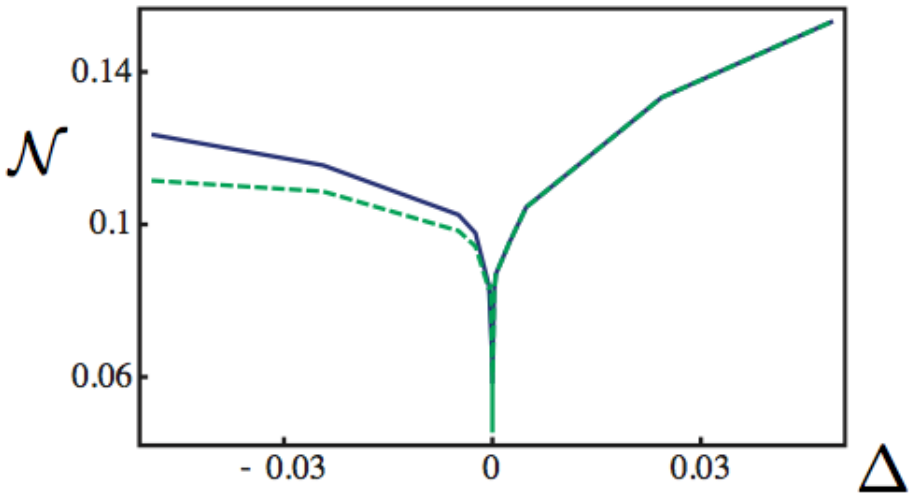

Figure 3.4: Short-time-scale dynamics: Non-Markovianity measure $\mathcal{N}$ for short time-scale truncation as a function of Δ for $N = 100$ (blue solid line) and $N = 1000$ (green dashed line).

derivative is not. A similar feature is found when one studies derivatives of thermodynamical and statistical quantities in presence of a classical and quantum phase transition. Obviously, this observation does not necessarily imply that $\mathcal{N}$ is a critical quantity in general.

3.6.2 Long time-scale in the thermodynamic limit

We now move to investigating the long-time scale behavior, corresponding to roughly $t_M \approx 5$ ms if we consider the set up in [33]. Here, the elapsed time t is long enough to allow for the direct observation of the soft-mode dynamics, as detected by the two-level system. The following discussion, however, is to be considered as a qualitative description of what happens in the thermodynamic limit only. In Coulomb crystals, such limit corresponds to taking the following limits $N \to \infty, L \to \infty$ and keeping a constant. In slow and coarse-grained regime, when the environment is pushed to criticality, anharmonic terms, arising from a Ginzburg-Landau expansion of the chain Hamiltonian (3.11) can become relevant [39] and lead to a breakdown of the harmonic approximation. Unfortunately, an exact and full ab-initio calculation of the collective dynamics of a Coulomb chain is still missing and all the existing models are based upon a perturbative approach in the neighborhood of the critical point. The following argument aims to suggest why, even in this long time-scale, a second order expansion could still be reasonable as long as we are approximately in the thermodynamic limit. Within the framework of Landau theory, it was shown in [39] that the 4^{th}-order contribution to a Taylor expansion of Hamiltonian (3.11), namely $V^{(4)}$ scales at criticality as ω_0^2/Na^2, whereas $\omega \approx \omega_0\Delta + \delta k$ for all the relevant modes near the soft mode ($\delta k = 0$). As the thermodynamic limit is defined via the condition that, for $N \to \infty$, a remains constant, it is easy to check that $\omega/V^{(4)} \gg 1$ for $N \gg 1$. For instance, if we take $N = 300$ and $\Delta = +10^{-6}$ we obtain that $\omega/V^{(4)} \approx 10^4$ for $0 \leq \delta k \leq 10^{-5}$. We again stress that this is an estimate based on an effective perturbative expansion of the crystal Hamiltonian. For a more detailed description, see [39].

The time-evolution of the optimal trace distance in this case is displayed in Fig. 3.5 again in the linear regime, for $\Delta = 0.1, 10^{-6}$ and $N = 300$. The colors are chosen as in Fig.3.3. Contrary to what happens in the short-time-scale regime, when the crystal is pushed closer and closer to criticality, the optimal trace distance displays wider and wider oscillations in time. Hence, the non-Markovianity measure should increase as the chain approaches the critical point. Fig.3.6 indeed confirms this idea: $\mathcal{N}$ displays a cusp-like maximum when $\Delta \to 0^{\pm}$.

As we mentioned earlier the soft-mode at $k = \pi/a$ drives the linear chain across the transition causing the periodic zig-zag deformation. The wide oscillations in red in Fig.3.5 are at the soft-mode frequency: the coupling between this mode and the single spin appears to dominate over all the modes, whose presence still manifest in a slowly damped dynamics of the optimal trance distance. The phononic background, which forces the system to dephase strongly at short-time-scales near criticality, is here overruled by an effective one-to-one coupling between the target ion and the

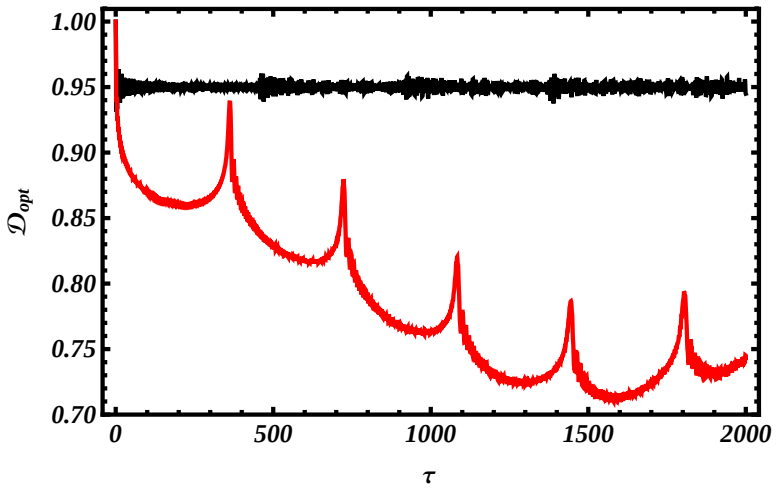

Figure 3.5: Long-time-scale dynamics: Time-evolution of the trace distance for the maximizing pair $\{|+\rangle, |-\rangle\}$ for $N = 300$, far from the critical point (black line, $\Delta = 0.1$) and very close to it (red line, $\Delta = 10^{-6}$).

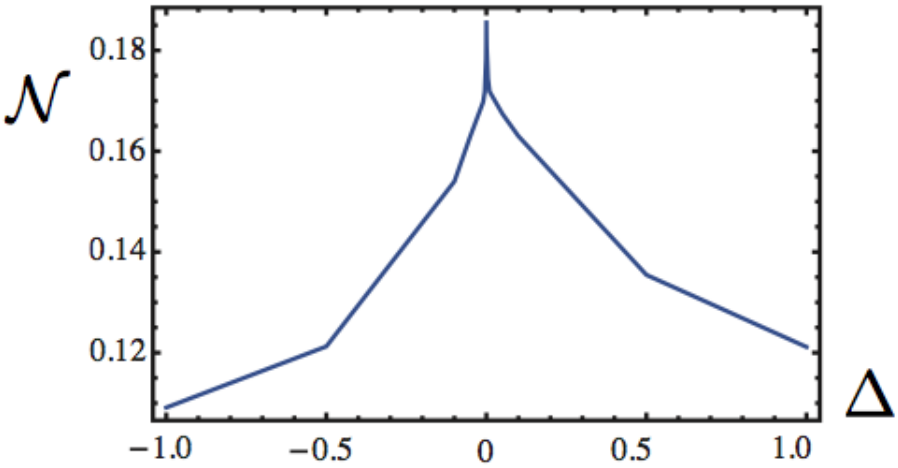

Figure 3.6: Long-time-scale dynamics: Non-Markovianity measure $\mathcal{N}$ for long time-scale truncation as a function of Δ for $N = 300$.

soft mode. In this sense, all the modes at $k \neq \pi/a$ act as a weak source of noise for the hybrid system composed by the 1/2 spin and the soft mode. These two opposite behaviors are not at all incompatible. Although the two-level system and the soft mode always couples very strongly at criticality, for short times the first is able to resolve only the high-energy part of the environment spectrum corresponding to lower momenta. Instead, when we wait long enough, revivals in the $D_{\text{opt}}(t)$ will show up resulting in a the peak in non-Markovianity.

3.6.3 Finite size effects

In this last subsection we study how a finite number of ions affects the above results. This is important for two reasons. First, in the standard theory of open quantum systems usually one assumes that the environment consists of an infinite and continuous number of degrees of freedom. Thus, to see what happens when this condition is not fulfilled is interesting from a foundational point of view. Second, since in the short-time regime we know the harmonic approximation to be valid to an excellent level of accuracy, we can calculate the non-Markovianity measure near criticality for an increasing number of ions in the chain and find out how quickly we approach the thermodynamic limit. The results are displayed in Fig. 3.7. The critical non-Markovianity $\mathcal{N}_{cr}$ saturates to a small non-zero value very soon and no significant deviation from this value is observed up to at least $N = 2000$ (not shown). Finite-size effects that translate to faster recurrences and would lead to a larger value of the non-Markovianity measure, are relevant only for relatively small N and no appreciable variation of $\mathcal{N}_{cr}$ is detectable as soon as $N > 100$. The thermodynamic limit is very quickly reached and the interesting fact is that the flow of information from the two-level system to the rest of the chain is never complete. At short-time sclaes only the high-energy part of the spectrum (small k) is resolved by the probe. This portion of the environment excitation spectrum is essentially flat ($\partial\omega(k)/\partial k|_{k=0} = 0$) meaning that all these modes dephase and rephase almost in sync. The system leaks information on average only since the dephasing and rephasing cycles repeat many times within the short time interval we consider. Some of this information does not flow out. This effect is further enhanced by short-time recurrences, which are simple mechanical excitations going back to the system.

3.7 Temperature

All the previous results were presented assuming the Coulomb crystal to be at zero-temperature. This means that no thermal excitations would be present at any point during the Ramsey protocol. All the excitations created in the chain would arise from pure laser-assisted interaction with the single two-level system and they would coherently evolve at all times. If we initialized the environment to a thermal state, we might expect some of the previous results to no longer hold true. This is precisely what this section is all about. We will repeat the same investigation, however focusing on a short-time regime only, assuming the following initial joint state of system and environment

$$\rho_I = |\phi_0\rangle\langle\phi_0| \otimes \rho_T, \tag{3.33}$$

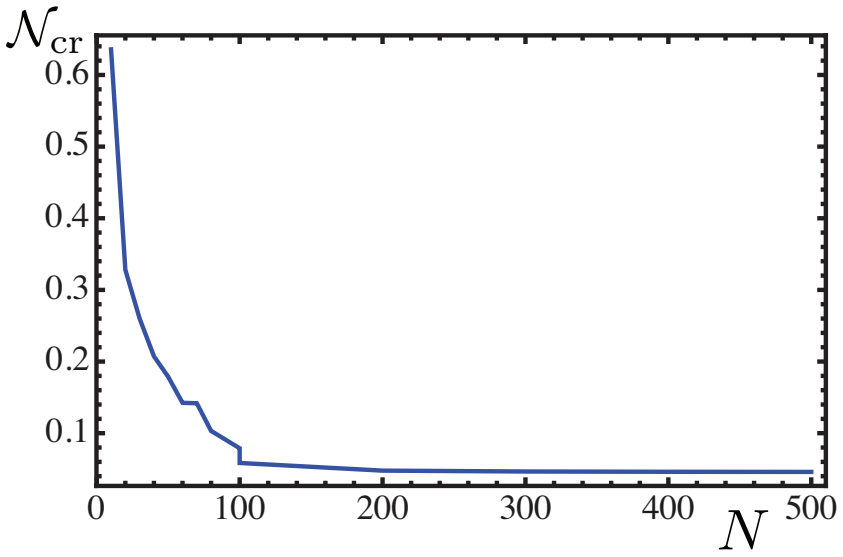

Figure 3.7: Short-time-scale: non-Markovianity measure $\mathcal{N}_{cr}$ at criticality as a function of the number of ions N.

where the initial system pure state is again generic linear superposition and the environment state is a multi-mode factorized thermal state

$$\begin{aligned} |\phi_0\rangle &= \cos\left(\frac{\theta}{2}\right)|e\rangle + e^{i\phi}\sin\left(\frac{\theta}{2}\right)|g\rangle, \\ \rho_T &= \bigotimes_{k,\sigma}\left(\sum_{n_{k,\sigma}=0}^{\infty}\frac{e^{-\beta\hbar\omega(k)n_{k,\sigma}}}{Z_{k,\sigma}}|n_{k,\sigma}\rangle\langle n_{k,\sigma}|\right), \end{aligned} \tag{3.34}$$

where $\beta = 1/k_BT, \omega(k) \equiv \omega_\perp(k)$, $Z_{k,\sigma} = \sum_{n_{k,\sigma}=0}^{\infty} e^{-\beta\hbar\omega(k)n_{k,\sigma}}$ and σ indicates the mode parity. Once again, the reduced density matrix for the system dynamics can be easily obtained from the global dynamics by partially tracing out the vibrational degrees of the chain. If the initial temperature of the chain is not too high, as compared to its largest transverse frequency, we can look at this thermal character as a weak perturbation to $S+E$ state initialization. Hence, the A, B, ξ quantities in Eq.(3.27) as well as the visibility $\mathcal{V}$ change as follows [101]

$$\begin{aligned} A(t,\beta) &= 2\sum_{k,\sigma}|\alpha_{k,\sigma}|^2\coth\left(\frac{\hbar\omega_k\beta}{2}\right)\sin^2\left(\omega_k t/2\right), \\ B(t,\beta) &= \sum_{k,\sigma}|\alpha_{k,\sigma}|^2\coth\left(\frac{\hbar\omega_k\beta}{2}\right)\sin(\omega_k t), \\ \xi(\beta) &= \exp\left[-\sum_{k,\sigma}|\alpha_{k,\sigma}|^2/2\coth\left(\frac{\hbar\omega_k\beta}{2}\right)\right], \\ \mathcal{V}(t,\beta) &= \exp\left[-A(t,\beta)\right]. \end{aligned} \tag{3.35}$$

It is straightforward to check that in the $T \to 0$ limit Eqs.(3.35) reduce to Eq.(3.27). In this low-temperature limit we assume the maximizing pair to be the same as in the $T = 0$ case, that is the eigenstates of $\hat{\sigma}_x$. The optimal trace distance reads as

$$D_{opt}(t,\beta) \approx \frac{1}{4}\left|1 + 2\cos\left[B(t,\beta)\right]\left(\mathcal{V}(t,\beta) - \frac{\xi^4(\beta)}{\mathcal{V}(t,\beta)}\right) + \mathcal{V}^4(t,\beta) + 2\xi^4(\beta)\right|, \quad (3.36)$$

The time-evolution of the optimal trace distance for increasing values of the chain's temperature, far from criticality at $\Delta = 0.1$ and for $N = 100$ is displayed in Fig.3.8. When we increase the initial temperature with respect to the largest frequency $\omega_{\max}$ the overall value of D_{opt} decreases. However, the amplitude of its oscillations in time increases. The flow of information is greatly amplified when the initial temperature of the chain is higher.

However, a simple argument can be used to understand this effect. Loosely speaking, as the environment is initialized in a thermal state, several modes are already well populated to begin with. Since the two-level system couples with the same strength to all the modes of the environment (see Eq.(3.16)) the more modes are initially excited, the more the interaction will be distributed among them. Another interesting feature of this regime is that the oscillations of D_{opt} are roughly in phase regardless of the initial temperature of the chain.

When, instead, the environment is pushed close to criticality a different behavior arises, see Fig.3.9. Now, an increasing initial temperature causes the optimal trace distance to decay much more rapidly. On the contrary, the amplitude of the very few oscillations we can observe does not appear to be significantly affected. Furthermore, all these curves saturate to the same value for later times. This behavior is exactly the opposite of what we observe far from criticality.

Similarly to the $T = 0$ scenario we again want to have a quantitative and time-independent picture of the connection between critical behavior and backflow of information. Hence, we study the non-Markovianity $\mathcal{N}$ as a function of Δ. The truncation time, that is the upper integration limit, is chosen to be $\omega_0 t_T \approx 120$. Once, again, we notice a clear dip in $\mathcal{N}$ in the proximity of the critical point, located at $\Delta = 0$. An interesting feature of Fig.3.10 is that when the temperature of the environment increases the steepness of the dip decreases. This effect is especially obvious when looking at the green curve, corresponding to the highest temperature, on the zig-zag side of the transition. It is also interesting to notice that far from criticality the higher the temperature the more non-Markovian the environment: this is in agreement with the dynamics of the trace distance displayed in Fig.3.8.

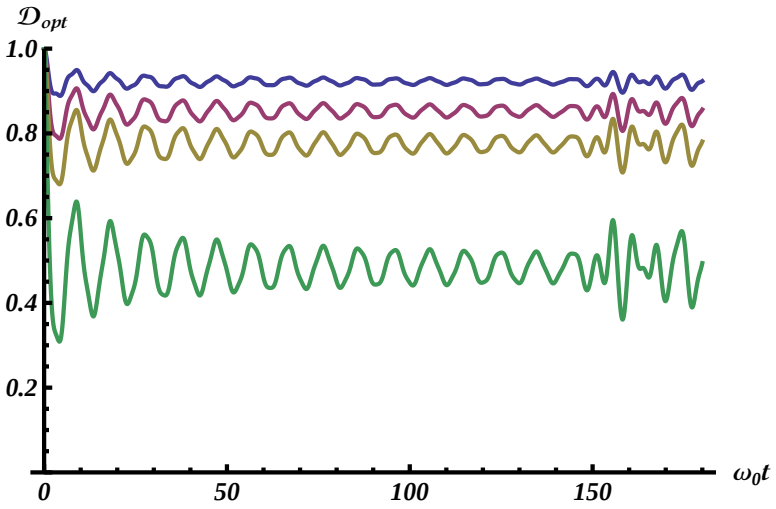

Figure 3.8: Time-evolution of $D_{opt}(t, \beta)$ at $\Delta = 0.1$ for $N = 100$ and four different values of temperature: $\beta\hbar\omega_{\max} = 0.3$ purple, $\beta\hbar\omega_{\max} = 0.7$ dark pink, $\beta\hbar\omega_{\max} = 1.2$ dark yellow and $\beta\hbar\omega_{\max} = 4.3$ green.

3.8 Conclusions

In this chapter we have used an open quantum system approach to investigate the critical dynamics of a Coulomb crystal. Equipped with a single and controllable quantum object, a 1/2 fictitious spin, and a probing protocol, Ramsey interferometry, we have proven the decoherence induced on the spin by the rest of the chain to be extremely sensitive to critical behavior.

To obtain quantitative results, we have investigated and quantified the non-Markovian character of the probing process, as measured by $\mathcal{N}$. Sudden changes in $\mathcal{N}$ as a function of the tuning parameter Δ are observed whenever the chain undergoes the linear-to-zig-zag phase transition. These result in extrema that not only unambiguously pinpoint criticality but whose nature also reflects the physics at different time-scales.

Furthermore, an analytical link between the backflow of information, as measured by $D(t)$, and the visibility of the Ramsey fringes has been established, allowing for a direct experimental observation of $\mathcal{N}$ near criticality and within the validity of the approximations used.

We have performed the analysis both in the case of zero and finite, but small, temperature. The findings are very similar and totally compatible with each other. In particular, accounting for an initial thermal character of the Coulomb crystal caused by a non-perfect state-initialization, provides a more realistic model.

Our results seem indicate that this type of approach allows one to successfully detect abrupt changes in the dynamics of a many-body systems, such as phase transitions, by means of a local quantum probe.

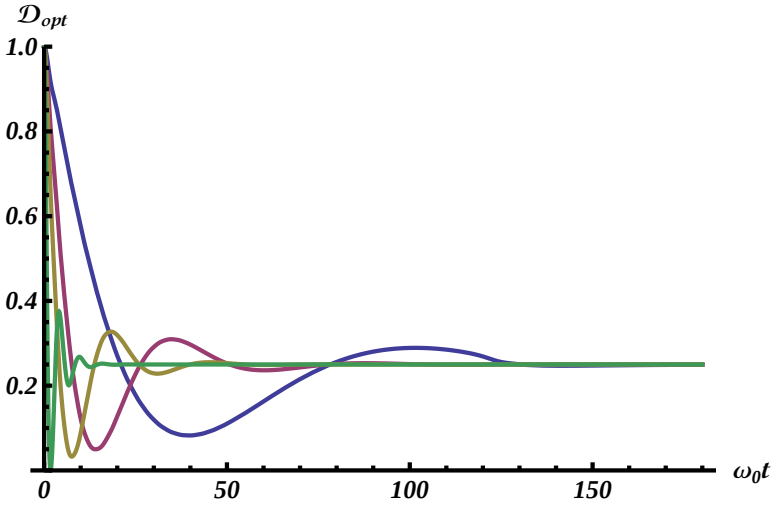

Figure 3.9: Time-evolution of $D_{opt}(t, \beta)$ at $\Delta = 10^{-5}$ for $N = 100$ and four different values of temperature: $\beta\hbar\omega_{\max} = 0.3$ purple, $\beta\hbar\omega_{\max} = 0.7$ dark pink, $\beta\hbar\omega_{\max} = 1.2$ dark yellow and $\beta\hbar\omega_{\max} = 4.3$ green.

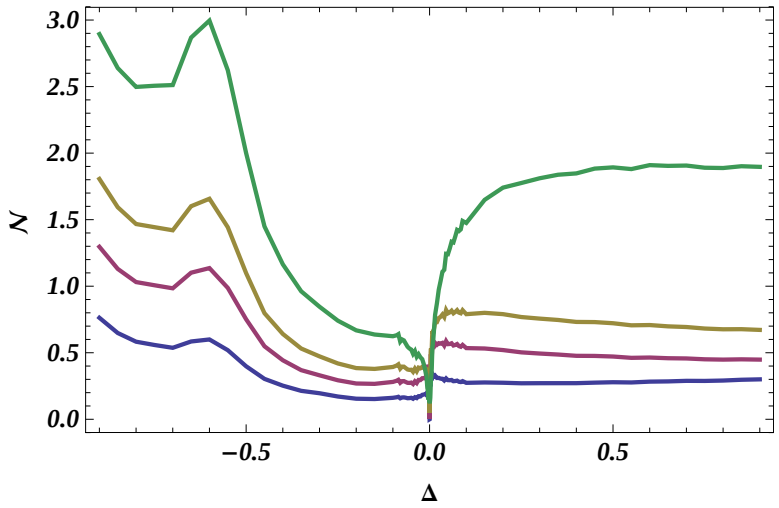

Figure 3.10: Non-Markovianity measure $\mathcal{N}$ as a function of the relative distance Δ for four different values of temperature: $\beta\hbar\omega_{\max} = 0.3$ purple, $\beta\hbar\omega_{\max} = 0.7$ dark pink, $\beta\hbar\omega_{\max} = 1.2$ dark yellow and $\beta\hbar\omega_{\max} = 4.3$ green. The truncation time in $\mathcal{N}$ is about $\omega_0 t_T \approx 120$.

Chapter 4

Quantum correlations in the two-atom Fermi problem

4.1 A brief introduction to the Fermi two-atom model

The Fermi model, in its original conception, can be seen as a *gedanken* experiment enquiring about the causal behavior of quantum probabilities. Suppose two identical atoms are located at two points in space and time, say $r_A = (x_A, 0, 0, t_A)$ and $r_B = (x_B, 0, 0, t_B)$ separated by a spatial distance $R = r_B - r_A$. They both independently interact with a multimode, quantized electromagnetic field $\hat{E}(r)$. Let us assume that at $t = 0$ the atom A is in an excited state $|e\rangle$, the atom B is in its ground state $|g\rangle$ and no photons are present. Because of the interaction, at some time $t > 0$ the atom A will decay to its ground state and emit a traveling photon that will be most likely absorbed by B at some later time.
As long as the two atoms are causally disconnected, that is their light cones do not intersect, is the excitation probability of B completely independent on the presence of A? Stated in a more general fashion: do transition probabilities in quantum mechanics respect the principle of causality?
This question was first addressed by Fermi back in 1932 [57] who gave it a positive answer: the probability amplitude of the state $|g_A, e_B, 0\rangle$, where the atoms have swapped the photonic excitation, starts increasing only after the they have become causally connected. Despite its simplicity, this result generated a long academic debate for the years to come. Most of the criticism to Fermi's solution was due to subtle technical flaws in his original calculation, such as use of the rotating-wave-approximation (RWA) and inclusion of negative frequencies of the field [58]. This problem was then further analyzed using different models and approximations. Generally speaking, all of the following results were obtained within the framework of

perturbation theory [59, 61, 62].
Through the years, it became clear how this question concerning the very foundations of quantum field theory, could be addressed from very different perspectives. In a series of papers a violation of Einstein's principle of causality was found and investigated in connection with the problem of state localization in quantum mechanics, the difficulties connected to using a bare-state representation for the atoms and the field and the attempt of defining in a rigorous operative way the act of measuring the excitation probabilities of the second atom [60, 104].
In a very recent paper, a strict proof of causality in the Fermi two-atom problem was given where, by causality, the authors mean a complete independence of the excitation probability of B upon A for $t < r/c$ [105]. On the other hand, it was also shown how two-point correlation functions can be non-zero outside the light cone. This result obviously does not violate causality: turning correlations into useful information implies transmission and that is proven to be causal.
In this chapter we address the problem of how more general types of quantum correlations behave in relation to causality. In particular we will focus our attention on entanglement [65], quantum discord [68, 69] and correlation functions [67]. Furthermore, we will also study non-locality, as quantified by the violation of Bell-type inequality [106, 107]. All the following results will be derived within the framework of second-order time dependent perturbation theory. The content of this chapter is mostly based on the findings reported in Ref. [64].

4.2 The Fermi model: perturbative time-evolution of the two-atom state

The Hamiltonian describing the two-atom Fermi problem in the two-level dipolar approximation can be expressed as follows [108]

$$\hat{H} = \frac{1}{2}\hbar(\Omega_A\hat{\sigma}_A^z + \Omega_B\hat{\sigma}_B^z) + \int_{-\infty}^{\infty} dk\, \hbar\omega_k \hat{a}_k^\dagger \hat{a}_k + \sum_{j=A,B} \hat{V}(x_j), \tag{4.1}$$

with the single-atom interaction potential given by

$$\hat{V}(x_j) = d_j \int dk \sqrt{N\omega_k} \left[e^{ikx_j}\hat{a}_k + e^{-ikx_j}\hat{a}_k^\dagger \right] \hat{\sigma}_j^x, \tag{4.2}$$

where $\hat{\sigma}_j^\alpha$ is the α Pauli operator for the j-th atom, we assume a linear dispersion relation $\omega_k = \upsilon|k|$ where $\upsilon = c$ in vacuum, $a_k, a_k^\dagger$ are the usual annihilation and creation operator satisfying boson commutation relations $[a_k, a_{k'}^\dagger] = \delta_{k,k'}$, $\Omega_j = \omega_{j,e} - \omega_{j,g}$ is the energy separations between the atomic internal levels and d_j is the

dipole operator amplitude $\langle e_j|\hat{\sigma}_j^x|g_j\rangle$ $(j = A, B)$. N is a normalization constant. As usual in QED, the size of the atoms are assumed to be much smaller that the relevant wavelengths $\lambda_j = \upsilon/(\Omega_j/(2\pi))$, that is, the atoms are localized and their positions can be considered as classical known variables [99]. The dynamics generated by the Hamiltonian (4.1) cannot be calculated exactly unless the counter rotating terms are neglected [99]. If we expand

$$\hat{\sigma}^x = \hat{\sigma}^+ + \hat{\sigma}^-, \tag{4.3}$$

where $\hat{\sigma}^\pm$ are the atom annihilation/creation operators, then the counter-rotating part $\hat{H}^{CR}$ of the Hamiltonian reads as

$$\hat{H}^{CR} = \sum_{j=A,B} d_j \int dk \sqrt{N\omega_k} \left[\hat{\sigma}_j^+ \hat{a}^\dagger e^{-ikx_j} + \hat{\sigma}_j^- \hat{a} e^{ikx_j}\right], \tag{4.4}$$

The above Hamiltonian creates or annihilates atom and field excitations simultaneously. This, in turn, translates to an infinite set of differential equations which is obviously an impossible task to address. Thus, a perturbative approach that relies on expanding the Heisenberg equations or, equivalently, the time evolution operator in interaction picture is necessary [108]. Furthermore, as demonstrated in [59], it is precisely the presence of non-rotating terms that accounts for the causal behavior of the equations of motions, already at the lowest order of perturbation. This constraints both the time-scale and the coupling regimes that we can access in our analysis.

The initial state of the composite system is

$$|\phi(0)\rangle = |e_A, g_B, 0\rangle\,. \tag{4.5}$$

As anticipated above both the atoms and the field are initialized in some precise bare states of the respective non-interacting Hamiltonians. We switch on the atom-field interactions $\hat{V}(x_j)$ and study the dynamics of the three-body system up to a certain time $t_{\max}$ compatible with our perturbative theory. In interaction picture with respect to the free Hamiltonian

$$\hat{H}_0 = \frac{1}{2}\hbar(\Omega_A\hat{\sigma}_A^z + \Omega_A\hat{\sigma}_A^z) + \int_{-\infty}^{\infty} dk\, \hbar\omega_k \hat{a}_k^\dagger \hat{a}_k, \tag{4.6}$$

the state of the system at time t reads as

$$|\phi(t)\rangle = T[e^{-i\int_0^t dt' \hat{V}_I(t')/\hbar}]|\phi(0)\rangle, \tag{4.7}$$

where

$$\hat{V}_I(t) = e^{-\frac{i\hat{H}_0 t}{\hbar}} \left[\sum_{j=A,B} \hat{V}(x_j) \right] e^{\frac{i\hat{H}_0 t}{\hbar}}, \tag{4.8}$$

and T is the time ordering operator. If we expand the time-evolution operator up to second order in the coupling amplitude d we obtain the following time-evolved state [64, 108]

$$\begin{aligned} |\phi(t)\rangle = &[(1+A)\,|eg\rangle + X\,|ge\rangle] \otimes |0\rangle + (U_A\,|gg\rangle + V_B\,|ee\rangle) \otimes |1\rangle \\ &+ (F\,|eg\rangle + G\,|ge\rangle) \otimes |2\rangle + \mathcal{O}(d^3). \end{aligned}$$

To compute the coefficients for the vacuum, single-photon, and two-photon states, we define the atom-action operator ($j = A, B$)

$$\mathcal{S}_\alpha^+ = -\frac{i}{\hbar} \int_0^t e^{i\Omega_j t'} \left\langle e_j | d\sigma_j^x | g_j \right\rangle V(x_j, t') dt' = -(\mathcal{S}_j^-)^\dagger, \tag{4.9}$$

and calculate its matrix elements among collective Fock states of the field $|n\rangle, n = 0, 1, 2 \ldots$, being

$$|n\rangle \langle n| = \frac{1}{n!} \int dk_1 .... \int dk_n \, |k_1 ... k_n\rangle \langle k_1 ... k_n| \,, \tag{4.10}$$

and $|k\rangle = a_k^\dagger |0\rangle$. Each of the coefficients in the perturbative expansion (4.9) is associated to a well-defined physical process. The first order terms U_A and V_B account for single-photon emission and absorption by a single atom. It is worth noticing that in these two terms no effective connection between the two atoms is present and hence we cannot expect them to manifest any causal behavior. The very contribution representing a photon exchange between A and B is

$$X = \langle 0 | T(\mathcal{S}_B^+ \mathcal{S}_A^-) | 0 \rangle. \tag{4.11}$$

This includes real photon exchange only inside the light cone, $vt > r$. However, vacuum fluctuations, associated to virtual photon clouds surrounding the atoms, are present for all values of t and r. The remaining terms are

$$\begin{aligned} A &= \frac{1}{2} \langle 0 | \, T(\mathcal{S}_A^+ \mathcal{S}_A^- + \mathcal{S}_B^- \mathcal{S}_B^+) \, |0\rangle \,, \\ F &= \frac{1}{2} \langle 2 | \, T(\mathcal{S}_A^+ \mathcal{S}_A^- + \mathcal{S}_B^- \mathcal{S}_B^+) \, |0\rangle \,, , \, G = \langle 2 | \, T(\mathcal{S}_B^+ \mathcal{S}_A^-) \, |0\rangle \,. \end{aligned} \tag{4.12}$$

The A term describes intra-qubit radiative corrections, while F and G correspond to single-photon emission events by more qubits resulting in a larger number of real photons. The coefficients in Eq. (4.9) can be computed analytically as a function of

two dimensionless parameters, ξ and K. The first one, $\xi = \upsilon t/r$, is a dimensionless time variable; $\xi = 1$ corresponds to the light-cone that separates two different space-time regions. $\xi < 1$ corresponds to the two atoms being causally disconnected with only virtual photons being exchangeable whereas for $\xi > 1$ the atoms are causally connected and real photons can be exchanged. The second parameter is a renormalized, dimensionless coupling strength

$$K = \frac{4d^2 N}{\hbar^2 \upsilon} = 2\left(\frac{g}{\Omega}\right)^2. \tag{4.13}$$

Since we are interested in classical and quantum correlations generated between the two atoms we need to discard the field. Thus we perform a partial trace over the field's degrees of freedom leading to the following atom-atom density matrix

$$\rho_{\mathrm{X}} = \frac{1}{c}\begin{pmatrix} \rho_{11} & 0 & 0 & \rho_{14} \\ 0 & \rho_{22} & \rho_{23} & 0 \\ 0 & \rho_{23}^* & \rho_{33} & 0 \\ \rho_{14}^* & 0 & 0 & \rho_{44} \end{pmatrix}, \tag{4.14}$$

in the basis formed by $|ee\rangle$, $|eg\rangle$, $|ge\rangle$, and $|gg\rangle$. The coefficients with the leading order of neglected contributions are [64, 108]

$$\begin{aligned} \rho_{11} &= |V|_B^2 + \mathcal{O}(d^4),\ \rho_{22} = 1 + 2\mathrm{Re}(A) + \mathcal{O}(d^4), \\ \rho_{33} &= |X|^2 + |G|^2 + \mathcal{O}(d^6),\ \rho_{44} = |U|_A^2 + \mathcal{O}(d^4), \\ \rho_{14} &= U_A^* V_B + \mathcal{O}(d^4) = \langle 0|\mathcal{S}_A^+ \mathcal{S}_B^+|0\rangle + \mathcal{O}(d^4), \\ \rho_{23} &= X^* + \mathcal{O}(d^4), \end{aligned} \tag{4.15}$$

and the state is normalized, $c = \sum_i \rho_{ii}$.

4.3 Quantum correlations and quantumness of correlations

In this section we shall introduce entanglement and geometric quantum discord. Loosely speaking, one can look at entanglement as the result of superposition principle acting in systems with more than one particle. Quantum discord can instead be seen as a direct consequence of the measurement-and-collapse postulate of quantum mechanics. Although they pertain to different aspects of quantum theory they both miss a classical counterpart.

4.3.1 Entanglement

Entanglement is a genuinely quantum property that arises in multipartite systems and manifests itself as correlations that can not be explained or predicted classically [65]. It is a consequence of the superposition principle along with the Hilbert space tensor product assumption for composite systems. Quantum entanglement has been proven to be a powerful resource as it allows for the implementation of quantum information protocols that are otherwise impossible, such as quantum teleportation [109], and for a significant speed-up in quantum computation [110]. Moreover, direct applications to cryptography have been demonstrated [111]. Entanglement has been the subject of intense studies in many different areas of quantum physics, ranging from quantum optics to many-body theory, and major efforts have been made to formulate a theory for entanglement both in discrete [65] and continuous variable systems [112]. Several ways of detecting and measuring entanglement have been theoretically proposed and, in most cases, experimentally tested [113]. Needless to say, the literature regarding this topic is extremely vast and a complete review goes well beyond the purpose of this thesis. Here, we focus our attention on bipartite systems, which are relevant for our following discussions.

Let us assume two quantum systems, whose Hilbert space we name $\mathcal{H}_A$ and $\mathcal{H}_B$ with dimensions d_A and d_B respectively. Given a composite state $|\psi\rangle$ of A and B we call it separable if two local states $|\psi_A\rangle \in \mathcal{H}_A$ and $|\psi_B\rangle \in \mathcal{H}_B$ exist such that

$$|\psi\rangle = |\psi_A\rangle \otimes |\psi_B\rangle \,. \tag{4.16}$$

On the contrary, if no such a representation exists, we call $|\psi\rangle$ entangled. This definition can be extended to mixed states. We say the composite mixed state $\hat{\rho}$ is separable if it can be written as a convex combination of local product states

$$\hat{\rho} = \sum_i p_i \hat{\rho}_i^A \otimes \hat{\rho}_i^B, \tag{4.17}$$

where $p_i \geq 0$, ρ_i^A, ρ_i^B belong to $\mathcal{H}_A, \mathcal{H}_B$ respectively for every i and $\sum_i p_i = 1$. Analogously to the pure state case we say $\hat{\rho}$ is entangled if no expansion (4.17) exists. A separable state can always be prepared by means of local unitary operations in $\mathcal{H}_A$ and $\mathcal{H}_B$ respectively, coordinated by classical communication between the two subsystems A and B (LOCC). Any kind of correlation, if present, is of purely classical origin.

For general bipartite systems a sufficient entanglement-detection criterion exists based on partial transposition of the total density matrix, known as PPT criterion [114, 115]. Furthermore, when applied to two-level system not only is the PPT criterion sufficient but also necessary. In the following we outline the main idea

behind PPT.
Separability can be revealed with the aid of positive maps. Partial transposition is a positive map. However, it is not completely positive and so it does not represent any physical process. It can be shown that when we partially transpose a separable state of the form (4.17) we are not affecting neither its separability nor its physicality. This implies that all of its eigenvalues will be still positive after partial transposition. Thus, if are given a physical state $\hat{\rho}$ (all eigenvalues are positive), we partially transpose it with respect to one of the two parties and at least one of its eigenvalues becomes negative we can conclude that $\hat{\rho}$ is entangled. Obviously the converse is not always true. If we label the partially transposed density matrix $\hat{\rho}^{T_j}$ with $j = A, B$, the following statement

$$\hat{\rho}^{T_j} \text{ has at least one negative eigenvalues } \iff \hat{\rho} \text{ is entangled} \tag{4.18}$$

can be proven to be true if $d_A d_B \leq 6$ [114, 115].
At this stage, we are provided only with a detection criterion or, equivalently, an entanglement witness. To actually quantify the amount of entanglement a measure can be defined, based on the PPT criterion. We call this measure negativity of entanglement N. This quantity is identically zero for all separable states and it does not increase under LOCC operations. In this respect it matches all the requirements for being a valid entanglement measure. For bipartite two-level systems negativity is easily computable. Given a general $d \otimes d$ quantum bipartite state (in our case we will have $d = 2$) $\hat{\rho}$, the (normalized to 1) negativity of entanglement is defined as [116]

$$N(\rho) \doteq \frac{1}{d-1} ||\hat{\rho}^{T_A} - \mathrm{I}_{AB}||_1, \tag{4.19}$$

where the partial transposition operation is taken here with respect to A, I_{AB} is the identity operator in the composed Hilbert space $\mathcal{H}_A \otimes \mathcal{H}_B$ and $||M||_1 = \mathrm{Tr}|M| = \sum_i |m_i|$ is the trace norm for a matrix M with eigenvalues $\{m_i\}$. The same quantity can be defined in terms of partial transposition with respect to B, leading to the same result. Other measures of entanglement for bipartite two-level systems can be introduced such as concurrence and entanglement of formation.

4.3.2 Quantum discord

Recently, a great deal of attention in the quantum physics community has been devoted to the study of quantum correlations other than entanglement. Among them, quantum discord has surely attracted most of the interest as well as skepticism. This quantity was first introduced independently in [68] and [69] as a measure of quantumness of correlations in bipartite systems. The following discussion briefly

summarizes the key points of Ref. [68]
Let us imagine we are given a bipartite system, whose subsystems we label A and B, with density matrix $\hat{\rho}$. We perform a local measurement on one of the parties only, say A. Since in quantum mechanics a measurement alway perturbs or even changes the state of the system to be measured, we can expect that in a two-party scenario such an act might disturb both A and B. Quantum discord can be defined as the minimum disturbance affecting B whenever we measure A in some suitable basis.
The way we operatively put this concept in formulas is by looking at the discrepancy, in the quantum case, between two classically equivalent definitions of mutual information. In classical information theory when we are given a random variable X we quantify the ignorance about it via the Shannon entropy [117]

$$H(X) = -\sum_x p_{X=x} \log p_{X=x}, \tag{4.20}$$

where x labels the possible values of X and $p_{X=x}$ is its probability distribution. When it comes to two random variables X, Y characterized by a joint probability distribution $p_{X,Y}$, we quantify the degree of correlation between the two by introducing the mutual information [118]

$$J(X:Y) = H(X) - H(X|Y), \tag{4.21}$$

where $H(X|Y) = \sum_y p_{Y=y} H(X|Y=y)$ is the conditional entropy of X given $Y=y$. The $p_{Y=y}$ probability distribution is the marginal of the joint one with respect to the X variable. Bayes rule allows us to write $H(X|Y) = H(X,Y) - H(Y)$ where $H(X,Y)$ is the joint entropy. Hence, we can recast Eq.(4.21) in an equivalent form

$$I(X:Y) = H(X) + H(Y) - H(X,Y). \tag{4.22}$$

Classically, Eq.(4.21) and Eq.(4.22) are completely equivalent. Now, let us turn our attention to the quantum scenario. In this case we replace the probability distributions with density matrices $\hat{\rho}$ and the Shannon entropy with the von Neumann entropy [119]

$$H_{VN}(\hat{\rho}) = -\mathrm{Tr}\left(\hat{\rho} \log \hat{\rho}\right). \tag{4.23}$$

With these new ingredients at hand we can straightforwardly generalize Eq.(4.22) to the quantum case whenever we are given a general bipartite state $\hat{\rho}$. The same, however, is not true for J. As anticipated before, in quantum mechanics it might be impossible to gain information about one of the two subsystems without perturbing the state of the other. Hence, the concept of conditional entropy has to be refor-

mulated keeping this fact into account. In other words, the Bayes rule is no longer applicable in the quantum domain. In fact, a conditional bipartite quantum state is such only after we have measured one of the two parties, say A. Projective measurements in quantum mechanics are formalized via a set of projective operators, namely $\{\hat{\Pi}_j^A\}$ corresponding to a certain observable. Assuming a j outcome, the conditional state of the bipartite system after the measurement reads as

$$\hat{\rho}_{j;A} = \frac{\hat{\Pi}_j^A \hat{\rho}\, \hat{\Pi}_j^A}{\mathrm{Tr}\left[\hat{\Pi}_j^A \hat{\rho}\right]}. \tag{4.24}$$

This leads to the following quantum version of Eq.(4.21)

$$J(\hat{\rho} : A)_{\{\hat{\Pi}_j^A\}} = H_{VN}(\hat{\rho}) - \sum_j p_j H_{VN}(\hat{\rho}_{j;A}), \tag{4.25}$$

where $p_j = \mathrm{Tr}\left[\hat{\Pi}_j^A \hat{\rho}\right]$. Quantum discord is defined as

$$\delta(\hat{\rho})_A = I(\hat{\rho}) - \min_{\{\hat{\Pi}_j^A\}} \left[J(\hat{\rho} : A)_{\{\hat{\Pi}_j^A\}}\right], \tag{4.26}$$

where the minimization, to be carried out over all the possible set of local projective measurements, assures that we obtain the minimum disturbance possible that a local measurement performed on A introduces in B. If we apply the same reasoning to B instead of A we will obtain that in general $\delta(\hat{\rho})_A \neq \delta(\hat{\rho})_B$: quantum discord is not symmetric under party exchange. It is straightforward to prove that a bipartite state of the form

$$\hat{\rho} = \sum_j \hat{\Pi}_j^A \hat{\tau} \hat{\Pi}_j^A, \tag{4.27}$$

with $\hat{\tau}$ a general density matrix, has vanishing discord. Conversely, if $\delta(\hat{\rho})_A = 0$ then $\hat{\rho}$ can be written in the form (4.27), in some suitable local basis.

It is important to underline that entanglement and quantum discord embody different aspects regarding correlations. As mentioned above, entanglement is a direct consequence of the linear superposition principle which, in turn, is a consequence of the first postulate of quantum theory regarding the state of a physical system and its preparation. Quantum discord comes instead straight from the measure-and-collapse axiom. The common ground these two concepts share is that they exist as such only when we look at composite systems or, more precisely, to a collection of distinguishable degrees of freedom. Although for two-level system pure states quantum discord and entanglement always coincide [68], this is no longer true in the case of mixed states. Furthermore, separable states can have non-vanishing discord [120–124]. The connection between these two quantities is still an open

problem. Also, the possibility for quantum discord to be a resource in quantum technologies has been long investigated. For an exhaustive review about the topic, see [125].

Even though the definition of quantum discord we have introduced above perfectly captures the key idea behind its formulation, it can be rather nasty to calculate due to the maximization process. In order to overcome this difficulty, the authors in [66] introduced a different definition based on a geometric approach: geometric quantum discord $D_A^{(2)}$. The underlying idea is pretty much the same as in (4.26) but geometric discord is much easier to compute for any general bipartite two-level system [126]. Once again, assuming a bipartite quantum state $\hat{\rho}$ with total Hilbert space $\mathcal{H}_A \otimes \mathcal{H}_B$ of dimension $d_A \times d_B$, we define geometric quantum discord as follows

$$D_A^{(2)}(\rho) \doteq \frac{d_A}{d_A - 1} \min_{\hat{\chi} \in \Omega_0} ||\hat{\rho} - \hat{\chi}||_2^2, \tag{4.28}$$

where $\hat{\chi}$ is a so-called classical-quantum state belonging to the set of zero-discord states Ω_0, $\hat{\chi} = \sum_i p_i |i\rangle\langle i| \otimes \hat{\rho}_{iB}$ and$||P - Q||_2^2 = \mathrm{Tr}(P - Q)^2$ is the squared Hilbert-Schmidt distance between a pair of operators P, Q. This definition can be proven to be equivalent to Eq.(4.26) and it has the same operative interpretation in terms of minimum disturbance on B whenever A is measured. For the case of interest, a bipartite two-level system, the geometric discord reads as follows [66]

$$D_A^{(2)}(\rho) = 2\mathrm{Tr}[S] - 2\lambda_{\max}(S), \tag{4.29}$$

where $\lambda_{\max}$ is the largest eigenvalue of the matrix S, that is defined as is defined as $S = \frac{1}{4}(\vec{x}\vec{x}^T + TT^T)$ where the upper T stands for transpose.

4.4 Dynamics of correlations in the two-atom Fermi problem

In this section we investigate the dynamics of negativity of entanglement N, the square root of geometric quantum discord $D^{(2)}$ and maximally connected spin-spin correlation function C for the two-atom state ρ_{X}. The maximally connected correlation function $C(\hat{\rho})$ function is defined as follows [67]

$$C(\hat{\rho}) \doteq \max_{n,n'} \left\{ \langle (\vec{\sigma} \cdot \hat{n})_A \otimes (\vec{\sigma} \cdot \hat{n}')_B \rangle_\rho - \langle (\vec{\sigma} \cdot \hat{n})_A \rangle_{\hat{\rho}} \langle (\vec{\sigma} \cdot \hat{n}')_B \rangle_{\hat{\rho}} \right\}, \tag{4.30}$$

where $\vec{\sigma}$ is the three-component Pauli-operator vector and $(\vec{\sigma} \cdot \hat{n})$ is the projection of such a spin vector along the direction pointed by $\hat{n}$. Obviously, this quantity is

definable both in the classical and the quantum case.
In the following we focus on their temporal behavior in relation to the question of causality and the analysis will involve both classical and quantum correlations, allowing for a direct comparison. One might wonder about the reason for this specific choice of correlations and also why we are comparing different powers. Since all the following results are derived using a time-dependent perturbative expansion of the general definitions (4.19), (4.29), (4.30), we need a test to check whether they are consistent with the limitations that such an approach imposes. A hierarchic relation exists between the three chosen quantities that is valid for any arbitrary state $\hat{\rho}$ of a bipartite two-level system

$$C(\hat{\rho}) \geq \sqrt{D}(\hat{\rho}) \geq N(\hat{\rho})\,. \tag{4.31}$$

The rightmost inequality in (4.31) was proven analytically in [127], while the leftmost one has been verified numerically in [128]. For pure two-qubit states Eq.(4.31) becomes a chain of equalities. Let us consider the following Bloch state representation of a bipartite two-level system [129]

$$\hat{\rho} = \frac{1}{4}\left(\mathrm{I}_1 \otimes \mathrm{I}_2 + \sum_{i=1}^{3} x_i \hat{\sigma}_i \otimes \mathrm{I}_2 + \sum_{j=1}^{3} y_j \mathrm{I}_1 \otimes \hat{\sigma}_j + \sum_{i,j=1}^{3} t_{ij} \hat{\sigma}_i \otimes \hat{\sigma}_j\right),$$

where σ_i $(i = 1, 2, 3)$ are the Pauli operators; $\vec{x} = \{x_i\}$ and $\vec{y} = \{y_i\}$ represent the three-dimensional Bloch vectors associated to the two-level systems A and B, respectively; and t_{ij} are the elements of the 3×3 spin-spin correlation matrix T. The square root of geometric discord of the state (4.14), up to the second order of expansion reads as

$$\sqrt{D_A^{(2)}(\rho_{\mathrm{X}})} = \sqrt{[\mathrm{Re}(U_A^* V_B)]^2 + |X|^2}\,. \tag{4.32}$$

The main contributions to Eq.(4.32) come from first and second order terms that account for 1 and 0-photon states respectively. As a explained above, the X term accounts for excitation-swap between the two atoms and carries all the information available about causal propagation of the traveling signal emitted by the first atom. The negativity of ρ_{X} reads as

$$N(\rho_{\mathrm{X}}) = \max\left\{0,\ \sqrt{(|U_A|^2 - |V_B|^2)^2 + 4|X|^2} - |U_A|^2 - |V_B|^2\right\}, \tag{4.33}$$

and it depends on the same matrix elements as the geometric discord. However, a space-time-dependent constraint for entanglement to grow exists: as long as the

following condition is fulfilled

$$\frac{|X|^2}{|U_A|^2|V_B|^2} \leq 1, \tag{4.34}$$

negativity will be zero. This entanglement activation time tells us that in order for the atoms to get entangled second-order processes must dominate over first-orders. This constraint is absent in the case of geometric discord. Finally, the maximum connected correlation function reads as

$$C(\rho_{\mathrm{X}}) = \max\left\{|U_A|^2 + |V_B|^2 + 2\mathrm{Re}(A), 2(|X| + |L|)\right\}, \tag{4.35}$$

where $L = U_A^* V_B$. Once again, only 0 and 1-photon processes contribute. Similarly to the previous two quantities, $C(\rho_{\mathrm{X}})$ also depends on X.

4.4.1 Results and Discussion

In this section we analyze and compare the time-evolution of the the quantities introduced in previous sections. We remark that the leading terms in the second order of perturbative expansion are U_A, V_B and X, which account for 0 and 1-photon state and are appear in all the correlations we consider here. Interestingly, the maximum connected correlation function C is also dependent upon the A coefficient. The square root of the geometric discord is displayed in Fig.4.1. The spatial distance between the atoms is set to $r = \upsilon\pi/4\Omega$ where $\Omega = \Omega_A = \Omega_B$. Different colors correspond to different values of the coupling parameter, ranging from weak to strong coupling. All the parameters have been set such that the effective coupling constant K (Eq.(4.13)) can be written as a linear function of a parameter Z ranging from 1 to 1000

$$K = \left(1.5 \times 10^{-4}\right) Z, \tag{4.36}$$

The first feature we see is a sharp peak at $\xi = 1$ after a slow but continuous growth starting at $\xi = 0$. The amplitude of such a peak and the global value of $\sqrt{D(\rho_{\mathrm{X}})}$ increase with the coupling strength. The point $\xi = 1$ represents the light-cone and that is when the two atoms become causally connected. After this time real photons can be exchanged. By looking at Eq.(4.32) we can easily understand these features. The square root of geometric quantum discord is the sum of first order contributions (U_A, V_B), which account for single atom processes and do not manifest any causality, and a second order term X that measures the probability of virtual and real photon swapping for $\xi < 1$ and $\xi > 1$ respectively. Thus, the stronger the coupling, the larger X. By recalling the operational interpretation of quantum discord we discussed above, we could argue that a one-party measurement performed

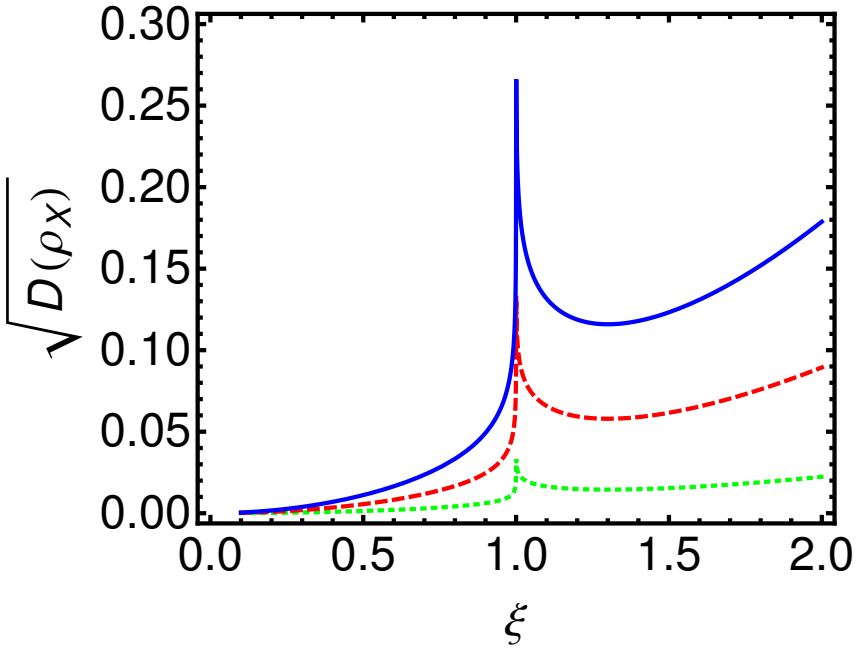

Figure 4.1: Time-evolution of the square root of geometric quantum discord $\sqrt{D(\rho_{\rm X})}$ for $Z = 50$ (dotted green), $Z = 200$ (dashed red), $Z = 400$ (continuous blue).

at any time will always disturb the second party and reveal the presence of the first. Fig.4.2 shows the time evolution of the negativity of entanglement for the same choices of the coupling strength K and the same atom-atom distance. Although a sharp peak is exhibited at $\xi = 1$, the dynamics of N for $\xi < 1$ greatly differs from geometric discord. In fact, entanglement starts increasing sharply just before $\xi = 1$ and it is zero otherwise. This feature was essentially anticipated by Eq.(4.34). Since in the $\xi < 1$ region only vacuum fluctuations are responsible for correlating the two atoms, we may conclude that entanglement is not as sensitive as geometric discord to such effect. Moreover, quantum discord is a more general property of quantum states than entanglement: as anticipated above, a separable quantum state can have non-vanishing discord. Similar results were found in [108] when studying the entanglement as measured by concurrence [130] in the same system.
Finally, Fig.4.3 shows the dynamics of the maximum connected correlation function $C(\hat{\rho}_{\rm X})$. Once again, all the parameters are the same as in previous figures. Pretty much like geometric discord, also the spin-spin correlation function starts increasing significantly for $\xi < 1$ and it as well displays a clear peak at $\xi = 1$. This quantity is not fully quantum *a priori* and tells us how, on average, the Bloch vectors of the two atoms influence each other. The optimal measurements $\hat{n}, \hat{n}'$ are different in different space-like regions. For $\xi < 1$, spin-spin correlations are maximized by measuring the $x - y$ plane component of $\vec{\sigma}$: no real excitation can reach the atom B yet. For $\xi \geq 1$, however, the optimal choice is to measure $\hat{\sigma}_z$ for both atoms. As

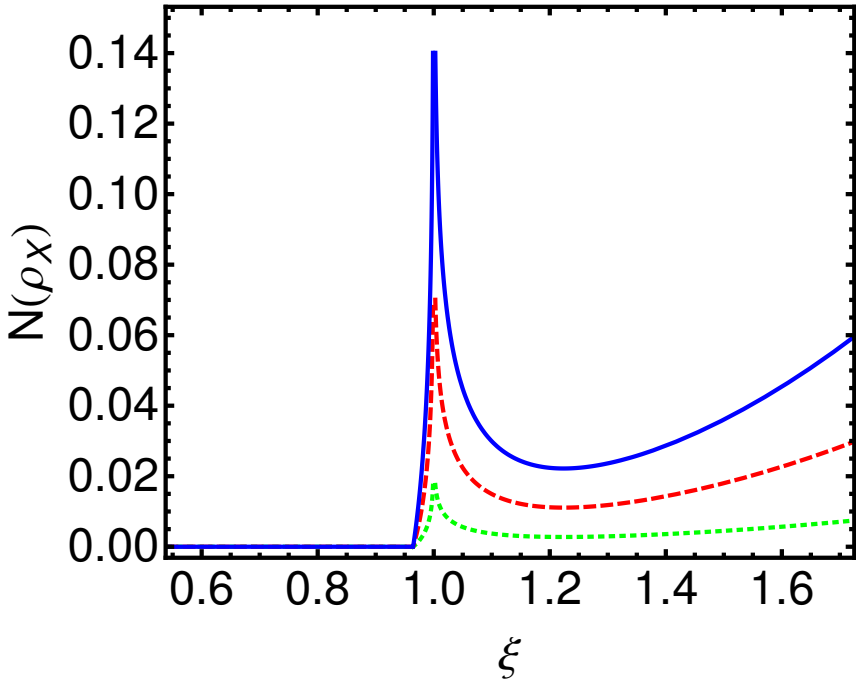

Figure 4.2: Time-evolution of the square root of the negativity of entanglement $N(\rho_{\rm X})$ for $Z = 50$ (dotted green), $Z = 200$ (dashed red), $Z = 400$ (continuous blue).

demonstrated in [108], only after the atoms become causally connected ($\xi = 1$) the excited state population of B is no longer independent on the presence of A. Vacuum fluctuations, whose role is important in connecting the atoms for $\xi < 1$ via virtual photons, are able to correlate transversal observables only. For a longitudinal $(z-z)$ correlation, one has to wait the arrival of the light signal, in agreement with the causality principle. Provided that a simultaneous space-time-region-dependent set of measurements on the two atoms could be efficiently performed in the laboratory frame, this result suggests that the spin-spin correlation function is a meaningful quantity to measure experimentally.

To conclude this section we compare of all the three quantities considered here in Fig. 4.4 as functions of Z and ξ. No violation of the general hierarchy (4.31) is observed confirming the consistency of the perturbative analysis that we have utilized.

In the last section we shall focus our attention on the non-locality of the model so far presented. To this aim, we will check if violations of Bell-type inequalities ever take place. Possible connections with the dynamics of the correlations that we have already studied will be investigated as well. The first part of the section will provide the reader with a minimum background for understanding the theory of Bell's inequalities.

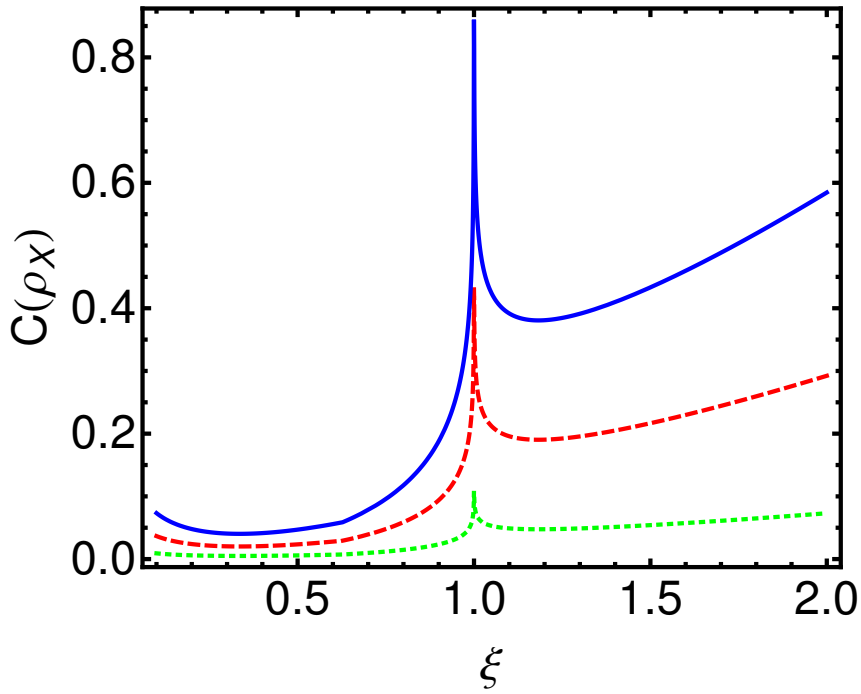

Figure 4.3: Time-evolution of the maximum connected correlation function $C(\rho_{\mathrm{X}})$ for $Z = 50$ (dotted green), $Z = 200$ (dashed red), $Z = 400$ (continuous blue).

4.5 Non-locality

In a famous paper published in 1935, Einstein, Podolsky and Rosen designed a *gedanken* experiment to show the incompleteness of quantum mechanics [131]. This result goes under the name of EPR paradox. Their conclusion was the following: if we postulate locality and realism as essential features for any physical theory, then quantum mechanics, with its predictions, cannot be complete. Locality meant that no action at a distance can ever take place or, equivalently, two distant objects cannot influence each other instantaneously. Realism implied that any observable property of an object exists with a well-defined value whether we observe it or not. Some consequences of quantum mechanics pose a rather clear difficulty to reconciling this theory with these concepts. In particular, the existence of entangled states seems to simultaneously contradict both realism and locality. This peculiarity was what bothered Einstein the most, so much that he renamed entanglement a "spooky action at a distance". The solution presented by the three authors was simple: quantum theory is only an approximation of a complete theory, in which "hidden variables" are the key to restoring both locality and realism.

The solution to such a speculative problem came in 1964 with a groundbreaking paper by John Bell [106]. Here, the author pictured an experiment whose outcome would definitely set the argument. He derived an inequality that any physical theory respecting locality and realism can never violate. We briefly summarize the idea.

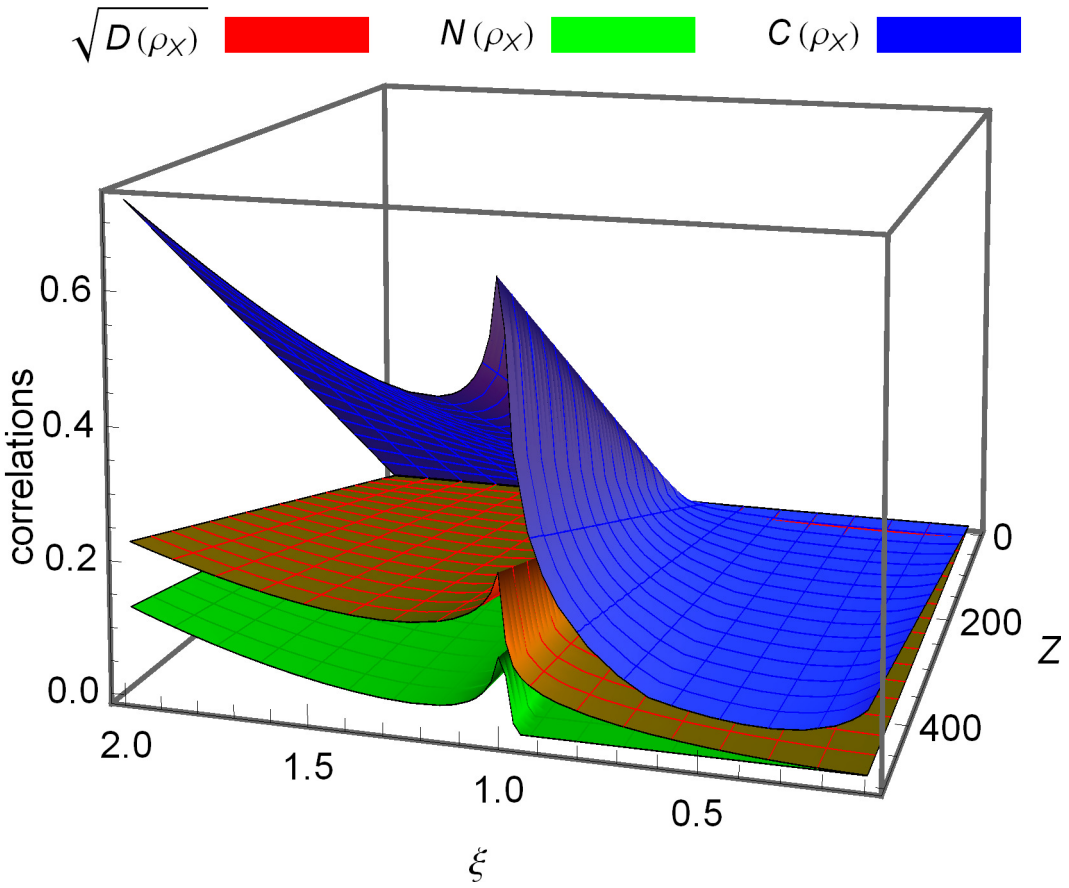

Figure 4.4: Comparative plot displaying the maximum connected correlation function C (topmost surface, blue online), the square root $\sqrt{D}$ of the geometric discord (middle surface, red online), and the negativity N (bottommost surface, green online), calculated for the state ρ_X as functions of the dimensionless time ξ and of the coupling strength Z, for $r = \upsilon\pi/4\Omega$.

Imagine we have two separated systems that do not interact with each other at any point. Let us fix a set of four possible joint measurements where each of the local measurements has a dichotomousc outcome, say ± 1. Starting from the constraint of locality and realism it is possible to write down a linear combination of the expectation values of these four joint measurements, which we label $\mathcal{B}$, that is always bounded from above by a certain value $\mathcal{B}_{\mathcal{C}}$. Any hidden variable theory satisfying the EPR requirements will never violate such an inequality. If quantum mechanics does represent the surface of a more complicated hidden-variable theory, then no violation of the Bell's inequality should be observed ever.

Unfortunately for Einstein, a clear violation of such an inequality was experimentally observed for the very first time in 1972 [132] and further confirmed in 1981-1982 in a fully quantum optical setup using pairs of entangled photons [133, 134]. Quantum mechanics has not been proven to be a complete theory. However, it certainly has been proven not to be consistent with either locality or realism. Further experimental tests conducted in different setups confirmed this feature of quantum theory [135–137]. Thus, the take-home message is simple: if we accept quantum mechanics as the best description of what happens in nature, we are forced to reject either realism or locality.

At this point, we wonder what the results we presented so far mean when one rethinks of the Fermi two-atom problem in terms of non-locality. The case of bipartite two-level systems has been extensively investigated in literature. The classical bound to Bell's inequality is $\mathcal{B}_{\mathcal{C}} = 2$ and an upper quantum bound of $2\sqrt{2}$ was computed by Tsirelson [138]. This corresponds to the value obtainable for maximally entangled states, such as Bell states. The connection between entanglement and Bell's inequality violation is not at all immediate though. If a quantum state does violate Bell's inequality we know for sure that it does not admit a classical description nor preparation by means of LOCC. Several entangled states of bipartite two-level systems fulfill this condition. However, examples of entangled states that do not violate this inequality are also well known in literature [139]. Hence, whenever we are given a quantum state $\hat{\rho}$ such that

$$2 < \mathcal{B}(\hat{\rho}) \leq 2\sqrt{2}, \tag{4.37}$$

we know that the state at hand is not predictable or reproducible classically. In the further analysis we will consider two slightly different definitions of the $\mathcal{B}$ parameter, the one derived by Clauser, Horne, Shimony and Holt (CHSH) [107] and an alternative optimized version for $X-$shaped states [140]. The first reads as follows

$$\mathcal{B}_{CHSH} = E(a_1, b_1) - E(a_1, b_2) + E(a_2, b_1) + E(a_2, b_2), \tag{4.38}$$

where $E(a_j, b_i) = \langle a_j b_i \rangle, j, i = 1, 2$ are the average correlations of the dihcotomic observable a_1, a_2 for system A and b_1, b_2 for system B. These can be thought of as spin-projections along different axis for a 1/2 spin particle, or different polarization states in a photonic system. Assuming that the outcomes are $a_j = \pm 1, b_i = \pm 1, j, i = 1, 2$ then the $\mathcal{B}_{\mathcal{C}} = 2$ bound can be easily computed assuming locality and realism. For a quantum state the observable a_j, b_i are replaced by operators and the statistical average $\langle \cdots \rangle$ has to be computed by using Born's rule. For an $X-$shaped state, such as the one at hand in the Fermi problem we find

$$\mathcal{B}_{CHSH}(\rho_{\mathrm{X}}) = -\sqrt{2}(\rho_{11} + \rho_{44} - \rho_{22} - \rho_{33} + 2\mathrm{Re}\rho_{23} + 2\mathrm{Re}\rho_{14}). \tag{4.39}$$

For a two-level system, which can always be mapped onto a fictitious 1/2 spin system, optimizing the Bell parameter means choosing projective angles for the set of joint spin measurements that maximize the violation of the Bell's inequality whenever this is present. The $X-$state optimized version of $\mathcal{B}_{CHSH}$ is given by [140]

$$\mathcal{B}_{OPT}(\rho_{\mathrm{X}}) = 2\sqrt{u_1 + \max[u_2, u_3]}\,, \tag{4.40}$$

where

$$u_1 = 4(|\rho_{14}| + |\rho_{23}|)^2, \qquad u_3 = 4(|\rho_{14}| - |\rho_{23}|)^2,$$

$$u_2 = (\rho_{11} + \rho_{44} - \rho_{22} - \rho_{33})^2\,.$$

Fig.4.5 shows the time evolution of the the Bell parameter $\mathcal{B}_{CHSH}$. The first feature worth noticing is the presence of a sharp peak at $\xi = 1$ for all of the three values of the coupling. This behavior surely reminds us of previous plots, where we looked at the dynamics of correlations. However, a clear difference is present here. In fact, in order to detect any appreciable violation of Bell's inequality we need to push the atom-field coupling to the strong limit and still such a violation would take place only in the neighborhood of $\xi = 1$. A direct comparison of this plot with Fig.4.2 shows us how a non-violation of Bell's inequality does not really tell us anything about the true nature of this state: if we took $\mathcal{B}_{CHSH}$ as a measure of quantumness of $\hat{\rho}_X$, we would be misled into believing that we might be able prepare it by means of LOCC operations. This is obviously not the case as the entanglement of this state starts increasing roughly around $\xi = 0.95$ and keeps increasing after the sharp peak-and-dip at $\xi = 1$. Fig.4.6 shows the time evolution of the optimized Bell parameter $\mathcal{B}_{OPT}$. Although, as predictable, the optimized Bell parameter $\mathcal{B}_{OPT}$ is larger than $\mathcal{B}_{CHSH}$ for all couplings and at all times, as further enlightened in Fig.4.7, still no appreciable violation of the classical threshold is observed unless the same conditions as in Fig.4.5 are matched. Hence, the same conclusions as in the case of $\mathcal{B}_{CHSH}$ apply: an analysis enquiring about the nature of the state $\hat{\rho}_X$ based

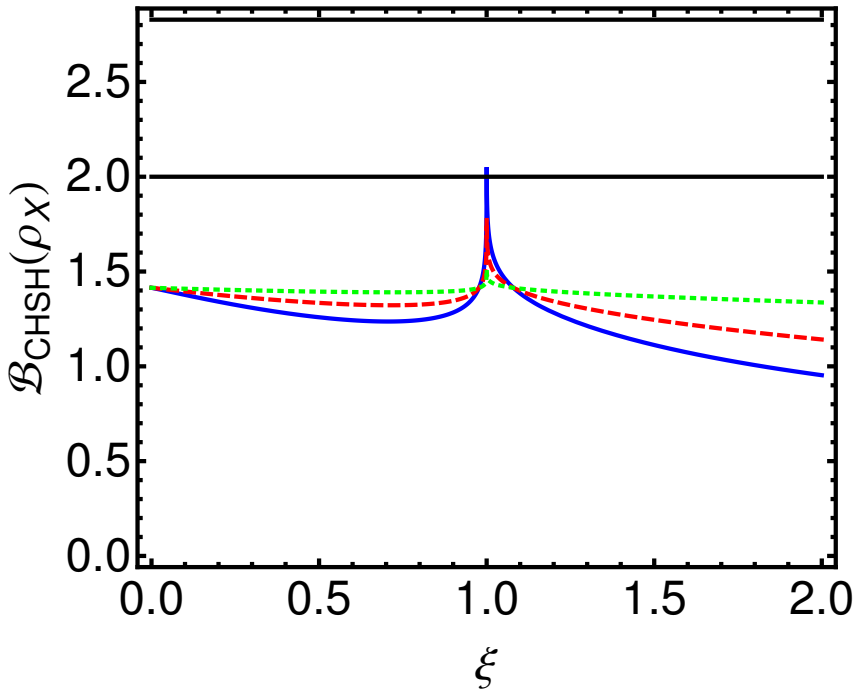

Figure 4.5: Bell-CHSH parameter $\mathcal{B}_{CHSH}$ and plotted for $Z = 100$ (dotted green), $Z = 400$ (dashed red) and $Z = 800$ (continuous blue), as a function of ξ. The straight line at $\mathcal{B} = 2$ gives the limit for a local realistic description.

on Bell's inequality only is insufficient as well as mainly inconclusive. The only real conclusion we can draw here is that measurement statistics we observe is compatible with locality and realism.

4.6 Conclusions

In this chapter a second order perturbation theory was developed to investigate the dynamics of classical and quantum correlations in the Fermi two-atom problem. All of the correlations studied turn out to be extremely sensitive to the light cone crossing point, at $\xi = 1$, where they all exhibit a sharp peak. Needless to say, this is when the signal emitted from the first atom can finally reach the second and further excite it.

We have seen that both geometric quantum discord and maximally connected correlation function start increasing at $\xi = 0$ unlike entanglement which displays a sudden birth just before $\xi = 1$. As all the correlations generated in the non-causal region are due to vacuum fluctuations effectively connecting the two atoms, we can conclude that geometric discord and spin-spin correlation functions are more sensitive to such an effect than entanglement. In particular, when one looks at C a sudden change in the nature of this function arises. For $\xi < 1$ these type of correlations can be only transverse allowing for virtual photon exchange, whereas for $\xi > 1$

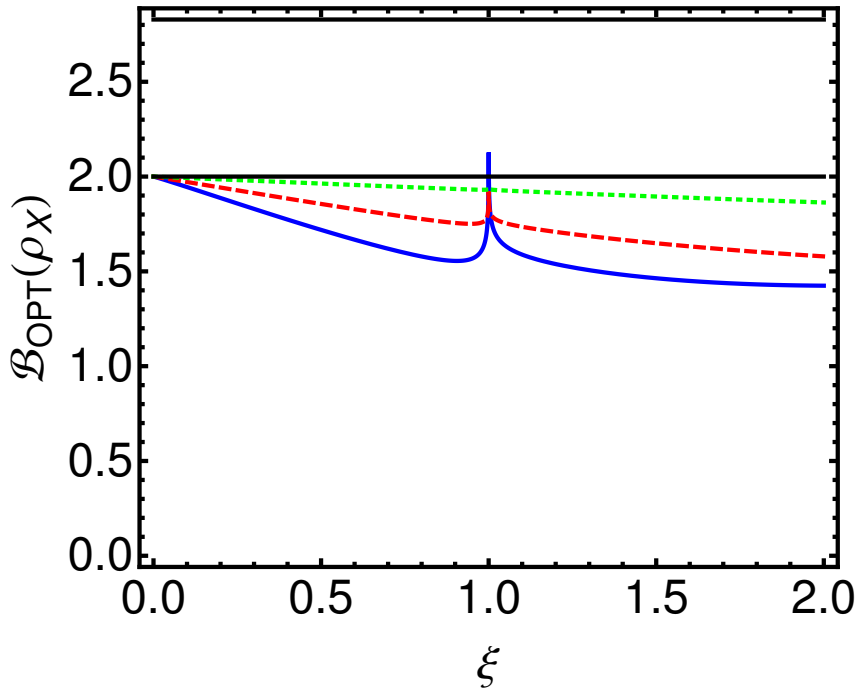

Figure 4.6: Optimized Bell-CHSH parameter $\mathcal{B}_{OPT}$ and plotted for $Z = 100$ (dotted green), $Z = 400$ (dashed red) and $Z = 800$ (continuous blue), as a function of ξ. The straight line at $\mathcal{B} = 2$ gives the limit for a local realistic description.

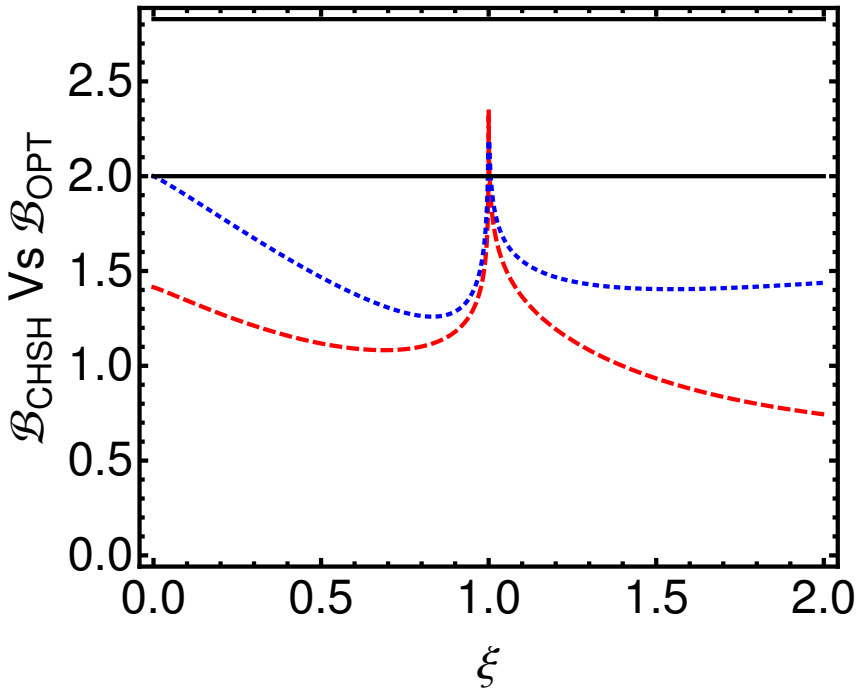

Figure 4.7: Comparison between $\mathcal{B}_{CHSH}$ (red dashed) and $\mathcal{B}_{\mathrm{OPT}}$ (blue dotted) for strong coupling $Z = 1000$. In all these plots $r = \upsilon\pi/4\Omega$.

longitudinal excitations (real photons) can be finally swapped. This is in agreement with recent results concerning the time-evolution of the excitation probability of the atom B [105].

Finally, a possible violation of Bell type inequalities was investigated in connection with the quantum or classical character of the state $\hat{\rho}_X$. Unfortunately, such an analysis has turned out to be not sufficiently illuminating as none or very weak violations were found.

Chapter 5

Conclusions and future perspectives

In this manuscript several aspects of the theory of open quantum system have been investigated. Major attention has been devoted to studying how interactions and/or correlations in open quantum system and its surrounding environment can be used for disparate purposes, such as implementing of quantum gates or probing critical phenomena.

In Chapter 2, we have introduced a novel scheme for implementing the C-NOT gate in trapped-ion systems. The use of many-body interactions and of an enlarged computational space makes it possible for stronger correlations between the ion's logic spin and the colletive motional state to develop during the execution of the protocol. This, in turn, results in a logic gate that is faster and more robust to dissipation and decoherence than the best experimental realization known so far. The result is presented for a small number of trapped ions, although the method is completely general and easily applicable to larger ion strings. Moreover, we believe it could serve as the starting point for constructing a set of N-body universal gates as an alternative to the traditional single and 2-qubit operations circuital decomposition.

In Chapter 3 we have analyzed the critical behavior of a Coulomb crystal, experimentally realizable in ion traps, from an open quantum system perspective. By means of Ramsey interferometry of a single 1/2 spin with the rest of the chain, intended as a phononic bath, we have witnessed a sudden transition in the reduced dynamics of the spin whenever the rest of the chain is pushed across criticality. In particular, we have seen how the backflow of information between the spin and the chain dramatically drops when the latter becomes mechanically unstable. Since we utilize this quantity as a quantifier of the degree of non-Markovianity of this process,

we have also related the critical behavior of the chain to the type of open dynamics that it can generate. Last, we have established an analytical link between the backflow of information and the visibility of the Ramsey fringes, providing a practical recipe for experimentally testing the theory presented. The study has been carried out in the zero and low temperature limit, leading to neat results in both cases. However, the model utilized has one limitation: it ignores non-harmonic contributions in the crystal Hamiltonian that arise at the critical point. This effect is particularly strong in the long time-scale regime and it can be neglected strictly in the thermodynamic limit. Hence, some open questions are left regarding the generalization of the Ramsey protocol to the full anharmonic case for a finite chain. For instance, one may wonder whether the backflow of information still drops drastically at criticality and whether a link between the visibility of the Ramsey fringes and the non-Markovian character of the single spin dynamics still exists. These two questions surely are of primary interest for future investigations. In a broader sense, since a quantum probe approach appears to be very advantageous when studying some critical phenomena in many-body physics, a general theory should be outlined.

In Chapter 4 we have presented a detailed perturbative study of the dynamics of quantum and classical correlations as well as the degree of non-locality in the two-atom Fermi problem. The general findings suggest that although this model can be proven to be strictly causal, atom-atom correlations can be generated in a non-causal space-time region as mediated by the electromagnetic field. This result does not obviously contradict general relativity as correlations do not represent physical information unless they are shared via communication, which cannot travel faster than light. Interestingly, we have observed how non-locality, as quantified by violations of Bell inequalities, is not sufficient to draw significant conclusions concerning the very nature of the atom-atom state at hand, whether this is quantum or classical. In fact, a very weak violation is observed only near that instant of time when the two atoms become causally connected. A question that we did not address is how other measures of quantum discord [125], other than the geometric one, behave in relation to the light-cone-crossing. For instance, during the completion of this project we have found the original definition by Ollivier and Zurek [68] to be unsuitable for a second order perturbative approach. However, such a measure could be compatible with a higher-order expansion of the dynamics. Another more general open question concerns the usefulness of these correlations for possible applications to quantum communication, such as quantum teleporation [142] or remote state preparation [143]. We believe this to be an interesting research path to take for future perspectives.

Appendix A

Stimulated Raman Transitions

Stimulated Raman transitions rely on the scheme illustrated in Fig.A.1 An atom in a lambda-type configuration interacts with two propagating lasers at frequency ω_{L_1} and ω_{L_2} respectively. The electronic levels $|\uparrow\rangle, |\downarrow\rangle$ forming the qubit are Zeeman sublevels and are split by a magnetic field. The effective Hamiltonian in this case reads as follows

$$\hat{H} = \hbar\Omega\hat{\sigma}_x\{e^{i\left[(\vec{k}_1-\vec{k}_2)\hat{\vec{r}}-(\omega_{L_1}-\omega_{L_2})t+\phi\right]} + \text{h.c.}\}, \tag{A.1}$$

where $\vec{k}_1$ and $\vec{k}_2$ are the wave-vector of the two lasers respectively, $\hat{\vec{r}}$ is the position operator of the atom and ϕ is a phase. The resonance condition can be easily matched by properly adjusting the propagation direction of the laser fields such that $|\omega_{L_1} - \omega_{L_2}| = \omega_0$ with ω_0 being the transition frequency between the Zeeman sublevels. The idea is then to drive transitions between these two levels by laser-coupling them strongly off-resonance to a third optical level $|\phi\rangle$. If we assume the detuning $\Delta \gg \delta$ the optical level $|\phi\rangle$ will be very unlikely to be populated and we can then employ the adiabatic elimination approximation [141] and eliminate it from the dynamics. The laser fields are plane waves

$$\vec{E}_j = E_j \cos(\vec{k}_j\hat{\vec{r}} - \omega_{L_j}t + \phi_j), \tag{A.2}$$

Hence, the original lambda structure will reduce to an effective two level-scheme where the energy of the qubit states will be Stark shifted by an amount $|g_{1(2)}|^2/\Delta$ where

$$g_{1(2)} \propto E_{1(2)}\langle\downarrow(\uparrow)|\hat{\vec{r}}|3\rangle \exp(-i\phi_{1(2)}). \tag{A.3}$$

The Stark shift that originates from the presence of the third optical level can be removed by properly adjusting the laser-laser detuning δ or incorporated in the ω_0 energy difference.

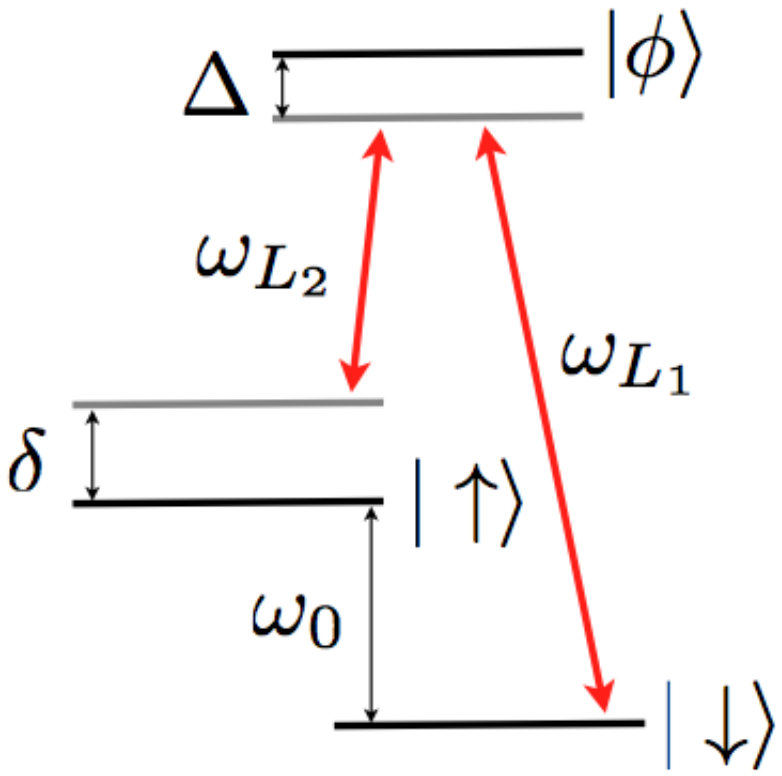

Figure A.1: Interaction scheme utilized to implement stimulated Raman transitions.

Appendix B

Quantum Process Tomography

A general completely positive dynamical map Φ_N acting over an N-qubit register can be completely characterized with quantum process tomography [81]. This technique allows one to determine of a complete set of orthogonal operators $\{\hat{\mathcal{K}}_m\}$ for which the Kraus operator decomposition can be performed $\hat{K}_i = \sum_m e_{im}\hat{\mathcal{K}}_m$ so as to get

$$\Phi_N \varrho = \sum_{m,n} \chi_{mn} \hat{\mathcal{K}}_m \varrho \hat{\mathcal{K}}_n^\dagger, \tag{B.1}$$

where the *channel matrix* $\chi_{mn} = \sum_i e_{im} e_{in}^*$ has been introduced. This is a very powerful tool: we only need to consider a fixed set of operators, whose knowledge is enough to characterize a channel through the matrix χ. We look at the specific case of a system of three qubits. The action of Φ over a element of a basis in the space of the $2^3 \times 2^3$ matrices can be determined by knowing the action of Φ over the fixed set of states constructed as the tensor product of the single-qubit ensemble of states $|0\rangle, |1\rangle, |+\rangle = (1/\sqrt{2})(|0\rangle + |1\rangle)$ and $|+_y\rangle = (1/\sqrt{2})(|0\rangle + i|1\rangle)$ as follows. Let us illustrate this argument by means of a single-qubit example. The action of Φ_1 on the generic element $|n\rangle\langle m|$ of a single-qubit density matrix ($n, m = 0, 1$) can be reconstructed as

$$\begin{aligned} \Phi_1(|n\rangle\langle m|) = {} & \Phi_1(|+\rangle\langle +|) + i\Phi_1(|+_y\rangle\langle +_y|) \\ & - (i+1)[\Phi_1(|n\rangle\langle n|) + \Phi_1(|m\rangle\langle m|)]/2. \end{aligned} \tag{B.2}$$

The argument can be easily extended to the case of three qubits, involving $4^3 = 64$ ensemble states. Therefore, it is straightforward to see that all the entries

$$\varrho_k = |n_1, n_2, n_3\rangle\langle m_1, m_2, m_3|,$$

($n_j, m_j = 0, 1$ with $k = 1, .., 64$) of a 8×8 density matrix can be found via state tomography of 64 fixed states. Clearly, $\Phi(\varrho_j) = \sum_k \lambda_{jk}\varrho_k$ as $\{\varrho_k\}$ form a basis. From

the above discussion we have

$$\Phi_3\varrho_j=\sum_{m,n}\hat{\mathcal{K}}_m\varrho_j\hat{\mathcal{K}}_n^\dagger\chi_{mn}=\sum_{m,n,k}\beta_{jk}^{mn}\varrho_k\chi_{mn}=\sum_k\lambda_{jk}\varrho_k, \tag{B.3}$$

where we have defined $\hat{\mathcal{K}}_m\varrho_j\hat{\mathcal{K}}_n^\dagger=\sum_k\beta_{jk}^{mn}\varrho_k$ so that we can write

$$\lambda_{jk}=\sum_{m,n}\beta_{jk}^{mn}\chi_{mn}. \tag{B.4}$$

The complex tensor β_{jk}^{mn} is set once we make a choice for $\{\hat{\mathcal{K}}_i\}$ and the λ_{jk}'s are determined from a knowledge of $\Phi\varrho_j$. By inverting Eq. (B.4), we get the channel matrix χ and characterize the map. Let $\hat{\mathcal{V}}^\dagger$ be the operator diagonalizing the channel matrix. Then it is straightforward to prove that if D_i are the elements of the diagonal matrix $\hat{\mathcal{V}}^\dagger\chi\hat{\mathcal{V}}$, then $e_{im}=\sqrt{D_i}\hat{V}_{mi}$, so that

$$\hat{K}_i=\sqrt{D_i}\sum_j\hat{\mathcal{V}}_{ji}\hat{\mathcal{K}}_j. \tag{B.5}$$

Bibliography

[1] R. Feynman, *Simulating physics with computers*, Int. J. Theoret. Phys. **21**, 467-488 (1982)

[2] I. J. Cirac and P. Zoller, *Quantum computations with cold trapped ions*, Phys. Rev. Lett. **74**, 4091 (1995)

[3] C. Monroe, D. M. Meekhof, B. E. King, W. M. Itano, and D. J. Wineland, *Demonstration of a fundamental quantum logic gate*, Phys. Rev. Lett. **75**, 4714 (1995)

[4] F. Schmidt-Kaler, H. Haffner, M. Riebe, S. Gulde, G. P. T. Lancaster, T. Deuschle, C. Becher, C. F. Roos, J. Eschner, and R. Blatt, *Realization of the Cirac-Zoller controlled-NOT quantum gate*, Nature **422**, 408-411 (2003)

[5] D. J. Wineland, J. Bergquist, W. M. Itano, and R. Drullinger, *Double-resonance and optical-pumping experiments on electromagnetically confined, laser-cooled ions*, Opt. Lett. **5**, 254 (1980)

[6] W. Nagourney, J. Sandberg, and H. Dehmelt, *Shelved optical electron amplifier: Observation of quantum jumps*, Phys. Rev. Lett. **56**, 2797 (1986)

[7] Th. Sauter, W. Neuhauser, R. Blatt, and P. E. Toschek, *Observation of quantum jumps*, Phys. Rev. Lett. **57**, 1696, (1986)

[8] J. C. Bergquist, Randall G. Hulet, Wayne M. Itano, and D. J. Wineland, *Observation of quantum jumps in a single atom* , Phys. Rev. Lett. **57**, 1699 (1986)

[9] J.J. Bollinger, D. J. Heinzen, W. M. Itano, S. L. Gilbert, and D. J. Wineland, *A 303 MHz frequency standard based on trapped Be^+ ions*, IEEE Trans. Instr. Meas. **40**, 126 (1991)

[10] D. Kielpinski, V. Meyer, M. A. Rowe, C. A. Sackett, W. M. Itano, C. Monroe, and D. J. Wineland, *A decoherence-free quantum memory using trapped ions*, Science **291**, 1013-1015 (2001)

[11] C. A. Sackett, D. Kielpinski, B. E. King, C. Langer, V. Meyer, C. J. Myatt, M. Rowe, Q. A. Turchette, W. M. Itano, D. J. Wineland, and C. Monroe, *Experimental entanglement of four particles*, Nature **404**, 256-259 (2000)

[12] D. Leibfried, E. Knill, S. Seidelin, J. Britton, R. B. Blakestad, J. Chiaverini, D. B. Hume, W. M. Itano, J. D. Jost, C. Langer, R. Ozeri, R. Reichle and D. J. Wineland, *Creation of a six-atom Schroedinger cat state*, Nature **438**, 639-642 (2005)

[13] Thomas Monz, Philipp Schindler, Julio T. Barreiro, Michael Chwalla, Daniel Nigg, William A. Coish, Maximilian Harlander, Wolfgang Hansel, Markus Hennrich, and Rainer Blatt, *14-Qubit entanglement: creation and coherence*, Phys. Rev. Lett. **106**, 130506 (2011)

[14] D. Deutsch, and R. Jozsa, *Rapid solution of problems by quantum computation*, Proc. R. Soc. Lond. A **439**, 553-558 (1992)

[15] S. Gulde, H. Haeffner, M. Riebe, G. Lancaster, C. Becher, J. Eschner, F. Schmidt-Kaler, I. L. Chuang and R. Blatt, *Quantum information processing with trapped Ca^+ ions*, Proc. R. Soc. Lond. A **361**, 1363-1374 (2003)

[16] B. DeMarco, A. Ben-Kish, D. Leibfried, V. Meyer, M. Rowe, B. M. Jelenkovi, W. M. Itano, J. Britton, C. Langer, T. Rosenband, and D. J. Wineland, *Experimental demonstration of a controlled-NOT wave-packet gate*, Phys. Rev. Lett **89**, 267901 (2009)

[17] M. D. Barrett, J. Chiaverini, T. Schaetz, J. Britton, W. M. Itano, J. D. Jost, E. Knill, C. Langer, D. Leibfried, R. Ozeri, and D. J. Wineland, *Deterministic quantum teleportation of atomic qubits*, Nature **429**, 737-739 (2004)

[18] M. Riebe, H. Haffner, C. F. Roos, W. Hansel, J. Benhelm, G. P. T. Lancaster, T. W. Korber, C. Becher, F. Schmidt-Kaler, D. F. V. James, R. Blatt, *Deterministic quantum teleportation with atoms*, Nature **429**, 734-737 (2004)

[19] J. Chiaverini, D. Leibfried, T. Schaetz, M. D. Barrett, R. B. Blakestad, J. Britton, W. M. Itano, J. D. Jost, E. Knill, C. Langer, R. Ozeri, and D. J. Wineland, *Realization of quantum error correction*, Nature **432**, 602-605 (2004)

[20] T. Monz, K. Kim, W. Hansel, M. Riebe, A. S. Villar, P. Schindler, M. Chwalla, M. Hennrich, and R. Blatt, *Realization of the quantum Toffoli gate with Trapped ions*, Phys. Rev. Lett. **102**, 040501 (2009)

[21] R. Gerritsma, G. Kirchmair, F. Zuhringer, E. Solano, R. Blatt, and C. F. Roos, *Quantum simulation of the Dirac equation*, Nature **463**, 68-71 (2010)

[22] B. P. Lanyon, C. Hempel, D. Nigg, M. Muller, R. Gerritsma, F. Zhringer, P. Schindler, J. T. Barreiro, M. Rambach, G. Kirchmair, M. Hennrich, P. Zoller, R. Blatt, and C. F. Roos, *Universal digital quantum simulation with trapped ions*, Science **334**, 57-61 (2011)

[23] Julio T. Barreiro, Markus Muller, Philipp Schindler, Daniel Nigg, Thomas Monz, Michael Chwalla, Markus Hennrich, Christian F. Roos, Peter Zoller, and Rainer Blatt, *An open-system quantum simulator with trapped ions*, Nature **470**, 486-491 (2011)

[24] D. J. Wineland, C. Monroe, W. M. Itano, D. Leibfried, B. E. King, and D. M. Meekhof, *Experimental issues in coherent quantum-state manipulation of trapped atomic ions*, J. Res. Natl. Inst. Stand. Technol. **103**, 259-328 (1998)

[25] H. Haeffner, C. F. Roos, and R. Blatt, *Quantum computing with trapped ions*, Phys. Rep. **469**, 155-203 (2008)

[26] M. Borrelli, L. Mazzola, M. Paternostro and S. Maniscalco, *Simple trapped-ion architecture for high-fidelity Toffoli gates*, Phys. Rev. A **84**, 012314 (2011)

[27] T. Toffoli, in *Automata, Languages and Programming*, J. W. de Bakker and J. van Leeuwen eds. (Springer, New York, 1980)

[28] P. K. Gosh, *Ion Traps*, 1995 (Clarendon, Oxford)

[29] D.H.E. Dubin and T.M. O Neil, *Trapped nonneutral plasmas, liquids, and crystals (the thermal equilibrium states)*, Rev. Mod. Phys. **71** 87 (1999)

[30] L. Hornekaer, N. Kjaergaard, A. M. Thommesen, and M. Drewsen, *Structural properties of two-component Coulomb crystals in linear Paul traps*, Phys. Rev. Lett. **86**, 1994 (2001)

[31] Niels Kjaergaard, and Michael Drewsen, *Observation of a structural transition for Coulomb crystals in a linear Paul trap*, Phys. Rev. Lett. **91**, 095002 (2003)

[32] A. Mortensen, E. Nielsen, T. Matthey, and M. Drewsen, *Observation of three-dimensional long-range order in small ion Coulomb crystals in an rf-trap*, Phys. Rev. Lett. **96**, 103001 (2006)

[33] G. Birkl, S. Kassner, and H. Walther, *Multiple-shell structures of laser-cooled* $^{24}Mg^{+}$ *ions in a quadrupole storage ring*, Nature **357**, 310-313 (1992)

[34] I.Waki, S. Kassner, G. Birkl, and H.Walther, *Observation of ordered structures of laser-cooled ions in a quadrupole storage ring*, Phys. Rev. Lett. **68**, 2007 (1992)

[35] D. F. V. James, *Quantum dynamics of cold trapped ions with application to quantum computation*, Appl. Phys. B **66**, 181-190 (1998)

[36] D. H. E. Dubin, *Theory of structural phase transitions in a trapped Coulomb crystal*, Phys. Rev. Lett. **71**, 2753 (1993)

[37] G. Piacente, I. V. Schweigert, J. J. Betouras, and F. M. Peeters, *Generic properties of a quasi-one-dimensional classical Wigner crystal*, Phys. Rev. B **69**, 045324 (2004)

[38] J. P. Schiffer, *Phase transitions in anisotropically confined ionic crystals*, Phys. Rev. Lett. **70**, 818 (1993)

[39] S. Fishman, G. De Chiara, T. Calarco, and G. Morigi, *Structural phase transitions in low-dimensional ion crystals*, Phys. Rev. B **77**, 064111 (2008)

[40] E. Shimshoni, G. Morigi, and S. Fishman, *Quantum zigzag transition in ion chains*, Phys. Rev. Lett. **106**, 010401 (2011)

[41] E. Shimshoni, G. Morigi, and Shmuel Fishman, *Quantum structural phase transition in chains of interacting atoms*, Phys.Rev.A **83**, 032308 (2011)

[42] P. Silvi, G. De Chiara, T. Calarco, G. Morigi, and S. Montangero, *Full characterization of the quantum linear-zigzag transition in atomic chains*, Ann. Phys. **525**, 827 (2013)

[43] M. Borrelli, P. Haikka, G. De Chiara and S. Maniscalco, *Non-Markovian qubit dynamics induced by Coulomb crystals*, Phys. Rev. A **88**, 010101(R) (2013)

[44] H.-P. Breuer and F. Petruccione, *The Theory of Open Quantum Systems* (Oxford University Press, Oxford, 2007)

[45] U. Weiss, *Quantum Dissipative Systems*, 2nd ed. (World Scientific, Singapore, 1999)

[46] M. M. Wolf, J. Eisert, T. S. Cubitt, and J. I. Cirac, *Assessing Non-Markovian Quantum Dynamics*, Phys. Rev. Lett. **101**, 150402 (2008)

[47] H. -P. Breuer, E.-M. Laine, J. Piilo, *Measure for the Degree of Non-Markovian Behavior of Quantum Processes in Open Systems*, Phys. Rev. Lett. **103**, 210401(2009)

[48] A. Rivas, S. F. Huelga, and M. B. Plenio, *Entanglement and Non-Markovianity of Quantum Evolutions*, Phys. Rev. Lett. **105**, 050403 (2010)

[49] S. Lorenzo, F. Plastina, and M. Paternostro, *Geometrical characterization of non-Markovianity*, Phys. Rev. A **88**, 020102(R) (2013)

[50] S. Luo, S. Fu, and H. Song, *Quantifying non-Markovianity via correlations*, Phys. Rev. A **86**, 044101 (2012)

[51] B. Bylicka, D. Chruscinski, and S. Maniscalco, *Non-Markovianity as a resource for quantum technologies*, arXiv:1301.2585

[52] P. Haikka, S. McEndoo, G. De Chiara, G. M. Palma, and S. Maniscalco, *Quantifying, characterizing, and controlling information flow in ultracold atomic gases*, Phys. Rev. A **84**, 031602(R) (2011)

[53] P. Haikka, J. Goold, S. McEndoo, F. Plastina, and S. Maniscalco, *Non-Markovianity, Loschmidt echo, and criticality: A unified picture*, Phys. Rev. A **85**, 060101(R) (20012)

[54] T. J. G. Apollaro, C. DiFranco, F. Plastina, and M. Paternostro, *Memory-keeping effects and forgetfulness in the dynamics of a qubit coupled to a spin chain*, Phys. Rev. A **83**, 032103 (2011)

[55] S. Lorenzo, F. Plastina, and M. Paternostro, *Role of environmental correlations in the non-Markovian dynamics of a spin system*, Phys. Rev. A **84**, 032124 (2011)

[56] F. Plastina, A. Sindona, J. Goold, N. Lo Gullo, and S. Lorenzo, *Decoherence in a Fermion Environment: Non-Markovianity and Orthogonality Catastrophe*, Open Sys. & Information Dyn. **20**, 1340005 (2013)

[57] E. Fermi, *Quantum Theory of Radiation*, Rev. Mod. Phys. **4** 87 (1932)

[58] M.I. Shirokov, Yad. Fiz. 4, 1077 (1966) [Sov. J. Nucl. Phys. **4**, 774 (1967)].

[59] A. K. Biswas, G. Compagno, G. M. Palma, R. Passante and F. Persico, *Virtual photons and causality in the dynamics of a pair of two-level atoms*, Phys. Rev. A **42**, 4291 (1990)

[60] D. Buchholz and J. Yngvason, *There are no causality problems for Fermi's two-atom system*, Phys. Rev. Lett. **73**, 613 (1994)

[61] P. W. Milonni, D. F. V. James and H. Fearn, *Photodetection and causality in quantum optics*, Phys. Rev. A **52**, 1525 (1995)

[62] E. A. Power and T. Thirunamachandran, *Analysis of the causal behavior in energy transfer between atoms*, Phys. Rev. A **56**, 3395 (1997)

[63] C. Sabín, B. Peropadre, M. del Rey, and E. Martín-Martínez, *Extracting Past-Future Vacuum Correlations Using Circuit QED*, Phys. Rev. Lett. **109**, 033602 (2012)

[64] M. Borrelli, C. Sabín, G. Adesso, F. Plastina, and S. Maniscalco, *Dynamics of atom-atom correlations in the Fermi problem*, New J. Phys. **14**, 103010 (2012)

[65] R. Horodecki, P. Horodecki, M. Horodecki, and K. Horodecki, *Quantum entanglement*, Rev. Mod. Phys. **81**, 865 (2009)

[66] B. Dakić, C. Brukner, and V. Vedral, *Necessary and sufficient condition for nonzero quantum discord*, Phys. Rev. Lett. **105**, 190502 (2010)

[67] M. M. Wolf, F. Verstraete, M. B. Hastings, and J. I. Cirac, *Area laws in quantum systems: mutual information and correlations*, Phys. Rev. Lett. **100**, 070502 (2008)

[68] H. Ollivier and W. H. Zurek, *Quantum discord: A measure of the quantumness of correlations*, Phys. Rev. Lett. **88**, 017901 (2001)

[69] L. Henderson and V. Vedral, *Classical, quantum and total correlations*, J. Phys. A **34**, 6899 (2001)

[70] D. Leibfried, R. Blatt, C. Monroe, and D. Wineland, *Quantum dynamics of single trapped ions*, Rev. Mod. Phys. **75**, 281 (2003)

[71] M. Abramowitz and I. A. Stegun, *Handbook of Mathematical Functions*, NBS Applied Mathematics Series No. 55, 1972 (Dover, New York)

[72] N. W. McLachlan, *Theory and Applications of Mathieu Functions*, 1974 (Clarendon, Oxford)

[73] W. Paul, *Electromagnetic traps for charged and neutral particles*, Rev. Mod. Phys. **62**, 531 (1990)

[74] R. J. Cook, D. G. Shankland and A. L. Wells, *Quantum theory of particle motion in a rapidly oscillating field*, Phys. Rev. A **31**, 564 (1985)

[75] R. J. Glauber, *Laser Manipulation of Atoms and Ions*, Proceedings of the International School of Physics Enrico Fermi (North-Holland, Amsterdam, 1002)

[76] C. Schneider, D. Porras and T. Schaetz, *Experimental quantum simulations of many-body physics with trapped ions*, Rep. Prog. Phys. **75**, 024401 (2012)

[77] A. Atland, and B. Simmons, *Condensed Matter Field Theory* (Cambridge University Press, 2010)

[78] J. A. Jones, *Quantum Computing with NMR*, Prog. NMR Spectrosc. **59**, 91-120 (2011)

[79] P. Kok, W. J. Munro, K. Nemoto, T. C. Ralph, J. P. Dowling, and G. J. Milburn, *Linear optical quantum computing with photonic qubits*, Rev. Mod. Phys. **79**, 135 (2004)

[80] A. Blais, R.-S. Huang, A. Wallraff, S. M. Girvin, and R. J. Schoelkopf, *Cavity quantum electrodynamics for superconducting electrical circuits: An architecture for quantum computation*, Phys. Rev. A **69**, 062320 (2004)

[81] M. A. Nielsen and I. L. Chuang, *Quantum Computation and Quantum Information* (Cambridge University Press, 2000)

[82] J. L. O'Brien, G. J. Pryde, A. Gilchrist, D. F. V. James, N. K. Langford, T. C. Ralph, and A. G. White, *Quantum Process Tomography of a Controlled-NOT Gate*, Phys. Rev. Lett. **93**, 080502 (2004)

[83] Alexei Gilchrist, Nathan K. Langford, and Michael A. Nielsen, *Distance measures to compare real and ideal quantum processes*, Phys. Rev. A **71**, 062310 (2005)

[84] F. Mintert, C. Wunderlich, *Ion-trap quantum logic using long-wavelength radiation*, Phys. Rev. Lett. **87**, 257904 (2001)

[85] P. A. Barton, C. J. S. Donald, D. M. Lucas, D. A. Stevens, A. M. Steane, and D. N. Stacey, *Measurement of the lifetime of the* $3d^2D_{5/2}$ *state in* $^{40}Ca^+$, Phys. Rev. A **62**, 032503 (2000)

[86] P. Richerme, C. Senko, J. Smith, A. Lee, S. Korenblit, and C. Monroe, *Experimental performance of a quantum simulator: Optimizing adiabatic evolution and identifying many-body ground states*, Phys. Rev. A **88**, 012334 (2013)

[87] C. F. Roos, M. Chwalla, K. Kim, M. Riebe, and R. Blatt, *'Designer atoms' for quantum metrology*, Nature **443**, 316-319 (2006)

[88] A. Sorensen, and K. Molmer, *Quantum computation with ions in thermal motion*, Phys. Rev. Lett. **82**, 1971 (1999)

[89] P. C. Haljan, P. J. Lee, K.-A. Brickman, M. Acton, L. Deslauriers, and C. Monroe, *Entanglement of trapped-ion clock states*, Phys. Rev. A **72**, 062316 (2005)

[90] G. J. Milburn, S. Schneider, and D. F. James, *Ion trap quantum computing with warm ions*, Fortschr. Phys. **48**, 801 (2000)

[91] D. Leibfried, B. DeMarco, V. Meyer, D. Lucas, M. Barrett, J. Britton, W. M. Itano, B. Jelenkovic, C. Langer, T. Rosenband, and D. J. Wineland, *Experimental demonstration of a robust, high-fidelity geometric two ion-qubit phase gate*, Nature **422**, 412-415 (2003)

[92] R.J. Glauber, *Coherent and incoherent states of the radiation field*, Phys. Rev. **131** 2766 (1963)

[93] M. Tavis, and F. W. Cummings *Exact Solution for an N-Molecule-Radiation-Field Hamiltonian*, Phys. Rev. **170**, 379 (1968)

[94] W. H. Zurek, *Decoherence and the transition from quantum to classical*, Phys. Today **44**, 36 (1991)

[95] N.W. Ashcroft and N.D. Mermin, *Solid State Physics* (Saunders College, Philadelphia, 1976)

[96] P. M. Chaikin, T. C. Lubensky, *Principles of Condensed Matter Physics* (Cambridge University Press, 2000)

[97] V. Gorini, A. Kossakowski, and E. C. G. Sudarshan, *Completely positive dynamical semigroups of $N-$level systems*, J. Math. Phys. **17**, 821 (1976)

[98] G. Lindblad, *On the generators of quantum dynamical semigroups*, Comm. Math. Phys. **48**, 119 (1976)

[99] C. Gerry and P. Knight, *Introductory Quantum Optics* (Cambridge University Press, 2005)

[100] D. F. Walls and G. J. Milburn, *Quantum Optics* (Springer, 2008)

[101] G. De Chiara, T. Calarco, S. Fishman and G. Morigi, *Ramsey interferometry with a spin embedded in a Coulomb chain*, Phys. Rev. A **78**, 043414 (2008)

[102] S. Wissmann, A. Karlsson, E.-M. Laine, J. Piilo, and H.-P. Breuer, *Optimal state pairs for non-Markovian quantum dynamics*, Phys. Rev. A **86**, 062108 (2012)

[103] N. Ashcroft, *Solid State Physics*, Holt-Saunders Int. Eds., Tokyo, (1976)

[104] G. C. Hegerfeldt, *Causality problems for Fermi two-atom system*, Phys. Rev. Lett. **72**, 596 (1994)

[105] C. Sabín, M. del Rey, J. J. García-Ripoll and J. León, *Fermi Problem with Artificial Atoms in Circuit QED*, Phys. Rev. Lett. **107**, 150402 (2011)

[106] J. S. Bell, *On the Einstein Podolsky Rosen paradox*, Physics **1**, 195-200 (1964)

[107] J. F. Clauser, M. A. Horne, A. Shimony, and R. A. Holt, *Proposed experiment to test local hidden-variable theories*, Phys. Rev. Lett. **23**, 880 (1969)

[108] C. Sabín, J. J. García-Ripoll, E. Solano and J. León, *Dynamics of entanglement via propagating microwave photons*, Phys. Rev. B **81**, 184501 (2010)

[109] C. H. Bennett, G. Brassard, C. Crepeau, R. Jozsa, A. Peres, and W. K. Wootters, *Teleporting an unknown quantum state via dual classical and Einstein-Podolsky-Rosen channels*, Phys. Rev. Lett. **70**, 1895 (1993)

[110] P. W. Shor, *Polynomial-time algorithms for prime factorization and discrete logarithms on a quantum computer*, J. Sci. Statist. Comput. **26**, 1484-1509 (1997)

[111] N. Gisin, G. Ribordy, W. Tittel, and H. Zbinden, *Quantum cryptography*, Rev. Mod. Phys. **74**, 145 (2002)

[112] G. Adesso, and F. Illuminati, *Entanglement in continuous-variable systems: recent advances and current perspectives*, J. Phys. A **40**, 7821 (2007)

[113] O. Guhne, and G. Toth, *Entanglement detection*, Phys. Rep. **474**, 1-75 (2009)

[114] A. Peres, *Separability criterion for density matrices*, Phys. Rev. Lett. **77**, 1413 (1996)

[115] R. Horodecki, P. Horodecki, and M. Horodecki, *Separability of mixed states: necessary and sufficient conditions*, Phys. Lett. A **210**, 377 (1996)

[116] G. Vidal, and R. F. Werner, *Computable measure of entanglement*, Phys. Rev. A **65**, 032314 (2002)

[117] C. E. Shannon, *A mathematical theory of communication*, Bell Sys. Tech. J. **27**, 379-423 (1948)

[118] T. M. Cover, and J. A. Thomas, *Elements of Information Theory* (J. Wiley, New York, 1991)

[119] I. Bengtsson, and K. Zyczkowky, *Geometry of Quantum States*, (Cambridge University Press, 2006)

[120] A. Ferraro, L. Aolita, D. Cavalcanti, F. M. Cucchietti and A. Acín, *Almost all quantum states have nonclassical correlations*, Phys. Rev. A **81**, 052318 (2010)

[121] M. Piani, S. Gharibian, G. Adesso, J. Calsamiglia, P. Horodecki and A. Winter, *All nonclassical correlations can be activated into distillable entanglement*, Phys. Rev. Lett. **106**, 220403 (2011)

[122] A. Streltsov, H. Kampermann and D. Bruss, *Linking quantum discord to entanglement in a measurement*, Phys. Rev. Lett. **106**, 160401 (2011)

[123] S. Campbell, T. J. G. Apollaro, C. Di Franco, L. Banchi, A. Cuccoli, R. Vaia, F. Plastina, and M. Paternostro, *Propagation of nonclassical correlations across a quantum spin chain*, Phys. Rev. A **84**, 052316 (2011)

[124] M. Piani, and G. Adesso, *Quantumness of correlations revealed in local measurements exceeds entanglement*, Phys. Rev. A **85**, 040301(R) (2012)

[125] K. Modi, A. Brodutch, H. Cable, T. Paterek, and V. Vedral, *The classical-quantum boundary for correlations: Discord and related measures*, Rev. Mod. Phys. **84**, 1655 (2012)

[126] S. Luo, and S. Fu, *Geometric measure of quantum discord*, Phys. Rev. A **82**, 034302 (2010)

[127] D. Girolami, and G. Adesso, *Interplay between computable measures of entanglement and other quantum correlations*, Phys. Rev. A **84**, 052110 (2011)

[128] G. Adesso (unpublished)

[129] S. Luo, *Quantum discord for two-qubit systems*, Phys. Rev. A **77** 042303 (2008)

[130] S. Hill and W. K. Wootters, *Entanglement of a pair of quantum bits*, Phys. Rev. Lett. **78**, 5022 (1997)

[131] A. Einstein, B. Podolsky, and N. Rosen, *Can quantum-mechanical description of physical reality be considered complete?*, Phys. Rev. **47**, 777 (1935)

[132] S. J. Freedman, and J. F. Clauser, *Experimental test of local hidden-variable theories*, Phys. Rev. Lett. **28**, 938 (1972)

[133] A. Aspect, P. Grangier, and G. Roger, *Experimental tests of realistic local theories via Bell's theorem*, Phys. Rev. Lett. **47**, 460 (1981)

[134] A. Aspect, P. Grangier, and G. Roger, *Experimental realization of Einstein-Podolsky-Rosen-Bohm gedankenexperiment: A new violation of Bell's inequalities*, Phys. Rev. Lett. **49**, 91 (1982)

[135] G. Weihs, T. Jennewein, C. Simon, H. Weinfurter, and A. Zeilinger, *Violation of Bell's inequality under strict Einstein locality conditions*, Phys. Rev. Lett. **81**, 5039 (1998)

[136] M. A. Rowe, D. Kielpinski, V. Meyer, C. A. Sackett, W. M. Itano, C. Monroe, D.J. Wineland, *Experimental violation of a Bell's inequality with efficient detection*, Nature **409**, 791-794 (2001)

[137] M. Ansmann, H. Wang, R. C. Bialczak, M. Hofheinz, E. Lucero, M. Neeley, A. D. O'Connell, D. Sank, M. Weides, J. Wenner, A. N. Cleland, J. M. Martinis, *Violation of Bell's inequality in Josephson phase qubits*, Nature **461**, 504-506 (2009)

[138] B. S. Cirel'son, *Quantum generalizations of Bell's inequality*, Lett. Math. Phys. **4**, 93-100 (1980)

[139] R. F. Werner, *Quantum states with Einstein-Podolsky-Rosen correlations admitting a hidden-variable model*, Phys. Rev. A **40**, 4277 (1989)

[140] B. Bellomo, R. Lo Franco, and G. Compagno, *An optimized Bell test in a dynamical system*, Phys. Lett. A **374**, 3007-3011 (2010)

[141] E. Brion, L. H. Pedersen, and K. Molmer, *Adiabatic elimination in a lambda system*, J. Phys. A: Math. Theor. **40**, 1033 (2007)

[142] C. H. Bennett, G. Brassard, C. Crepeau, R. Jozsa, A. Peres, W. K. Wootters, *Teleporting an unknown quantum state via dual classical and EinsteinPodolskyRosen channels*, Phys. Rev. Lett. **70**, 18951899 (1993)

[143] C. H. Bennett, D. P. DiVincenzo, P. W. Shor, J. A. Smolin, B. M. Terhal, and W. K. Wootters, *Remote state preparation*, Phys. Rev. Lett. **87**, 077902 (2001)